NUMERICAL INVESTIGATION OF HYDROGEN PRODUCTION FROM METHANE FOR SMALL SCALE STATIONARY PEM FUEL CELL APPLICATIONS

by

Özgür Tan

B.S., Chemical Engineering, Istanbul Technical University, 2005

Submitted to the Institute for Graduate Students in
Science and Engineering in partial fulfillment of
the requirements for the degree of
Master of Science

Graduate Program in Chemical Engineering
Boğaziçi University

2007

dedicated to my mother
and father

ACKNOWLEDGEMENTS

I would like to express my truthful gratitude to my thesis supervisors, Professor Zeynep İlsen Önsan and Assistant Professor Ahmet Kerim Avcı for their guidance and understanding. I am indebted to them for their patience for my never-ending questions and for the assistance and support they provided throughout the course of the project. It was a great opportunity and privilege for me to work with them and learn from their great expertise and experiences in catalysis and reaction engineering.

I would like to thank Mustafa Karakaya for sharing his scientific background with me and for his valuable suggestions on the framework of the project. I would also like to express my thanks to Emre Maşalacı for his partnership and true friendship that continues since our undergraduate education.

Finally, I must express my cordial feelings to my family. This work would have never been possible without everlasting support, patience and encouragement they provided throughout my entire life. I dedicate this work to my father, who showed me how a father should be, and my mother, who is the most self-sacrificing mother in the world; but I know, no dedications, no words or no phrases can be used to thank to them, all I can say is that I am very proud of being their son.

The financial support for this research was provided by TÜBİTAK through project 104M163 and by Boğaziçi University Research Fund (BAP) through project 06HA501.

ABSTRACT

NUMERICAL INVESTIGATION OF HYDROGEN PRODUCTION FROM METHANE FOR SMALL SCALE STATIONARY PEM FUEL CELL APPLICATIONS

The steady-state behaviour of the fuel processor system consisting of a catalytic indirect partial oxidation reactor (combined total oxidation/steam reforming), a water-gas shift converter and a preferential carbon monoxide oxidation reactor for conversion of methane to hydrogen for use in small scale fuel cell applications is investigated using computer-based modeling/simulation techniques. Steady-state simulation and sizing of reactors, which are considered to be packed-bed tubular type, are carried out for six different feed ratio ((methane/oxygen, steam/methane) = (2.24, 1.17), (1.89, 1.56)) /PEMFC power output (500, 1000, 1500 W) configurations. Material balance calculations are executed to obtain the flow rates of each species at each stream. These results are then used in reactor modeling and simulation studies as boundary conditions to estimate the size of the reactors in terms of catalyst weight. A one-dimensional pseudohomogeneous reactor model is used for modeling and simulation purposes. Reactor dimensions and catalyst particle diameter are then estimated by using a set of criteria to quantify interfacial heat and intraparticle mass transfer resistances and flow behaviour in packed beds. Total pressure change along the reactor tube is also checked such that the dimensions do not lead to excessive pressure drop. Catalyst quantity in each reactor is found to increase almost linearly with the power output of the PEMFC at both feed compositions. Lengths and diameters estimated for IPOX, WGS and PROX reactors are also found to increase with increasing PEMFC power output. Total system volume, excluding the piping, pumping and heat exchange units, is estimated to be 0.49, 0.98 and 1.51 liters for 500, 1000 and 1500 W of PEMFC power outputs, respectively.

ÖZET

KÜÇÜK ÖLÇEKLİ DURAĞAN PEM TİPİ YAKIT PİLİ UYGULAMALARI İÇİN METAN GAZINDAN HİDROJEN ÜRETİMİNİN SAYISAL OLARAK ARAŞTIRILMASI

Metan gazının küçük ölçekli yakıt pili uygulamalarında kullanılmak üzere, katalitik dolaylı kısmi oksidasyon (toplam oksidasyon + buhar reformlama) reaktörü, su-gazı değişim reaktörü ve seçimli karbon monoksit oksidasyon reaktörü içeren yakıt dönüşüm sisteminde hidrojene dönüşümü bilgisayar destekli modelleme/benzetim yöntemleriyle incelenmiştir. Dolgulu yataklı tipte ve tüp şeklinde olduğu kabul edilen reaktörlerin kararlı durum benzetimleri ve boyutlandırılmaları altı değişik besleme oranı ((metan/oksijen, buhar/metan) = (2.24, 1.17), (1.89, 1.56))/yakıt pili çıkış gücü (500, 1000, 1500 W) düzeninde yapılmıştır. Her bileşenin her akımdaki akış değeri kütle dengesi hesaplamaları yürütülerek elde edilmiştir. Daha sonra bu sonuçlar, katalizör ağırlığı cinsinden reaktör boyutlarını hesaplamak için, reaktör modelleme ve benzetiminde sınır değerleri olarak kullanılmıştır. Modelleme ve benzetim çalışmaları bir boyutlu türdeş reaktör modeli kullanılarak yapılmıştır. Uzunluk cinsinden reaktör boyutları ve katalizör parçacığının çapı, akışkan ve katalizör arayüzündeki ısı iletimini, katalizör parçacığının içindeki kütle iletimini ve dolgulu yataklı reaktörlerdeki akış rejimini belirleyen ölçütlerin kullanılmasıyla bulunmuştur. Reaktör tüpü boyunca toplam basınç değişimi, boyutlandırmanın aşırı basınç düşüşüne sebep olmaması için ayrıca kontrol edilmiştir. Her reaktörün içindeki katalizör miktarının iki farklı besleme oranında da yakıt pilinin gücüyle doğrusal olarak arttığı bulunmuştur. Ayrıca her reaktör için elde edilmiş uzunluk ve çap değerlerinin de yakıt pilinin gücüyle arttığı gözlemlenmiştir. Boru donanımlarının, pompaların ve ısı değiştiricilerinin dâhil olmadığı toplam sistem hacmi, 500, 1000 ve 1500 W gücündeki yakıt pilleri için sırasıyla 0.49, 0.98 ve 1.51 litre olarak hesaplanmıştır.

TABLE OF CONTENTS

LIST OF FIGURES

LIST OF TABLES

LIST OF SYMBOLS/ABBREVIATIONS

A_c	Cross-sectional area of the reactor, m^2
$c_{p,j}$	Heat capacity of species *j*, kJ $kmol^{-1}$ K^{-1}
C_{sj}	Surface concentration of species *j*, kmol m^{-3}
D_e	Effective diffusivity inside catalyst, m^2 h^{-1}
D_{kj}	Binary diffusivity of component *k* into component *j*, m^2 h^{-1}
D_{km}	Diffusivity of component *k* diffusing into a homogeneous gas mixture, m^2 h^{-1}
D_p	Catalyst particle diameter, µm or mm
D_t	Diameter of the reactor tube, cm
E_i	Activation energy of reaction *i*, kJ $kmol^{-1}$, kJ mol^{-1} or kcal mol^{-1}
$F_{1,j}$	Flow rate of species *j* in the feed, kmol h^{-1} or mol h^{-1}
$F_{2,j}$	Flow rate of species *j* in IPOX reactor after total oxidation, kmol h^{-1} or mol h^{-1}
$F_{3,j}$	Flow rate of species *j* at the exit of IPOX reactor, kmol h^{-1} or mol h^{-1}
$F_{4,j}$	Flow rate of species *j* at the exit of the WGS converter, kmol h^{-1} or mol h^{-1}
$F_{5,j}$	Flow rate of species *j* at the air inlet stream, kmol h^{-1} or mol h^{-1}
$F_{6,j}$	Flow rate of species *j* at the exit of the PROX reactor, kmol h^{-1} or mol h^{-1}
G	Superficial mass velocity, kg m^{-2} s^{-1}
h_s	Particle-to-fluid heat transfer coefficient, kJ m^{-2} h^{-1} K^{-1}
i	Reaction index
j	Species index
k	Species index

k_i	Rate constant for reaction *i*, mol kgcat^{-1} s^{-1}, mol gcat^{-1} s^{-1} or kmol kgcat^{-1} h^{-1}
$k_{0,i}$	Pre-exponential factor of reaction *i* in Arrhenius equation, mol kgcat^{-1} s^{-1}, mol gcat^{-1} s^{-1} atm^{-1} or mol gcat^{-1} s^{-1}
K_j	Adsorption constant for species *j* (reforming), bar^{-1}
$K_{0,j}$	Pre-exponential factor of species *j* in van't Hoff equation, bar^{-1}
K_{eq}^{SR}	Equilibrium constant for steam reforming reaction, bar^2
K_{eq}^{WGS1}	Equilibrium constant for water-gas shift reaction (in IPOX)
K_{eq}^{WGS2}	Equilibrium constant for water-gas shift reaction,
$K_{CH_4}^{c}$	Adsorption constant for methane (oxidation), bar^{-1}
$K_{O_2}^{c}$	Adsorption constant for oxygen (oxidation), bar^{-1}
L	Length of the reactor tube, cm
m_{cat}	Amount of catalyst needed for reaction *i*, kg
M_j , M_k	Molecular weights of species *j* and *k*, g mol^{-1}
P_j	Partial pressure of species *j*, bar
P_{out}	Total outlet pressure of the reactor of interest, bar
P_T	Total pressure, bar
Pr	Prandtl number
r_i	Rate of reaction *i*, kmol kgcat^{-1} h^{-1}
R	Universal gas constant, kJ kmol^{-1} K^{-1}
Re	Reynolds number
T	Temperature, K
T_1^{in}	Temperature of the inlet stream of IPOX reactor, K
T_2^{in}	Temperature of the inlet stream of WGS converter, K
T_3^{in}	Temperature of the inlet stream of PROX reactor, K
$V_{particle}$	Particle volume of the catalyst, m^3
$V_{particle,ex}$	Particle volume of the catalyst excluded pores, m^3
V_{pore}	Pore volume of the catalyst, m^3

V_{total}	Total volume of the catalyst, m^3
V_{void}	Volume of the catalyst, m^3
W	Catalyst weight, g
X_i	Degree of conversion of reaction *i*
Y_j	Mole fraction of component *j*
α_j	Constant in heat capacity equation, kJ $kmol^{-1}$ K^{-1}
β_j	Constant in heat capacity equation, kJ $kmol^{-1}$ K^{-2}
γ_j	Constant in heat capacity equation, kJ $kmol^{-1}$ K^{-3}
δ_j	Constant in heat capacity equation, kJ $kmol^{-1}$ K^{-4}
ΔH^o_{298}	Standard heat of reaction at 298 K, kJ mol^{-1}
ΔH_i	Heat of reaction *i* at *T*, kJ $kmol^{-1}$
ΔH_j	Heat of adsorption of species *j*, kJ $kmol^{-1}$ or kJ mol^{-1}
ε_f	Void fraction
ε_p	Pellet porosity
λ_f	Thermal conductivity of the bulk fluid, kJ m^{-1} h^{-1} K^{-1}
λ_{N_2}	Thermal conductivity of nitrogen, W m^{-1} K^{-1}
μ	Viscosity of the gas mixture, kg m^{-1} s^{-1}
v	Velocity of the gas mixture, m s^{-1}
v_a	Atomic diffusion volume,
v_{ij}	Stoichiometric coefficient of species *j* in reaction *i*
ρ_b	Bulk density of the catalyst, kg m^{-3}
ρ_c	Solid density of the catalyst, kg m^{-3}
ρ_m	Density of the gas mixture, kg m^{-3}
ρ_p	Particle density of the catalyst, kg m^{-3}
σ	Constriction factor
τ	Tortuosity
ϕ	Porosity

AFC	Alkaline fuel cell
ATR	Autothermal reforming
CHP	Combined heat and power
HTM	Hydrogen transport membrane
HTS	High-temperature shift
IPOX	Indirect partial oxidation
LNG	Liquefied natural gas
LPG	Liquefied petroleum gas
LTS	Low-temperature shift
MCFC	Molten carbonate fuel cell
MCR	Microchannel/microstructured reactor
OTM	Oxygen transport membrane
PAFC	Phosphoric acid fuel cell
PEMFC	Polymer electrolyte/Proton exchange fuel cell
PROX	Preferential oxidation of carbon monoxide
ppm	Parts per million
SOFC	Solid oxide fuel cell
SR	Steam reforming
TOX	Total oxidation
WGS	Water-gas shift

1. INTRODUCTION

Hazardous emissions caused by conventionally used energy conversion technologies such as internal combustion engines are constituting an important environmental risk that forces automobile industry and developing technology to find innovative solutions for the development of clean energy conversion systems, which is also imposed by stringent legislative regulations (Trimm and Önsan, 2001). Therefore, development of fuel-efficient engines that release less pollutant has been a major objective for many years. Promising alternatives have been identified in four key areas: direct-injection compression ignition engines, hybrid electric vehicles, fuel cell powered electric vehicles and the use of lightweight materials (Trimm and Önsan, 2001). Fuel cell powered electrically driven vehicles have become one of the most promising candidates for clean energy production.

Fuel cells offer significant advantages compared to the conventional technologies in clean and efficient power generation. Moreover, when pure hydrogen is used, they can operate at zero emission levels. They produce lower noises, have fewer moving parts, represent comparably longer service life and operate efficiently because of the electrochemical conversion of the fuel into electrical power without the need of a heat generation step; such attractive features make fuel cells a promising alternative of conventional combustion engines for use in automobiles (Ahmed and Krumpelt, 2001; Trimm and Önsan, 2001). In addition to transportation purposes, fuel cells can also be used in a variety of areas ranging from small portable devices to stationary residential applications and mega-watt scale power stations (Avcı, 2003).

Types of fuel cells operating with different fuels and electrolytes are investigated for their potential use in such application areas. For vehicular and transport applications, the most promising fuel cell technology appears to be the Polymer Electrolyte/Proton Exchange Membrane Fuel Cell (PEMFC) fueled by hydrogen due to its compactness, low weight, potential for low cost and volume, high power density, modularity, dynamic response and ability to start-up quickly (Ahmed and Krumpelt, 2001; Avci, 2003; Ralph

and Hards, 1998; Ghenciu, 2002). Despite the advantages of it, some problems exist in the use of PEMFC such as the lack of hydrogen distribution infrastructure which is a handicap for the need of continuous hydrogen availability and the low-energy density of today's hydrogen storage technology. Also, as a method of having hydrogen on-board, storage of hydrogen on-board needs excessive volumes and is still an expensive way when the current technological status is considered. Nevertheless, it is an option very likely to be commercialised in the long term (Satyapal *et al.*, 2007). Therefore, compact, efficient devices that convert hydrocarbon fuels into hydrogen-rich gas mixture on-board the vehicle with a system called fuel processor seems to be a promising alternative (Trimm and Önsan, 2001).

A fuel processor converts a primary, hydrocarbon-based fuel to a hydrogen-rich gas mixture in the context of a catalytic process within different possible kinds of reactors such as membrane, monolithic and fixed-bed types (Ma and Trimm, 1996; de Smet *et al.*, 2001; Avcı *et al.*, 2000). Three catalytic reactions are proposed to take place in series in the configuration of a fuel processor system (Avcı *et al.*, 2002). Primary fuel is first converted catalytically into a hydrogen-rich gas mixture by steam reforming, direct partial oxidation or by indirect partial oxidation. One promising route for hydrogen production is indirect partial oxidation (IPOX), which is the combination of total oxidation (TOX) of part of the fuel and steam reforming (SR) of the remaining fuel. Steam reforming is an endothermic reaction, i.e. heat must be supplied for this reaction, while total oxidation is an exothermic reaction which produces heat. During indirect partial oxidation reaction, heat released by the exothermic total oxidation is harnessed by the endothermic steam reforming (Ma, 1995; Ma and Trimm, 1996). Coupling of total oxidation and steam reforming reactions is also called as autothermal reforming (ATR) or autothermal hydrogen production (Brown, 2001).

Reformed gas mixture is then treated by water-gas shift (WGS) reaction in a subsequent catalytic reactor for reducing the level of carbon monoxide, a poison for the fuel cell catalysts, and for enriching the hydrogen concentration. Hydrogen-rich gas mixture is finally sent to a preferential carbon monoxide oxidation reactor (PROX) where carbon monoxide concentration is reduced to the levels below the tolerable limits of the PEMFC electrodes of 10 ppm (Cheng *et al.*, 2007).

The objective of this study is to investigate the steady-state conversion of methane to hydrogen in a fuel processor system that includes IPOX, WGS and PROX reactors and to design and to size these reactors by a series of computer-based modeling and simulation techniques. A parametric study is conducted by considering two different feed ratios ((methane/oxygen, steam/methane) = (2.24, 1.17), (1.89, 1.56)) and three different power sizes of PEMFC (500, 1000, 1500 W), summing up to six different configurations of the fuel processor system. For every configuration, component flow rates within the system are figured out by material balances. Catalyst quantities within the reactors to deliver these calculated throughput rates and compositions are estimated by use of a reactor model. Reactors are considered to be catalytic packed-bed type; they are modeled and simulated using one-dimensional pseudohomogeneous model. Evaluation of catalyst quantities is followed by sizing of the reactors and determination of appropriate catalyst particle sizes. The latter are carried out by incorporating equations of mechanical energy balance and a set of criteria for quantifying interfacial (fluid-to-catalyst) and intraparticle (within the catalyst) transport resistances, axial dispersion and fluid flow profile into the reactor model. In each of the configuration of the fuel processor system, for every reactor, it is aimed to come up with a reactor length, diameter and particle size that can offer reactor operation almost free of transport resistances with minimal pressure drop and with a fluid flow profile as assumed in the pseudohomogeneous reactor model.

A literature survey related to fuel cell technology, total oxidation and steam reforming of methane, partial oxidation processes, water-gas shift reaction and preferential carbon monoxide oxidation is presented Chapter 2. Material balance equations, the mathematical model and the set of quantitative criteria employed for the simulation and sizing of IPOX, WGS and PROX reactors are given in Chapter 3. Component flow rates in every stream of the fuel processor system obtained from material balances and simulation results, which are the component flow and temperature profiles along the reactor for every feed/power output configuration, used in reactor design and sizing, are presented and discussed in Chapter 4. An exploratory study for the intensification of the fuel processor system using process intensification techniques is outlined in Chapter 5. Chapter 6 involves the major conclusions that can be drawn from this study and the recommendations for future work.

2. LITERATURE SURVEY

2.1. Fuel Cell Technology

2.1.1. Fuel Cell Operation

Fuel cells are energy conversion devices in which chemical energy stored in a fuel is converted into electrical energy by series of electrochemical reactions. Electro-chemical fuel cell process is a simpler, cleaner and more efficient operation compared to fuel conversion in internal combustion engines (Song, 2002).

A typical fuel cell consists of electrodes, i.e. anode and cathode and an electrolyte which is placed between these porous electrodes. In a fuel cell operation, fuel is fed to anode where the fuel is oxidized to give positive ions and electrons. The electrolyte between the two electrodes conducts positive ions selectively from anode to cathode. On the other hand, electrons are transferred from anode to cathode by means of an external circuit in which the electrical power is generated. Oxygen molecules (that is generally supplied in the form of air), protons and electrons react at the cathode to give the products of the fuel cell conversion process. A typical fuel cell operation is given in Figure 2.1 in which the operation of a hydrogen-driven fuel cell with a positively charged-hydrogen ion conducting electrolyte is demonstrated (Karakaya, 2006).

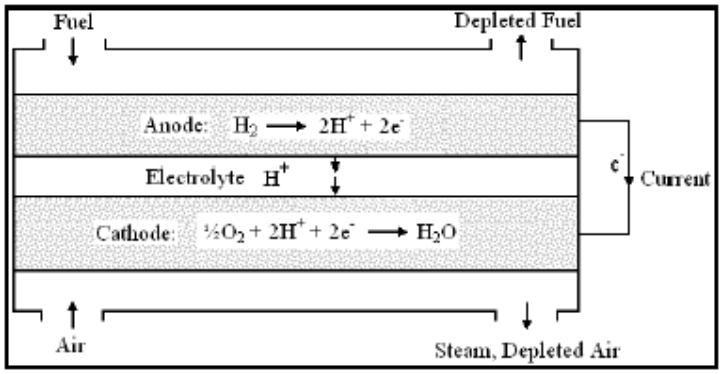

Figure 2.1. Fuel Cell Operation (Karakaya, 2006)

The output electrical potential of an individual fuel cell, e.g. of hydrogen driven fuel cells is given about 0.6-0.7 volts (Trimm and Önsan, 2001). In general, voltage of a single fuel cell is insufficient and therefore, combination of fuel cells in the form of stacks is necessary for achieving the desired power output.

2.1.2. Types and Applications of Fuel Cells

Fuel cells are categorized as low temperature fuel cells which are Proton Exchange/Polymer Electrolyte Membrane Fuel Cells (PEMFC), Alkaline Fuel Cells (AFC) and Phosphoric Acid Fuel Cells (PAFC) and high temperature fuel cells which are Molten Carbonate Fuel Cells (MCFC) and Solid Oxide Fuel Cells (SOFC) (Perry and Green, 1997).

Each type of fuel cell has a set of specific features that are associated with their efficiencies, type of electrolyte material, operating temperature, cost etc. PAFC has high efficiency which can be considered as the ratio of generated power to per unit of fuel feed and it can tolerate carbon monoxide concentration of about 1.5 mole per cent. However, it has low power generation and large size and weight that are not compatible for vehicular applications. AFC can achieve power generating efficiencies up to 70 per cent and has advantages of being simple in design and less expensive (Hirschenhofer *et al.,* 1998), whereas it requires pure hydrogen as feed and is sensitive to carbon monoxide. MCFC and SOFC promise high fuel-to-electricity efficiencies up to 85 per cent and they can process hydrocarbon fuels. However, they operate at elevated temperatures about 923 K and 1273 K, respectively, possibly requiring high external energy demand and relatively high capital cost due to the need of materials of construction having improved thermal resistances (Perry and Green, 1997).

PEMFC uses pure hydrogen as fuel and operates with a solid polymer (perfluorosulfonic acid) electrolyte which is an excellent conductor for hydrogen ions and has ability to reduce corrosion, safety and management problems. Compared to other types of fuel cells, PEMFC has high power density, quick start-up ability, about 40 per cent of efficiency and low operation temperatures between 343 and 363 K (Larminie and Dicks, 2003; Cheng *et al.,* 2007). Due to its such features, PEM fuel cells are primarily

investigated to suit for residential, commercial and transportation applications (Larminie and Dicks, 2003; Santarelli and Torchio, 2007; Lee *et al.*, 2007). The major properties of PEMFC are presented in Table 2.1.

Table 2.1. Major properties of PEMFCs (Selen, 2003)

Operating temperature	343 – 363 K
Cathode/Anode catalyst	Pt/Pt
Efficiency (5 kW size)	30 – 40 per cent
Efficiency (50 kW size)	35 – 45 per cent
Estimated cost	$200/kW
Major challenges	Membrane durability System complexity
Major advantages	High power density Quick start-up Reduced corrosion and management problems Low operating temperatures
Major applications	Transportation Small scale CHP Portable/leisure

PEMFC has anode and cathode electrodes that are composed of one or more precious metal catalysts such as platinum (mostly used), platinum alloys, palladium, rhodium, supported by high surface area materials such as carbon powder or fibers, conducting polymers such as a composite of polypyrrole and polystyrenesulfonate, carbon nanohorn (Litster and McLean, 2004). Due to the usage of platinum catalysts on both surfaces, the cost of operation rises. In order to lower the cost, platinum loadings as low as 0.014 mg/cm^2 is reported using novel sputtering methods (Cha and Lee, 1999; O'Hayre *et al.*, 2002) where conventional catalyst layers generally featured expensive platinum loadings of 4 mg/cm^2 (Litster and McLean, 2004). As a consequence, cost of catalyst loading may no longer be a major barrier for PEMFC use.

The PEMFC does not tolerate more than 10 ppm carbon monoxide since the platinum catalysts used on electrodes are highly sensitive to the poisonous carbon monoxide gas (Cheng *et al.*, 2007). In addition, water management is an important issue for PEMFC operation since the solid polymer electrolyte has to be humidified which means that by-product water should not evaporate faster than it is produced – a factor requiring low temperature operation (Larminie and Dicks, 2003).

2.2. Fuels and Fuel Conversion Processes Used in On-board Hydrogen Production

The potential use of fuel cells in applications such as transportation facilities brought significant challenges associated with generation, storage and distribution of hydrogen which is used as a common fuel in fuel cells (Trimm and Önsan, 2001). There are two methods for fuelling a fuel cell vehicle with hydrogen: storing hydrogen on-board or producing it on-board. For on-board hydrogen storage, pressurized vessels are considered to store hydrogen under cryogenic conditions (i.e. in the form of liquid) and high-pressure cylinders are considered to store hydrogen as compressed gas. Alternatively, hydrogen can be chemisorbed on a metal or alloy to form metal hydrates or can be adsorbed on carbon nanotubes (Trimm and Önsan, 2001; Avcı, 2003). However, at the moment, these hydrogen storage methods are somewhat expensive, occupy excessive volume, increase the weight, decrease the energy conversion efficiency and they are not easily refillable. Because of these reasons, storage of hydrogen on-board does not seem to be feasible for passenger vehicles and requires further improvements. Nevertheless, it may be feasible for use in big vehicles like buses and lorries, where volume and weight constraints are minimal. As a result, design and operation of efficient and compact fuel processors which convert hydrocarbons to hydrogen on-board the vehicle has taken great attention and served as a promising way for usage of fuel cells in transportation (Trimm and Önsan, 2001; Ralph and Hards, 1998).

2.2.1. Fuels

Various types of fuels have been considered for their conversion to hydrogen. Natural gas, LPG (liquefied petroleum gas), gasoline, methanol, ethanol and diesel are some of the fuels of interest. However, diesel conversion requires well-controlled

conditions, since it can deposit coke easily during the fuel conversion processes mentioned in Section 2.2.2. Nevertheless, its ease of on-board storage because of its liquid form, well-established delivery infrastructure, high energy density and price advantage keep diesel as one of the important candidates for on-board conversion (Cheekatamarla and Lane, 2005; Kopasz *et al.*, 2005; Kang and Bae, 2006).

Methanol has received most interest for on-board conversion since it is in liquid form at ambient temperatures, having high energy density and, when compared with other fuels, it can be reformed at lower temperatures, as seen in Table 2.2. Methanol has also the advantage of having low carbon monoxide concentration in product stream (0.8 mol per cent) compared to other fuels (Brown, 2001). Although many studies reported successful demonstration of on-board methanol conversion, methanol has some problems about its production volume and a lacking-distribution network; current supply of methanol can only meet the demands of a certain number of fuel cell vehicles (Thomas *et al.*, 2000; Thomas and Dawe, 2003). Hence, investments for establishing additional methanol synthesis facilities and distribution networks are required for the use of methanol as fuel (Avcı, 2003). Furthermore, methanol is a toxic chemical which can cause serious hazards for health and for environment (Brown, 2001).

Table 2.2. Temperature ranges of steam reforming for different fuels (Brown, 2001)

Fuel	Temperature Range (K)
Methane	1000 – 1100
Methanol	500 – 560
Ethanol	800 – 1000
Multi-carbon Hydrocarbons	1000 – 1150

Gasoline is another fuel considered for on-board hydrogen production. It has a high energy density, is already available for on-board applications and has a widespread refuelling infrastructure. Unlike methanol, gasoline does not require an extra synthesis step; it can be obtained by refining crude oil (Avcı, 2003). Despite the many advantages of gasoline, it contains aromatic hydrocarbons which can easily lead to coke formation during

its steam reforming (Rostrup-Nielsen, 1984). Catalyst deactivation due to high sulphur content in gasoline is another problem for on-board gasoline conversion. Nevertheless, prototypes with gasoline fuel processor/PEM fuel cell system are being developed by major car manufacturers (Springman *et al.*, 2004).

Ethanol is a renewable liquid fuel, which can be produced from biomass with biochemical processes i.e. any starch or sugar source via fermentation and can be converted to hydrogen on-board a vehicle. Ethanol has important advantages compared with other fuels such as being almost CO_2 neutral since the carbon dioxide produced in the process is consumed for biomass growth and offering a nearly closed carbon loop by this way. Moreover, it offers high energy density, safety, ease of handling, storage and transport because of its liquid form and non-toxicity (Liguras *et al.*, 2004). Thus, ethanol seems to be promising potential as a fuel for on-board conversion.

LPG (Liquefied Petroleum Gas) is a well-known and widely used fuel. It can be stored in liquid form in pressurized vessels for mobile and portable use. LPG is by-product of crude oil processing in refineries and is a mixture of propane and n-butane, whose amounts change with the processed crude oil. Moreover, LPG has very low sulphur content, high power density and is a cheaper fuel compared to others. Therefore, its on-board conversion in small-scale applications has been investigated by several groups (Ahmed and Krumpelt, 2001; Laosiripojana and Assabumrungrat, 2005; Recupero *et al.*, 2005; Cipiti *et al.*, 2006).

Natural Gas is mainly composed of 75 to 85 percent methane, with the remainder being ethane, propane and trace of carbon dioxide (Dicks, 1996). It gives the lowest carbon dioxide emissions and the highest hydrogen-to-carbon ratio among the other hydrocarbon fuels. Moreover, natural gas has major advantages in storage and distribution: it can be shipped in the form of liquefied natural gas (LNG) or distributed through widespread pipeline networks worldwide. Thus, natural gas is considered to be the ideal and suitable fuel for hydrogen production due to its good storage properties, existing infrastructure and high hydrogen/carbon ratio (Barz *et al.*, 2003). However, it is not a suitable fuel for on-board hydrogen production, because it needs heavy and large pressurized vessels for on-board storage. In addition to its complicated storage, which is because of its gaseous form

in ambient temperatures, considerable energy input is needed for its conversion due to the stability of natural gas molecules. Therefore, instead of using it in small-scale vehicular applications, it is much more promising to use it in on-site hydrogen production for stationary residential and commercial applications (Avcı, 2003; Dicks, 1996).

2.2.2. Fuel Conversion Processes

Several methods such as steam reforming, thermal cracking, carbon dioxide reforming, partial oxidation and autothermal reforming are suggested for the conversion of hydrocarbon fuels to hydrogen (Jamal and Wyszynski, 1994; Trimm and Önsan, 2001; Pena *et al.*, 1996). Autothermal reforming and steam reforming have been considered as the basic processes for hydrogen production in commercial applications. However, most of the industrial hydrogen production is based on methane steam reforming currently (Muradov and Veziroğlu, 2005).

Thermal cracking is direct decomposition of hydrocarbons to carbon and hydrogen:

$$C_nH_m \longrightarrow nC + \tfrac{1}{2}mH_2 \qquad (2.1)$$

For methane cracking, the reaction is:

$$CH_4 \longrightarrow C + 2H_2, \qquad \Delta H^o_{298} = 74.8 \text{ kJ/mol} \qquad (2.2)$$

The process has some basic advantages: no carbon dioxide and carbon monoxide are produced during the reaction, thus there is no need for an extra step to reduce the carbon monoxide level and hydrogen is produced in a single step. However, there are some difficulties associated with thermal cracking: high energy input is required to sustain the reaction due to its endothermicity and this process occurs at high temperatures, around 1673 K and higher where the use of transition metal catalysts (e.g. Ni, Fe, Co) may reduce the maximum temperature of the process (Muradov, 2003). Because of the high operation temperature, catalyst can be deactivated by coke formation. As a result, due to the high-energy demand and potential coke formation problems, thermal cracking seems not to be a feasible solution process for on-board hydrogen production (Trimm and Önsan, 2001).

Steam reforming of hydrocarbons is a well-known route for hydrogen production and favoured by high temperatures:

$$C_nH_m + nH_2O \longrightarrow nCO + (½m+n)H_2, \qquad (2.3)$$

Steam reforming of hydrocarbons to produce hydrogen runs generally on nickel-based catalysts and is a well-established industrial process described in detail (Twigg, 1989; Rostrup-Nielsen, 1984) while steam reforming of methanol is an attractive alternative for small-scale applications (Joensen and Rostrup-Nielsen, 2002).

Catalytic steam reforming offers higher hydrogen concentrations reaching up to 80 per cent (for partial oxidation and autothermal reforming 40-50 percent on dry basis) in the crude reformed gas (Ming *et al.*, 2002) and it leads to the best gas quality (Heinzel *et al.*, 2002) compared with partial oxidation and autothermal reforming. During steam reforming, water-gas shift reaction takes place as a side reaction which occur on same catalyst as steam reforming; it lowers the carbon monoxide concentration and increases the hydrogen production, so it is important to the final product spectra (Trimm and Önsan, 2001):

$$CO + H_2O \longleftrightarrow CO_2 + H_2, \qquad \Delta H^{o}_{298} = -41.2 \text{ kJ/mol} \qquad (2.4)$$

Steam reforming is endothermic and heat must be added to the system to sustain the reaction. Due to the considerable heat demand, requirement of large reactors and high amounts of catalyst loading, steam reforming by itself is not applicable for vehicular on-board applications. However, for on-board applications, the energy requirement of Reaction (2.3) can be provided by combusting the part of the fuel by total oxidation reaction which generally runs on Pt-based catalysts (Golunski, 1998; Trimm and Önsan, 2001):

$$CH_4 + 2O_2 \longrightarrow CO_2 + 2H_2O, \quad \Delta H^{o}_{298} = -802.3 \text{ kJ/mol} \qquad (2.5)$$

The combination of total oxidation (2.5), steam reforming (2.3) and water-gas shift reaction (2.4) is called indirect partial oxidation (IPOX). In the indirect partial oxidation

process, water addition is needed to sustain steam reforming and water-gas shift reactions, since water produced by total oxidation is not sufficient for this purpose (Rostrup-Nielsen, 1998). Besides, for temperature control of catalyst bed and to minimize the coke formation during steam reforming reaction, extra water has to be added into the system (Avcı *et al.*, 2001b; Trimm, 1999). The process is called autothermal reforming (ATR) when extra water is integrated to the system. The carbon monoxide and carbon dioxide in the product gas stream can be removed by various techniques such as water-gas shift reaction, carbon dioxide absorption, methanation and preferential oxidation (Ahmed and Krumpelt, 2001).

Another route for hydrogen production is the direct partial oxidation method in which methane is oxidized to give a mixture of carbon monoxide and hydrogen in a single step (Hickman and Schmidt, 1993; Trimm and Önsan, 2001):

$$CH_4 + \tfrac{1}{2}O_2 \longrightarrow CO + 2H_2, \qquad \Delta H^{o}_{298} = -35.7 \text{ kJ/mol} \qquad (2.6)$$

Direct partial oxidation process is thermodynamically favored at high temperatures, around 1023 K and at short residence times between 10^{-4} and 10^{-2} s (Hickman and Schmidt, 1992; Pena *et al.*, 1996). In case of longer residence times the process may turn into indirect partial oxidation or may even result in carbon dioxide reforming (Trimm and Önsan, 2001):

$$CH_4 + CO_2 \longrightarrow 2CO + 2H_2, \qquad \Delta H^{o}_{298} = -247 \text{ kJ/mol} \qquad (2.7)$$

Basic hydrogen production processes, steam-reforming, indirect partial oxidation method which is combination of steam reforming, water-gas shift and total oxidation reaction, and direct partial oxidation process are investigated in depth in following sections.

Among fuel conversion processes mentioned above, direct partial oxidation and autothermal reforming seem to be more attractive than others although steam reforming itself gives the highest hydrogen production per unit amount of fuel converted. Compared with others, ATR and direct partial oxidation processes have superiorities: they have relatively short response times to changes in the application of interest, e.g. in vehicular

applications and can be designed more compactly in hardware, i.e. requires smaller reactor volumes (Ahmed and Krumpelt, 2001). When compared to direct partial oxidation method, ATR is reported to have similar carbon monoxide and hydrogen selectivities and the latter route has also the ease of operation and control (Avcı *et al.*, 2001a). Therefore, ATR is considered as the fuel-processing route for hydrogen production in this work.

2.3. Total Oxidation of Methane

Steam reforming reaction is an endothermic reaction and necessary heat input can be supplied in several ways. Electric heaters could be considered as heaters; however, due to its high cost and low overall efficiency, other options should be investigated (Trimm and Önsan, 2001; Rakass *et al.*, 2006; Karakaya, 2006). Total oxidation is a possible way to generate necessary heat for endothermic steam reforming reaction (Trimm and Önsan, 2001):

$$CH_4 + 2O_2 \longrightarrow CO_2 + 2H_2O, \quad \Delta H^{o}_{298} = -802 \text{ kJ/mol} \qquad (2.5)$$

Indirect partial oxidation is a combination of total oxidation and steam reforming reactions and is an autothermal, self-sustaining reaction, i.e. heat released by exothermic total oxidation reaction is utilized by endothermic steam reforming reaction (Trimm and Önsan, 2001). However, total oxidation reaction needs high temperatures to initiate which changes with the hydrocarbon fuel-to-oxygen ratio in the feed. For example, methane is reported to initiate to oxidize at 623 K for methane-to-oxygen ratio of 2.53 over $Pt/\delta\text{-}Al_2O_3$ catalyst (Ma *et al.*, 1996). Therefore surrounding room temperature may not be enough for most hydrocarbons and pre-heating is usually necessary for this purpose (Trimm and Önsan, 2001). This can be achieved by energy integration in fuel processor system by heat exchangers to heat the feed stream (Avcı *et al.*, 2001a; Avcı *et al.*, 2002) or by oxidizing methanol and hydrogen which are reported to have oxidized at room temperature over a precious metal catalyst such as platinum (Ma *et al.*, 1996; Jiang, 1992; Jiang *et al.*, 1995).

2.3.1. Catalysts

Precious metal catalysts such as platinum, palladium and rhodium are reported for combustion of hydrocarbons since their stability at high temperatures is suitable for total oxidation conditions of hydrocarbons (Trimm, 1983; Ma *et al.*, 1996; Burch *et al.*, 1999). Moreover, the effect of support material on the catalytic performance of methane combustion for platinum, palladium and rhodium catalysts has been investigated: Rh supported on ZrO_2, Ce-ZrO_2 and α-Al_2O_3 is investigated by Eriksson and co-workers (2006), palladium catalyst was studied by using a series of metal oxides as the support by Yoshida *et al.* (2007). Also, catalytic performance of bimetallic palladium-platinum catalyst is investigated for methane combustion (Persson *et al.*, 2006).

An important parameter in total oxidation of light hydrocarbons is the light-off temperature. This temperature is defined as the point at which approximately 10 per cent of the hydrocarbon is oxidized and is the starting point of the activity of the oxidation catalyst (Trimm and Lam, 1980; Avcı *et al.*, 2002). Figure 2.2 shows experimentally measured hydrocarbon conversion versus inlet temperature curves for methane, ethane and propane at a hydrocarbon/oxygen ratio of 0.9 over platinum based catalyst Pt/δ-Al_2O_3 (Ma *et al.*, 1996). It can also be seen from the graph that at ca. 10 per cent hydrocarbon conversion, i.e. at light-off temperature, oxidation of hydrocarbons begins and also, as the length of the carbon chain and hydrocarbon conversion increase, light-off temperature decreases and reactivity increases.

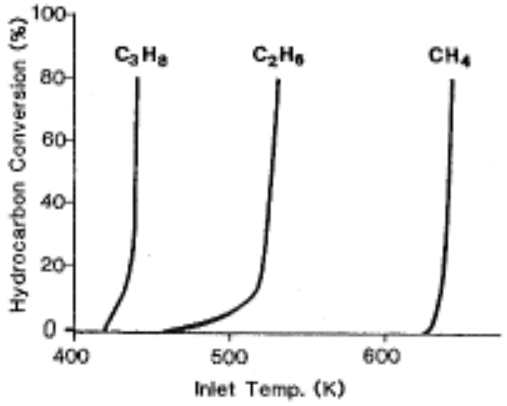

Figure 2.2. Hydrocarbon conversion vs. inlet temperature for methane, ethane and propane at a hydrocarbon/oxygen ratio of 0.9 over Pt/δ-Al_2O_3 (Ma *et al.*, 1996)

Palladium-based catalysts have the lowest light-off temperature of methane oxidation (Burch *et al.*, 1999; Ciuparu and Pfefferle, 2001); platinum-based (Ma *et al.*, 1996; Veser and Schmidt, 1996) and rhodium-based (Burch *et al.*, 1999) catalysts are also being utilized. They could also be classified in the order palladium-based > platinum-based > rhodium-based on the basis of their activity (Aryafar and Zaera, 1997).

Light-off temperature of a hydrocarbon depends strongly on hydrocarbon/oxygen ratio. Table 2.3 shows the results of Ma *et al.* (1996) that indicates variation of light-off temperatures of methane oxidation over $Pt/\delta\text{-}Al_2O_3$ at different methane-to-oxygen ratios. Veser and Schmidt (1996) mention about amount of methane at inlet and inform that light-off temperature of platinum-based catalysts decreases as methane inlet composition increases. Light-off temperature is an important concept for design and operation of oxidation systems; therefore needs certain comprehension for process safety and regular operation (Bui *et al.*, 1997).

Table 2.3. Light-off temperatures of methane oxidation at different CH_4/O_2 ratios (Ma *et al.*, 1996)

CH_4/O_2	Light-off Temperature (K)
0.27	724
0.9	641
2.53	623
5.04	589

2.3.2. Kinetics of Methane Oxidation

Several studies about the kinetics of oxidation of hydrocarbons can be found in the literature, which suggest different rate expressions in the form of Langmuir-Hinshelwood (Trimm and Lam, 1980; Ma *et al.*, 1996) and Power-Law (Ma, 1995; Opoku-Gyamfi and Adesina, 1999) types, proposed for certain ranges of operating conditions and catalysts.

Langmuir-Hinshelwood and power-law type rate expressions describing methane oxidation over Pt-based catalysts are presented in Table 2.4 (Trimm and Lam, 1980; Ma, 1995, Ma *et al.*, 1996). Rate expressions reported by Trimm and Lam (1980) are Langmuir-Hinshelwood type, in which first term is based on the reaction between molecularly adsorbed methane and oxygen, whereas the second term demonstrates the Elay-Rideal mechanism between molecularly adsorbed methane and oxygen in the gas phase.

Table 2.4. Rate equations for total oxidation of methane for Pt-based catalysts

Catalyst	Rate Equation	Reference
Pt/Al_2O_3	$-r_{TOX} = \frac{k_{TOXa} P_{CH_4} P_{O_2}^{0.5}}{1 + K_{CH_4}^c P_{O_2}^{0.5}} + \frac{k_{TOXb} P_{CH_4} P_{O_2}}{1 + K_{CH_4}^c P_{O_2}}$ (2.8)	Trimm and Lam, 1980
Pt/Al_2O_3	$-r_{TOX} = \frac{k_{TOXa} P_{CH_4} P_{O_2}}{(1 + K_{CH_4}^c P_{CH_4} + K_{O_2}^c P_{O_2})^2} + \frac{k_{TOXb} P_{CH_4} P_{O_2}}{(1 + K_{CH_4}^c P_{CH\,4} + K_{O_2}^c P_{O_2})}$ (2.9)	Trimm and Lam, 1980
$Pt/\delta\text{-}Al_2O_3$	$-r_{TOX} = \frac{k_{TOX} K_{CH_4}^c P_{CH_4} \sqrt{K_{O_2}^c P_{O_2}}}{(1 + K_{CH_4}^c P_{CH_4} + \sqrt{K_{O_2}^c P_{O_2}})^2}$ (2.10)	Ma *et al.*, 1996
$Pt/\delta\text{-}Al_2O_3$	$-r_{TOX} = 1.57*10^5 * \exp\left(\frac{-21068}{1.987*T}\right) * (P_{CH_4})^{0.95} * (P_{O_2})^{-0.17}$ (2.11)	Ma, 1995

In Table 2.4, k_{TOX} is reaction rate constant for methane oxidation (Reaction 2.5) and is described with an Arrhenius-type relationship:

$$k_i = k_{0,i} \exp\left(\frac{-E_i}{RT}\right) \tag{2.12}$$

where *i* is the reaction index.

$K^c_{CH_4}$ and $K^c_{O_2}$ are oxidation adsorption constants for methane and oxygen, respectively. Temperature dependency of these coefficients is estimated by using van't-Hoff equation:

$$K_j = K_{0,j} \exp\left(\frac{-\Delta H_j}{RT}\right) \tag{2.13}$$

where *j* is the component index.

2.4. Steam Reforming of Methane

Steam reforming of hydrocarbons is a well-established process that is currently used in hydrogen production at industrial scale (Twigg, 1989; Armor, 1999). Hydrogen needed to drive PEM fuel cells is produced by steam reforming of hydrocarbons, as part of the ATR mechanism as mentioned in Section 2.2.2, in on-board fuel conversion systems.

Hydrocarbons are converted to carbon monoxide and carbon dioxide directly by two generic reactions:

$$C_nH_m + nH_2O \longrightarrow nCO + (½m+n)H_2, \tag{2.3}$$

$$C_nH_m + (2n)H_2O \longleftrightarrow nCO_2 + (½m+2n)H_2 \tag{2.14}$$

For steam reforming of methane, the reaction is as follows:

$$CH_4 + H_2O \longleftrightarrow CO + 3H_2, \qquad \Delta H^{o}_{298} = 206.2 \text{ kj/mol} \tag{2.15}$$

An important side reaction, water-gas shift (WGS), runs simultaneously with the steam reforming reactions (Reactions (2.3) and (2.14)) and affects the product composition. In water-gas shift reaction, carbon monoxide treated with steam is converted to carbon dioxide and hydrogen:

$$CO + H_2O \longleftrightarrow CO_2 + H_2, \qquad \Delta H^{o}_{298} = -41.2 \text{ kJ/mol} \tag{2.4}$$

Steam reforming is an endothermic reaction and thermodynamically favored at high temperatures. Considerable energy requirement of the steam reforming reaction is one of the major difficulties of the process. External heaters and burners are reported as usable equipments for heat transfer to catalyst bed during reaction (Rakass *et al.*, 2006). It is also reported that heat transfer is the most important factor that determines the product distribution and reactor performance (Kvamsdal *et al.*, 1999).

Steam requirement is another difficulty for the operation since steam reforming reaction takes place at high temperatures -typically above 1070 K- and at high temperature steam activates the catalyst sintering.

2.4.1. Catalysts

Ni-based catalysts are currently being used in the conventional steam-reforming processes since, compared with the precious metal catalysts such as Rh-based ones, they are cheap but still offer sufficient activity (Twigg, 1989; Rostrup-Nielsen, 1984; Trimm and Önsan, 2001).

Coke formation is the most important difficulty which has to be overcome during steam reforming reactions. In order to minimize catalyst coking, steam to carbon ratio (Equation 2.16) should have a minimum value of ca. 2.5 (Rostrup-Nielsen, 1984; Trimm and Önsan, 2001). In an indirect partial oxidation operation which is a combination of total oxidation and steam reforming reactions, steam-to-carbon ratio is defined as follows (Avcı *et al.*, 2002):

$$steam/carbon\ ratio = \frac{moles\ of\ \ water\ \ fed + moles\ of\ \ water\ \ produced\ by\ TOX}{moles\ of\ \ methane\ \ fed - moles\ of\ \ methane\ consumed\ in\ TOX} \quad (2.16)$$

It is reported that coke formation is much less on Rh and Ru (Rostrup-Nielsen, 1984); however, their high cost makes it difficult for commercial use. The specific activities of several metals doped on alumina or magnesia are reported to be in the order of Rh, Ru > Ni, Pd, Pt > Re > Co (Rostrup-Nielsen, 1973).

Supports used for Ni-based catalysts have also been investigated to minimize coke formation in recent studies. Ross (1974) reported that magnesia or potassia, both of which are alkaline components, eliminates coke formation. In addition, Trimm (1999) reported that ceria support can reduce coke formation. Bradford and Vannice (1996) arranges Ni-based catalysts according to their activity in the order of Ni/TiO_2 > Ni/C > Ni/SiO_2 > Ni/MgO. A comprehensive summary about coke formation during steam reforming is available in the literature (Rostrup-Nielsen, 1998; Ma, 1995).

2.4.2. Kinetics of Methane Steam Reforming

There are many investigations about methane steam reforming kinetics in the literature (Rostrup-Nielsen, 1984; Xu and Froment, 1989; Elnashaie *et al.*, 1990; Ma, 1995; Numaguchi and Kikuchi, 1988). The main difference in these kinetic studies and, hence the observed rate expressions, is the order of steam partial pressure, which can have positive, negative or zero values. This difference is reported to be because of non-monotonic behavior of partial pressure of steam on the reaction mechanism (Elnashaie *et al.*, 1990).

Xu and Froment (1989) reported Langmuir-Hinshelwood type rate equations which are determined using elementary-step kinetic model proposal. They also reported rate expressions for water-gas shift side reaction. The rate expressions for methane steam reforming and water-gas shift which are derived for the $Ni/MgAl_2O_4$ catalyst, are given in Table 2.5 and Table 2.6, respectively.

Numaguchi and Kikuchi (1988) have also proposed a kinetic model for methane steam reforming and water-gas shift reactions run over Ni/Al_2O_3 catalyst. In their kinetic model, they considered surface reaction as the rate-determining step. The resulting rate laws are of Langmuir-Hinshelwood type, which are given in Table 2.5 and Table 2.6 for steam reforming and water-gas shift, respectively. They reported rate equation for methane steam reforming towards formation of carbon monoxide, thus the parallel reaction, i.e. steam reforming of methane towards carbon dioxide is not taken into account (Numaguchi and Kikuchi, 1988). Ma (1995) also recommended a rate expression for methane steam reforming which is also given in Table 2.5.

Table 2.5. Rate equations for steam reforming of methane

Rate Equation	Reference
$-r_{SR} = \frac{k_{SR}/P_{H_2}^{2.5}(P_{CH_4}P_{H_2O} - P_{H_2}^3 P_{CO}/K_{eq}^{SR})}{(1+K_{CO}P_{CO}+K_{H_2}P_{H_2}+K_{CH_4}P_{CH_4}+K_{H_2O}P_{H_2O}/P_{H_2})^2}$ (2.17)	Xu and Froment (1989)
$-r_{SR} = \frac{k_{SR}(P_{CH_4} - P_{H_2}^3 P_{CO}/K_{eq}^{SR})}{P_{CH_4}^{\alpha_2} P_{H_2O}^{\beta_2}}$ (2.18)	Numaguchi and Kikuchi (1988)
$-r_{SR} = \frac{k_{SR}K_{CH_4}K_{H_2O}P_{CH_4}P_{H_2O}}{P_{H_2}^{1.5}(1+K_{CH_4}\frac{P_{CH_4}}{P_{H_2}^{0.5}}+K_{H_2O}\frac{P_{H_2O}}{P_{H_2}})^2}$ (2.19)	Ma (1995)

Table 2.6. Rate equations for water-gas shift side reaction

Rate Equation	Reference
$-r_{WGS1} = \frac{k_{WGS1}/P_{H_2}(P_{CO}P_{H_2O} - P_{H_2}P_{CO2}/K_{eq}^{WGS1})}{(1+K_{CO}P_{CO}+K_{H_2}P_{H_2}+K_{CH_4}P_{CH_4}+K_{H_2O}P_{H_2O}/P_{H_2})^2}$ (2.20)	Xu and Froment (1989)
$-r_{WGS1} = \frac{k_{WGS1}(P_{CO} - P_{H_2}P_{CO_2}/K_{eq}^{WGS1})}{P_{CH_4}^{\alpha_3} P_{H_2O}^{\beta_3}}$ (2.21)	Numaguchi and Kikuchi (1988)

k_i is the reaction rate constant for reaction *i* and K_j is adsorption constant for species *j* in all reaction rate expressions. Arrhenius equation (2.12) and van't-Hoff equation (2.13) are used to determine the temperature dependencies of these coefficients. K_{eq}^i is the equilibrium constant for reaction *i*. All parameters in equations (2.12) and (2.13) are given in Table 2.7.

Table 2.7. Parameters of k_i and K_j in Equations (2.17) and (2.20)

(Xu and Froment, 1989)

Reaction	$k_{0,i}$ (mol kgcat^{-1} s^{-1})	E_i (kJ kmol^{-1})
(2.15)	1.17 x 10^{15} bar$^{-0.5}$	240,100
(2.4)	5.43 x 10^{5} bar^{-1}	67,130

Species	$K_{0,j}$ (bar^{-1})	ΔH_j (kJ kmol^{-1})	Equilibrium Constants
CH_4	6.65 x 10^{-4}	- 38,280	$K_{eq}^{SR} = 4.707\times10^{12}\exp\left(\frac{-224{,}000}{RT}\right)\ bar^2$
H_2O	1.77 x 10^{5}	88,680	
CO	8.23 x 10^{-5}	- 70,650	$K_{eq}^{WGS1} = 1.142\times10^{-2}\exp\left(\frac{-37{,}300}{RT}\right)$
H_2	6.12 x 10^{-9}	- 82,900	

Power-law rate expressions have also been proposed to describe the methane steam reforming (Rostrup-Nielsen, 1984; Ma, 1995). Rate law parameters for steam reforming of methane and referred catalysts are given in Table 2.8.

Catalysts that are used in experiments by Xu and Froment (1989) and Numaguchi and Kikuchi (1988) differ from each other; both are Ni-based catalysts, but supporting materials are different. The catalyst properties are shown in Table 2.9. Metal surface areas are nearly identical; however, a nickel content of catalysts differs from each other.

Table 2.9. Catalyst properties

	Xu and Froment (1989)	Numagchi and Kikuchi (1988)
Catalyst	$Ni/MgAl_2O_4$	Ni/Al_2O_3
Metal Content (wt per cent)	15.2	8.7
Metal Surface Area (m^2/g)	4.1	3.6
Density (kg/m^3)	1,870	1,970

Table 2.8. Power-law rate equation parameters for methane steam reforming

Reference	Hydrocarbon	Catalyst	Temp. Range (K)	Pressure (MPa)	Orders			E_{SR} (kJ/mol)
					CH_4	H_2O	H_2	
Rostrup-Nielsen (1984)	CH_4	Ni/MgO	723-823	0.1	1	-	-	110
Ma (1995)	CH_4	Ni/MgO	623-673	0.1	0.96	-0.17	0.25	60

2.5. Partial Oxidation Process

As mentioned before, catalytic steam reforming of hydrocarbons is well-known route for hydrogen production that gives offers highest hydrogen concentration (Ming *et al.*, 2002; Heinzel *et al.*, 2002). However, due to its high endothermicity, steam reforming requires high energy input and elevated operating temperatures, and, therefore, it seems not to be suitable for use in on-board fuel cell applications. On the other hand, partial oxidation of hydrocarbons, once started, is energetically self sustaining, it is much faster than steam-reforming and it can run over smaller amounts of catalyst and within smaller reactor volumes. Due to these advantages, partial oxidation seems to be the promising fuel processing route for hydrogen production from hydrocarbons for driving hydrogen fuel cells.

Partial oxidation of hydrocarbons is known to occur by two major mechanisms:

- Direct Partial Oxidation, which involves hydrocarbon conversion to synthesis gas – a mixture of carbon monoxide and hydrogen – in a single step

- Indirect Partial Oxidation, which involves the coupling of total oxidation and steam reforming reactions.

2.5.1. Direct Partial Oxidation

In direct partial oxidation, hydrocarbons are converted to a mixture of carbon monoxide and hydrogen in a single step reaction (Trimm and Önsan, 2001; Hickman and Schmidt, 1993). This reaction is given for methane as follows:

$$CH_4 + \tfrac{1}{2}O_2 \longrightarrow CO + 2H_2, \qquad \Delta H^{o}_{298} = -35.7 \text{ kJ/mol} \qquad (2.6)$$

Direct partial oxidation produce synthesis gas at advantageous CO/H_2 ratios for use in processes. However, carbon monoxide-to-hydrogen ratio of 2 is less than optimal for fuel cell applications in which maximal hydrogen and reduced carbon monoxide concentration are desired (Trimm and Önsan, 2001).

Direct partial oxidation of hydrocarbons has been investigated on different types of catalysts such as platinum group metals Pt, Pd, Rh on alumina, ceria, titania supports and on NiO-MgO. Schmidt and co-workers have studied the partial oxidation of various hydrocarbons such as methane, n-hexane, cyclohexane, isooctane and decane (Hickman and Schmidt, 1993; Bharadwaj and Schmidt, 1995; Hickman and Schmidt, 1992; Schmidt *et al.*, 2003; Bodke *et al.*, 1998; Dietz *et al.*, 1998). In these studies, it has been reported that high CH_4 conversions close to 100 per cent and high selectivities (greater ~90 per cent) to hydrogen was achieved on Rh-coated monoliths at very low contact times (~5 ms) at ~ 1270 K and at near stoichiometric hydrocarbon-to-oxygen feed ratios, without any carbon formation over the catalysts.

Direct partial oxidation of methane has received interest by different researchers. Choudhary and coworkers have studied methane direct partial oxidation on nickel-based catalyst such as $Ni/AlPO_4$ (Choudhary *et al.*, 1997; Choudary *et al.*, 1998a; Choudary *et al.*, 1998b). They observed high selectivity to H_2 around 95 per cent and activities, i.e. methane conversions around 90 per cent at temperatures around 1073 K. Jin *et al.* (2000) reported investigation about the direct partial oxidation of methane on Ni/Al_2O_3. Ru/TiO_2 is another catalyst that has been investigated for its possible use in direct partial oxidation of methane at lower temperatures (Boucouvalas *et al.*, 1996).

Direct partial oxidation, which allows use of small size reactors, is compatible with instant changes in feed conditions and offers coke-free operation. Such advantages make direct partial oxidation process a promising technology for on-board hydrogen production in mobile applications. However, high operating temperatures, millisecond-level contact times and near-explosive feed and operating conditions are the challenges that limit the practical use of this conversion route (Trimm and Önsan, 2001).

2.5.2. Indirect Partial Oxidation

Although steam reforming offers the highest hydrogen yield among other conversion routes, it suffers from the need of high temperatures. Thus, considerable heat must be given to the reaction system, which can be supplied either by external means or by combusting the part of reactants. The concept of combustion of part of the fuel has

received attention in many practices and applications. Indirect partial oxidation (IPOX) is basically based on the same concept; it is the combination of exothermic total oxidation and endothermic steam reforming, and heat needed to drive the latter reaction is generated by combusting part of the fuel by the former reaction (Ma, 1995; Ma and Trimm, 1996; Ma *et al.*, 1996). External heat supply is therefore not necessary once the process is triggered and become self-sustaining. The concept of indirect partial oxidation has commercial applications such as the Johnson Matthey Hot Spot^{TM} reactors (Golunski, 1998).

In indirect partial oxidation operation, various types of fuels such as natural gas (simulated by methane), LPG (liquefied petroleum gas), gasoline, methanol, ethanol and diesel may be considered their conversion to a hydrogen-rich stream (Trimm and Önsan, 2001). However, except in the case of methanol, conversion of hydrocarbons cannot be initiated at room temperature and they have to heated up to the light-off temperatures for conversion (Ma, 1995; Ma and Trimm, 1996). Ma (1995) has suggested a solution for this purpose in which hydrocarbons can reach to their light-off temperatures by the heat generated by methanol or by hydrogen combustion, both of which can be initiated at room temperatures.

Coke formation is a phenomenon that is possible and needs careful control within indirect partial oxidation. External water injection into the reaction system can help in gasifying the coke deposited over the catalysts. Water injection is also needed for temperature control of catalyst bed and for meeting the water demand for steam reforming reaction, as mentioned formerly (Avcı *et al.*, 2002). Coke formation over nickel-based catalysts can be minimized by keeping the steam-to-carbon ratio (defined in Equation (2.16)) around 2.5 (Rostrup-Nielsen, 1984).

Pt and Ni-based catalysts are used in total oxidation and steam reforming of methane respectively, as mentioned in Sections 2.3 and 2.4, and extensively studied in depth by many researches (Ma, 1995, Ma and Trimm, 1996). Various configurations of these catalysts are experimented for indirect partial oxidation of methane. These configurations are named as dual-bed, mixed-bed and uniform-bed (bimetallic). In the dual-bed system, Pt-based total oxidation catalyst is placed upstream and Ni-based steam reforming catalyst is placed downstream of a tubular reactor. In such a system, total

oxidation and steam reforming is assumed to occur consecutively where the steam reforming is thought to be triggered by the heat released by total oxidation reaction. The mixed-bed system corresponds to a physical mixture of two catalysts where the total oxidation and steam reforming is believed to take place simultaneously. In the uniform-bed configuration, both reactions occur over a bifunctional catalyst having Pt and Ni metals on the same support. Investigations on these catalyst bed configurations came up with different hydrogen production efficiencies which can be considered as hydrogen produced per unit of hydrocarbon fuel (Trimm and Önsan, 2001). Trimm and Önsan (2001) have experimented three configurations with the carbon:oxygen ratio of 1.55 at the inlet and steam:carbon ratio of 2.34, and reported a graph that compares relative hydrogen production efficiencies of various bed configurations, which is presented in Figure 2.3.

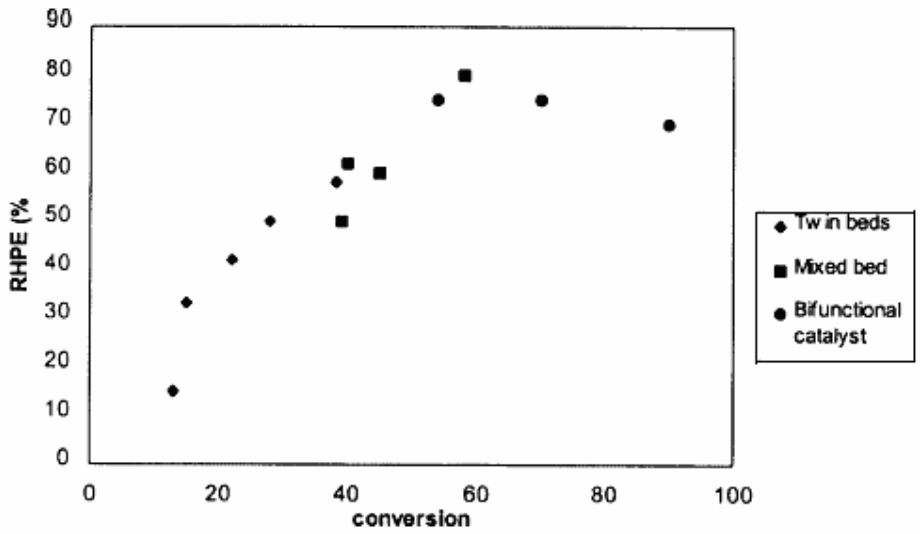

Figure 2.3. Comparison of relative hydrogen production efficiencies obtained over different catalyst bed configurations. Feed conditions: carbon:oxygen=1.55, steam:carbon=2.34 (Trimm and Önsan, 2001)

The bifunctional catalyst is reported to give the optimal performance, with methane conversion of up to 92 per cent and hydrogen production efficiencies of ~80 per cent at an operation temperature of 903 K. Similar results also obtained by Ma and Trimm (1996), optimal performance is reported for bimetallic catalyst with 60-65 per cent conversion of methane and 80-85 per cent selectivity to hydrogen.

2.6. Water-gas Shift Reaction

The water-gas shift reaction (WGS)

$$CO + H_2O \longleftrightarrow CO_2 + H_2, \qquad \Delta H^{o}_{298} = -41.2 \text{ kJ/mol} \qquad (2.4)$$

is an industrially important reaction since it is one of the steps in overall process of hydrogen production from natural gas, LPG and oil for ammonia synthesis and other important industrial processes such as hydro treating of petroleum stocks and refining heavy oil (Choi and Stenger, 2003; Saito *et al.*, 2003).

In recent years, there has been a renewed interest on water-gas shift reaction due to its important roles in fuel processing systems for hydrogen fuel cells, especially for PEMFC (Sun *et al.*, 2005; Saito *et al.*, 2003).

The moderately exothermic water-gas shift reaction can be carried out at two different temperatures:

- High-temperature shift (HTS) taking place between 623 and 673 K
- Low-temperature shift (LTS) taking place between 453 and 523 K

Majority of carbon monoxide is converted to hydrogen by HTS and LTS after which the CO level is reduced down to approximately 7,000 ppm (Sun *et al.*, 2005) or ~2 mol per cent (Avcı *et al.*, 2002). It is reported that in many processes, WGS is considered as secondary hydrogen producer and the primary CO clean-up system (Kamarudin *et al.*, 2004). Moreover, water-gas shift reaction is reported as a preferable reaction than the oxidation for carbon-monoxide removal due to a lower calorific value and regarded as a CO removal process for reformed gas before the preferential oxidation of CO (Utaka *et al.*, 2000). Furthermore, Sekizawa *et al.* (1998) studied CO removal carried out over Cu-supported oxide catalysts such as Cu/Al_2O_3-ZnO by coupled water-gas shift and CO oxidation in the presence of large amount of H_2O and H_2. They investigated the effects of addition of small amount of O_2 to the gas mixture and found that it is effective in

promoting CO removal by WGS since it enhance the CO removal through oxidation in coupled WGS and CO oxidation reaction.

2.6.1. Catalysts

In most fuel processor systems, the water-gas shift reactor is reported to be the biggest and heaviest component due to relatively slow reaction kinetics and is inhibited at higher temperatures by thermodynamics (Choi and Stenger, 2003). Therefore, the size of the water-gas shift reactor has to be reduced to the acceptable limits for fuel processor system economics which is possible by the use of high performance catalysts such as $Cu/ZnO/ZrO_2/Al_2O_3$ (Saito *et al.*, 2003).

Iron-based and copper-based catalysts are used on commercial basis to run high-temperature (623 K-673 K) (HTS) and low-temperature (453 K-523 K) (LTS) water-gas shift reactions on industrial scale, respectively (Amadeo and Laborde, 1995). The copper-based LTS catalysts are reported to have good activities at low temperatures around 480-500 K. Moreover, high selectivity to carbon monoxide and fewer side reactions at high temperatures are reported as extra advantages of these catalysts (Amadeo and Laborde, 1995). In recent studies, authors have tried to improve the activity of copper-based catalysts for water-gas shift reaction. Saito *et al.* (2003) investigated the effects of pretreatment of Cu/ZnO-based catalysts such as calcination temperature and treatment in H_2 at high temperatures to improve the activity of LTS catalysts. Consequently, Saito *et al.* (2003) expressed that activity of the catalyst could be correlated mainly to the Cu surface area of the catalyst.

Sun *et al.* (2005) demonstrated that in comparison with the conventional Cu/ZnO catalyst, noble metal catalysts have the advantage of high activity; Au, Pd and Pt are reported to offer high activities up to 95 per cent CO conversion in a wide temperature range for WGS reaction (Lian *et al.*, 2006). Different support materials such as CeO_2 (Andreeva *et al.*, 2002; Zhao *et al.*, 2004), Fe_2O_3 (Tabakova *et al.*, 2000; Boccuzzi *et al.*, 1999) and TiO_2 (Idakiev *et al.*, 2004; Panagiotopoulou and Kondarides, 2004) for use in gold-based catalysts have also been explored. In the studies of Andreeva *et al.* (2002), Au/Fe_2O_3 catalyst is shown to have high catalytic activity for LTS because of the specific

interaction between gold and the ferric oxide support. It is also reported that Au/ZnO may be an active catalyst for low-temperature WGS reaction, though; its catalytic activity is lower than those of Au/Fe_2O_3 and Au/ZrO_2 (Tabakova *et al.*, 2000).

Lei *et al.* (2005) have investigated the effect of promotion of Fe_3O_4-Cr_2O_3 by precious metals and found that rhodium doped Fe_3O_4-Cr_2O_3 to be greatly effective on reactivity of carbon monoxide. Moreover, Radhakrishnan *et al.* (2006) have made investigations on rhenium promotion of ceria-zirconia supported platinum catalysts and found that they enhanced the WGS activity.

2.6.2. Kinetics of Water-gas Shift Reaction

There are numerous studies reported about the kinetics and mechanisms of low-temperature water-gas shift reaction. Despite this large number of investigations, there are still controversies and disagreements on the kinetics and mechanism of WGS. Two kinetic mechanisms are proposed for water-gas shift reaction: the “adsorptive mechanism” and the “regenerative mechanism” (Choi and Stenger, 2003). The regenerative-the surface redox mechanism is based on the adsorption and dissociation of water on the catalytic surface (Amadeo and Laborde, 1995), while in the adsorptive mechanism, CO and H_2O adsorb on the catalyst surface and form an intermediate which results in desorbed H_2 and CO_2 (Choi and Stenger, 2003).

Various rate expressions can be derived from the two mechanisms (Choi and Stenger, 2003). Many research groups have investigated adsorptive mechanism and redox mechanism to derive rate expressions for water-gas shift reaction during past fifty years (Choi and Stenger, 2003). Unlike the rate expressions derived from detailed mechanisms, there are also empirical, power-law type rate expressions which are found to be sufficient for most reactor design studies (Keiski *et al.*, 1993, Choi and Stenger, 2003, Lei *et al.*, 2005).

Amadeo and Laborde (1995) studied five different models that describe five different rate expressions for water-gas shift reaction on $Cu/ZnO/Al_2O_3$ between 453 and

503 K. Models I and II represent a redox mechanism, while models III-V are Langmuir-Hinshelwood type. These models are represented in Table 2.10.

It is reported that among five models, model III presents the best fit with the experimental data. In this model, adsorption constant of each species are taken into account (Amadeo and Laborde, 1995). Heats of adsorption and apparent activation energy of model III are shown in Table 2.11. Specific reaction rate and adsorption constant of species are calculated by Arrhenius Equation (2.12) and van't-Hoff Equation (2.13), respectively.

Table 2.10. Five models describing rate expressions (Amadeo and Laborde, 1995)

Model I	$r_{WGS2} = \frac{k_{WGS2} P_{H_2O}(1-\beta)}{A P_{H_2O} + P_{CO}}$	(2.22)
Model II	$r_{WGS2} = \frac{k_1 k_2 P_{CO} P_{H_2O}(1-\beta)}{k_1 P_{CO} + k_2 P_{H_2O} + k_3 P_{CO_2}}$	(2.23)
Model III	$r_{WGS2} = \frac{k_{WGS2} P_{CO} P_{H_2O}(1-\beta)}{1+\sum K_i P_i}$	(2.24)
Model IV	$r_{WGS2} = \frac{k_{WGS2} P_{CO}(1-\beta)}{(1+K_{H_2CO_2} P_{H_2} P_{CO_2} P_{H_2O}^{-1} + K_{H_2} P_{H_2} + K_{H_2O} P_{H_2O} + K_{CO_2} P_{CO_2}}$	(2.25)
Model V	$r_{WGS2} = \frac{k_{WGS2} P_{CO} P_{H_2O}(1-\beta)}{1+K_{CO_2} P_{CO_2} + K_{H_2} P_{H_2}}$	(2.26)

where $\beta = P_{CO_2} P_{H_2} / (P_{CO} P_{H_2O} K_e)$

Table 2.11. Adsorption heats and apparent activation energies of model III (Amadeo and Laborde, 1995)

	CO	CO_2	H_2O	H_2
ΔH_j (kJ mol^{-1})	-0.91	-24.72	-1.42	-14.4
$K_{0,j}$ (atm^{-1})	2.21	0.0047	0.40	0.052
E_{WGS2} (kJ $kmol^{-1}$) : 4,080			$k_{0,WGS2}$ (mol $gcat^{-1}$ s^{-1} atm^{-1}) : 0.92	

Choi and Stenger (2003) offered an empirical power-law rate expression derived from numerical fitting for water-gas shift reaction between 393 and 523 K occurring over $Cu/ZnO/Al_2O_3$ catalyst:

$$r_{WGS2} = 2.96x10^5 \exp\left(-\frac{47{,}400}{RT}\right)\left(P_{CO}P_{H_2O} - \frac{P_{CO_2}P_{H_2}}{K_{eq}^{WGS2}}\right) \quad (2.27)$$

Also, a comparison of activation energies and frequency factors with other empirical power-law rate equations derived from different catalysts are given in Table 2.12 (Choi and Stenger, 2003).

Table 2.12. Parameter comparison for empirical expressions (Choi and Stenger, 2003)

$$r_{WGS2} = k_{0,WGS2}\exp(-E_{WGS2}/RT)P_{CO}^m P_{H_2O}^n(1-\beta)$$

Catalyst	*m*	*n*	$\ln k_{0,WGS2}$	E_{WGS2} (kJ kmol^{-1})
ICI-$Cu/ZnO/Al_2O_3$	1	1	15.2	52,800
Cu/Al_2O_3	1	1.9	-	69,300
$Cu/ZnO/Al_2O_3$	0	1	-	41,800
CuO/MnO_2	1	1	-	55,000

Radhakrishnan *et al.* (2006) reported empirically measured rates after kinetic experiments which are modeled by the equation

$$rate = A\times\exp(-E_{WGS2}/RT)\times[CO]^a\times[H_2O]^b\times[CO_2]^c\times[H_2]^d\times(1-\beta) \quad (2.28)$$

where $\beta = ([CO_2]\times[H_2])/(K_{eq}^{WGS2}\times[CO]\times[H_2O])$

Radhakrishnan *et al.* (2006) observed equation (2.28) under LTS conditions and for two types of catalysts which are platinum and platinum-rhenium catalysts. Table 2.13 gives the parameters and comparison of the two catalysts.

Table 2.13. Kinetic parameters for Pt and Pt/Re catalysts between 483-513 K (Radhakrishnan *et al.*, 2006)

Parameter	Pt	Pt/Re
CO order (*a*)	0.07	-0.05
H_2O order (*b*)	0.67	0.85
CO_2 order (*c*)	-0.16	-0.05
H_2 order (*d*)	-0.57	-0.32
E_{WGS2} (kcal mol^{-1})	17	17
A	2.5×10^7	4.5×10^6

2.7. CO Oxidation Reaction

Proton exchange membrane fuel cells require purified hydrogen as fuel. Precious metals such as platinum and nickel are widely used as fuel-cell anodes (Ralph and Hards, 1998). However, these metals could be deactivated by carbon monoxide adsorption at low temperatures (Schmidt *et al.*, 1994). In order to prevent poisoning of the fuel cell electrodes, it is reported that the CO concentration in hydrogen-rich streams should be below 10 ppm (Cheng *et al.*, 2007), which is the tolerable limit of the anodes.

There are various methods for reducing the carbon monoxide level in hydrogen-rich streams for fuel cell applications. Diffusing hydrogen through a Pd/Ag membrane is one of the recommended methods, but this needs fairly high temperatures and pressures, which may not be practical for use in vehicular applications (Trimm and Önsan, 2001). Methanation of carbon monoxide is another route for removal of CO. However, this method causes significant loss in hydrogen and results in the emission of methane which is an unwanted greenhouse effect (Trimm and Önsan, 2001). Among all possible methods, selective oxidation of carbon monoxide seems to be the most plausible option (Choi and Stenger, 2004; Özkara and Aksoylu, 2003; Trimm and Önsan, 2001).

In the selective oxidation of CO (or preferential oxidation of carbon monoxide (PROX)), desired CO oxidation reaction (2.29) is accompanied by the undesired H_2 oxidation reaction (2.30) which causes loss of efficiency of fuel due to hydrogen consumption:

$$CO + ½\ O_2 \longrightarrow CO_2, \quad \Delta H^o_{298} = -283\ kJ/mol \tag{2.29}$$

$$H_2 + ½\ O_2 \longrightarrow H_2O, \quad \Delta H^o_{298} = -242\ kJ/mol \tag{2.30}$$

Hence, selectivity of carbon monoxide, defined in Equation (2.31), needs to be high for preferential oxidation (Chin *et al.*, 2005; Choi and Stenger, 2004):

$$Selectivity\ (\%) = \frac{0.5(n_{CO}^{in} - n_{CO}^{out})}{n_{O_2}^{in} - n_{O_2}^{out}} \times 100 \tag{2.31}$$

In addition, as H_2 may be oxidized by the excess O_2, the amount of oxygen to be injected to the system has to be carefully controlled. Therefore, catalyst that can selectively oxidize CO has to be chosen and stoichiometric amounts of oxygen have to be fed to the PROX system (Trimm and Önsan, 2001).

Trimm and Önsan (2001) presented three obvious possibilities to increase the selectivity of CO in preferential oxidation reaction: an appropriate catalyst that adsorbs CO but not H_2, catalyst on which both CO and H_2 oxidized, but small amounts of H_2 oxidation and preferential CO oxidation is leaded by kinetic parameters and an operation temperature where CO is oxidized but H_2 is not. It is also recommended that in all cases, deterministic oxygen:carbon monoxide ratios and temperature have to be controlled carefully.

2.6.1. Catalysts

Choi and Stenger (2004) classified the PROX catalysts into three categories which are presented in Figure 2.4.

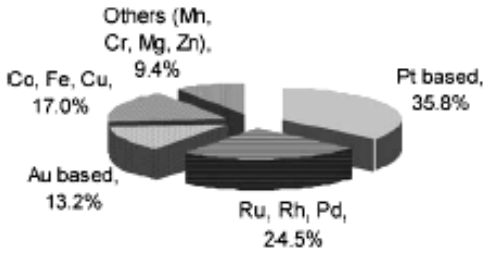

Figure 2.4. Typical formulation of PROX catalysis in 30 recently published papers (Choi and Stenger, 2004)

It can be seen from Figure 2.4 that that the most commonly used PROX catalyst is platinum-based ones which is usually dispersed on alumina. Kahlich *et al.* (1999) reported that the commonly used PROX catalysts (alumina-supported Pt, Ru and Rh) operate at 423-473 K and because of the high temperature operation they lose activity and selectivity. For low temperatures between 353 and 373 K, which is close to PEMFC operation temperature, oxide supported gold catalysts are reported to be the promising alternative and show good performance (Kahlich *et al.*, 1999; Choi and Stenger, 2004). Gold-based catalysts are confirmed to be more active for carbon monoxide oxidation than hydrogen oxidation since they can operate at low temperatures, and are moisture-resistant (Trimm and Önsan, 2001).

In comparison with well-known Pt-based PROX catalysts, Au-based ones demonstrate better activities and selectivities (Kahlich *et al.*, 1999). Gold-based catalysts exhibit different behaviour, depending on the type of support material. A set of investigations show that, among the gold catalysts supported on TiO_2, α-Fe_2O_3, ZrO_2 and Co_3O_4 (Kahlich *et al.*, 1999; Cameron *et al.*, 2003; Haruta *et al.*, 1993; Rossignol *et al.*, 2005; Schumacher *et al.*, 2004), Au/α-Fe_2O_3 gave the best activity and selectivity. Similarly, Pt supported on various materials such as zeolites and TiO_2 are reported to give higher activities and selectivities than Pt/Al_2O_3 did (Watanabe *et al.*, 1997; Schumacher *et al.*, 2004). The method of reduction of the size of platinum particles is also reported to improve the activity and selectivity of the Pt/γ-Al_2O_3 catalyst (Son *et al.*, 2002).

Sedmak *et al.* (2003) studied the selective CO oxidation in excess of H_2 over $Cu_{0.1}Ce_{0.9}O_{2-y}$ nanostructured catalyst and found that this catalyst has the best activity and

selectivity compared to the Pt/γ-Al_2O_3 and Au/α-Fe_2O_3. They also claimed that the catalyst has the price advantage compared to others.

Trimm and Önsan (2001) give an extensive review about the catalysts used in low temperature CO oxidation in H_2 rich gas streams.

It is reported that effects of CO_2 and H_2O is an important issue in the PROX process (Chin *et al.*, 2005). As a result of their experimental study on Au/α-Fe_2O_3, Schubert *et al.* (2004) reported that addition of CO_2 to PROX reduces the rate of CO oxidation and the selectivity, whereas addition of H_2O increases the selectivity.

2.6.3. Kinetics of CO Oxidation Reaction

Several rate equations describing PROX over different catalysts have been reported in the literature (Kahlich *et al.*, 1997; Kahlich *et al.*, 1999; Sedmak *et al.*, 2003). Although there are many studies that report kinetic rate expressions about carbon-monoxide oxidation, only a few of them consider hydrogen oxidation simultaneously with CO oxidation. Some of the studies that consider simultaneous H_2 oxidation with CO oxidation assume constant selectivity for carbon monoxide in PROX reactions at certain temperatures (Lin *et al.*, 2005), whereas some others consider only carbon monoxide oxidation, due to the high CO selectivity (~100 per cent) of the catalyst used (Sedmak *et al.*, 2003).

Kahlich *et al.* (1997) recommended a rate expression for CO oxidation over Pt/γ-Al_2O_3 catalyst for temperature range between 423 and 523 K by introducing a process parameter λ, which is defined as the concentration ratio of oxygen to carbon monoxide:

$$r_{PROX} = k_{PROX} . P_{CO}^{0.4} . \lambda^{0.82} = k_{0,PROX} . \exp(\frac{-E_{PROX}}{RT}) . P_{CO}^{-0.42} . P_{O_2}^{0.82} \qquad (2.32)$$

where $\lambda = \frac{2P_{O_2}}{P_{CO}}$.

Kahlich *et al.* (1999) also studied the selective low temperature oxidation of CO over Au/α-Fe_2O_3 and gave the parameters of the rate equation in comparison with those of observed with Pt/γ-Al_2O_3 catalyst. The parameter comparison is tabulated in Table 2.14.

Table 2.14. Power-law rate constants for Au/ α-Fe_2O_3 and Pt/γ-Al_2O_3 catalyst systems (Kahlich *et al.*, 1999)

System	$k_{0,PROX}$ (mol gcat^{-1} s^{-1})	α_{CO}	α_{O2}	E_{PROX} (kJ kmol^{-1})
Au/α-Fe_2O_3 at 353 K	9.81 x 10^{-4}	0.55	0.27	31,000
Pt/γ-Al_2O_3 at 473 K	13.8 x 10^{-4}	-0.42	0.82	71,000

Sedmak *et al.* (2003) studied the kinetics of CO oxidation over $Cu_{0.1}Ce_{0.9}O_{2-y}$ nanostructured catalyst which they found it to be 100 per cent selective in the temperature range of 318-363 K and considered two models to describe the observed reaction rate. One of the models is Mars and van Krevelen type which is derived on the basis of a redox mechanism:

$$r_{PROX} = \frac{k_{CO} k_{O_2} P_{CO} P_{O_2}^n}{0.5 k_{CO} P_{CO} + k_{O_2} P_{O_2}^n} \tag{2.33}$$

where $k_{CO} = A_{CO}.\exp(-E_{a,CO}/RT)$ and $k_{O_2} = A_{O_2}.\exp(-E_{a,O_2}/RT)$.

Liu and Flytzani-Stephanapoulos model is another kinetic expression that Sedmak *et al.* (2003) evaluated:

$$r_{PROX} = \frac{k_L K_L P_{CO} P_{O_2}^m}{1 + K_L P_{CO}} \tag{2.34}$$

where $k_L = A_L.\exp(-E_{a,L}/RT)$ and $K_L = B_L.\exp(Q/RT)$.

The parameters of the two kinetic model rate expressions calculated by Sedmak *et al.* (2003) are presented in Table 2.15.

Table 2.15. Parameters of the two kinetic models of CO oxidation in H_2-rich stream (Sedmak *et al.*, 2003)

Mars and van Krevelen model		Liu and Flytzani-Stephanapoulos model	
A_{CO} (mol gcat^{-1} s^{-1} bar^{-1})	1.44 x 10^5	A_L (mol gcat^{-1} s^{-1} bar^{-m})	2.64 x 10^3
$E_{a,CO}$ (kJ kmol^{-1})	5.72 x 10^4	$E_{a,L}$ (kJ kmol^{-1})	5.9 x 10^4
A_{O_2} (mol gcat^{-1} s^{-1} bar^{-n})	2.39 x10^3	B_L (bar^{-1})	7.53 x 10^0
E_{a,O_2} (kJ kmol^{-1})	6.02 x 10^4	Q (kJ kmol^{-1})	8.7 x 10^3
n	0.2 ± 0.05	m	0.15 ± 0.025

Özyönüm (2002) has also investigated the kinetics of selective CO oxidation over Pt-Co-Ce/Al_2O_3 catalyst by studying on five different reaction paths and determined the plausible mechanisms to obtain rate expressions. Choi and Stenger (2004) expressed that in most of the PROX reactor feed gases, the concentration of H_2 and CO_2 are approximately 70 and 20 per cent, which can influence the reverse WGS reaction. Therefore, they concluded that the kinetics of WGS reaction has to be also considered simultaneously to predict the concentration of all gas components.

3. STEADY STATE MODELING OF METHANE CONVERSION IN FUEL PROCESSOR SYSTEM

In this chapter, modeling of a fuel processor system that converts methane to hydrogen by a series of catalytic reactions is investigated. Operating characteristics of the fuel processor system, typical temperatures and molar compositions of streams are obtained from literature. Material balance calculations and stream flow rates are based on hydrogen throughput rates corresponding to 500, 1000 and 1500 W electrical power output of a PEM fuel cell, and are done using typical stream compositions and temperature values obtained from the literature. Sizing and design of the catalytic reactors involved in the fuel processor system are performed using one-dimensional pseudohomogeneous packed-bed reactor model tailored to simulate multiple reactions and appropriate heat and mass transfer criteria to minimize transport resistances. Expressions used to quantify the reaction rates in reactor models are obtained from literature as well.

3.1. Generalized Fuel Processor System

Various fuels and fuel processor systems have been investigated for hydrogen production for fuel cell applications. Conversion of natural gas, modeled as methane, propane, i-octane and methanol to hydrogen via indirect partial oxidation and direct partial oxidation mechanisms have been studied using computer-based techniques (Avcı, 2003; Avcı *et al.*, 2001a; Avcı *et al.*, 2002). Avcı *et al.* (2002) investigated quantitatively the possible use of natural gas as a fuel for hydrogen generation in small-scale stationary applications. The fuel processor-fuel cell operation proposed in their study is investigated in this work as the fuel processor system for hydrogen generation from methane, which is presented in Figure 3.1. Avcı *et al.* (2002) placed a sulphur trap in front of the natural gas feed stream for preventing catalyst deactivation by poisoning due to the sulphur existing in natural gas. However, since pure methane is considered as fuel in this work, there is no need to place a sulphur trap in the fuel processor system.

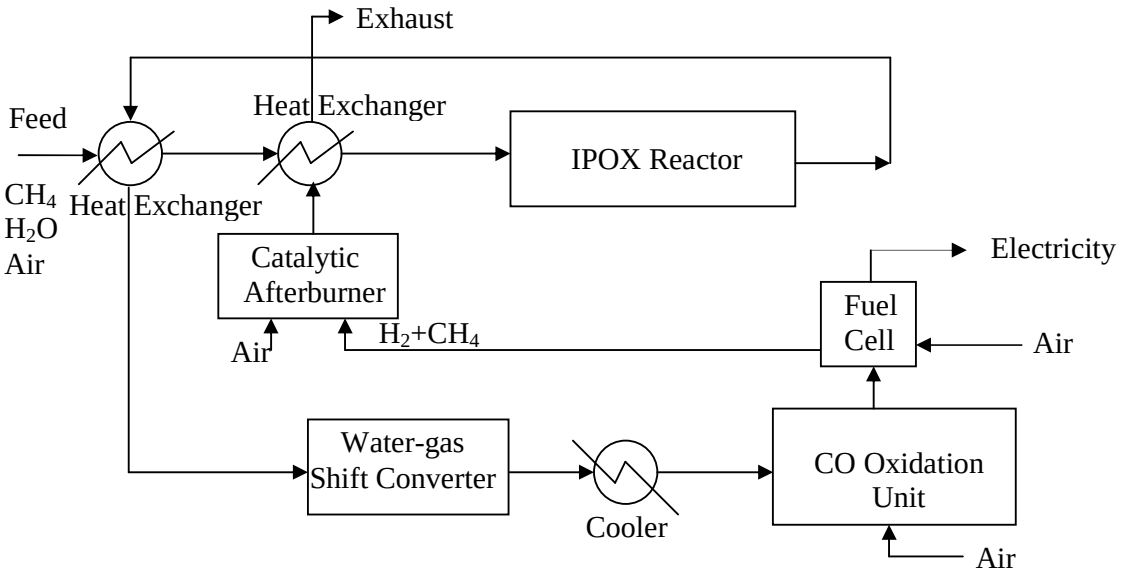

Figure 3.1. Fuel processor system (adapted from Avcı *et al.*, 2002)

The fuel processor system considered in this work contains three main reactors: Indirect partial oxidation (IPOX) reactor, water-gas shift (WGS) converter and CO oxidation unit in which preferential oxidation of CO (PROX) takes place. In addition to the main reactors, there is a catalytic afterburner unit in which unreacted methane and hydrogen rejected from the fuel cell are oxidized and a PEM fuel cell stack that provides electricity by using the generated hydrogen. Heat exchangers are also implemented to obtain energy integration and to ensure proper operation within the fuel processor system.

In the IPOX reactor, methane is converted to hydrogen over physical mixture of Pt/δ-Al_2O_3 and Ni/MgO-Al_2O_3 catalysts via indirect partial oxidation, which is the combination of total oxidation (TOX), steam reforming (SR) and water-gas shift (WGS) reactions (Ma *et al.*, 1996):

$$CH_4 + 2O_2 \longrightarrow CO_2 + 2H_2O, \quad \Delta H^{o}_{298} = -802 \text{ kJ/mol} \qquad (2.5)$$

$$CH_4 + H_2O \longleftrightarrow CO + 3H_2, \quad \Delta H^{o}_{298} = 206.2 \text{ kJ/mol} \qquad (2.15)$$

$$CO + H_2O \longleftrightarrow CO_2 + H_2, \quad \Delta H^{o}_{298} = -41.2 \text{ kJ/mol} \qquad (2.4)$$

In this process, heat needed by endothermic steam reforming reaction is provided by exothermic total oxidation reaction. In addition, this reaction supplies part of the steam needed by steam reforming. Steam reforming is thermodynamically favored at high temperatures. However, reaction temperature should not be above ca. 1100 K to prevent catalyst deactivation due to thermal sintering and carbon deposition (Rostrup-Nielsen, 1998; Ma, 1995). In order to help avoiding the possibility of coke formation, steam to carbon ratio defined in equation (2.16) has to be kept around 2.5 which can be achieved by adding extra water into the system, as shown in Figure 3.1 (Rostrup-Nielsen, 1984; Trimm and Önsan, 2001).

In water-gas shift converter, carbon monoxide is removed from hydrogen rich stream over $Cu/ZnO/Al_2O_3$ catalyst particles, within a temperature range of 393 -523 K by the following reaction (Choi and Stenger, 2003):

$$CO + H_2O \longleftrightarrow CO_2 + H_2, \qquad \Delta H^{o}_{298} = -41.2 \text{ kJ/mol} \qquad (2.4)$$

The main goal in using the water-gas shift converter is to reduce the majority of carbon monoxide down to approximately 2 mol per cent, while increasing hydrogen production rate. Since carbon monoxide is a poison for fuel cell anode catalyst, its concentration must be below 10 ppm in the hydrogen rich stream which can be achieved by the CO oxidation unit afterwards, as shown in Figure 3.1 (Avcı, 2003). In this system, WGS converter is therefore considered to function as a CO clean-up system and as a secondary reactor producing hydrogen.

Carbon monoxide level in hydrogen rich stream can be reduced below 10 ppm level in a catalytic CO oxidation unit (Figure 3.1) by selectively combusting carbon monoxide:

$$CO + \tfrac{1}{2} O_2 \longrightarrow CO_2, \qquad \Delta H^{o}_{298} = -283 \text{ kJ/mol} \qquad (2.29)$$

In CO oxidation unit, CO oxidation reaction is accompanied by the undesired hydrogen oxidation reaction:

$$H_2 + \tfrac{1}{2}O_2 \longrightarrow H_2O, \qquad \Delta H^{o}_{298} = -241.8 \text{ kJ/mol} \qquad (2.30)$$

This unit should be able to operate at a temperature around 353 K, since the exit stream will be fed to the PEM fuel cell which operates at 343-363 K (Sedmak *et al.*, 2003; Santarelli and Torchio, 2007). Therefore a proper catalyst, which can selectively oxidize CO in the desired temperature range, should be selected. In a recent study, a $Cu_{0.1}Ce_{0.9}O_{2-y}$ nanostructured catalyst is reported to give 100 per cent selectivity for carbon monoxide during the oxidation reaction in the temperature range of 318-363 K, which is in accordance with the operating temperature range of the CO oxidation unit. Therefore, this catalyst is considered to be the selective CO oxidation catalyst in this work.

After CO oxidation unit, CO-purified hydrogen rich stream is sent through PEMFC to produce desired electrical power by converting chemical energy stored within hydrogen to electricity through the reactions occurring on the anode and cathode of fuel cell:

Anode reaction: $H_2 \longrightarrow 2H^+ + 2e^-$ (3.1)

Cathode reaction: $½O_2 + 2H^+ + 2e^- \longrightarrow H_2O$ (3.2)

It has been reported that PEMFC rejects about 25 per cent of the hydrogen that is fed into it (Golunski, 1998). Moreover, methane that remains unconverted in the IPOX reactor is also fed into the fuel cell. Rejected hydrogen and unconverted methane are oxidized in a separate catalytic afterburner unit packed with a Pt-based oxidation catalyst to enable heat recovery and to exhaust a gas free from hydrocarbons by the reactions:

$H_2 + ½O_2 \longrightarrow H_2O,$ $\Delta H^o_{298} = -241.8$ kJ/mol (2.30)

$CH_4 + 2O_2 \longrightarrow CO_2 + 2H_2O,$ $\Delta H^o_{298} = -802.3$ kJ/mol (2.5)

In this study, three main reactors, i.e. IPOX reactor, WGS converter and CO oxidation unit of the fuel processor/fuel cell system are simulated and designed for meeting a range of electrical power outputs of the PEM fuel cell. The system is modeled at steady state and reactors are assumed to operate adiabatically. Design, i.e. sizing of the reactors are conducted using one-dimensional pseudohomogeneous packed-bed reactor model. For each reactor type, reaction kinetics is implemented into the mathematical model using rate

laws given in the literature for the catalysts of interest. Reactor dimensions are determined using interfacial and intraparticle mass and heat transfer criteria for porous catalysts and packed beds such that transport resistances are minimized.

3.1.1. Operating Characteristics

In order to design the IPOX, WGS and CO oxidation reactors of the fuel processor system (Figure 3.1), boundary conditions defined by the inlet/exit temperatures and stream compositions have to be determined. In this context, typical composition and temperature values of the feed stream of the fuel processor/fuel cell system can be determined from the data published previously in the literature.

Ma and Trimm (1996) worked on alternative catalyst bed configurations for the autothermal conversion of methane to hydrogen at different CH_4/O_2 and H_2O/CH_4 ratios for feedstock. They measured maximum temperature for IPOX reactor, amount of methane conversion and product yields for nine different feed ratios which are tabulated in Table 3.1. Two distinct CH_4/O_2 and H_2O/CH_4 ratios are selected to be the feed ratios of present work, which are 2.24 & 1.17 and 1.89 & 1.56.

Feed stream, composed of methane, water and air, is mixed at a certain composition and is fed into the system at 298 K. This stream has to be heated up to the inlet temperature of the IPOX reactor which is equal to the light-off temperature of methane at the selected CH_4/O_2 ratio. Such a processing is needed for the IPOX mechanism to be initiated. It is thus preheated by the hot exit stream of the IPOX reactor through a heat exchanger and by the hot exhaust stream of catalytic afterburner unit through a secondary heat exchanger (Figure 3.1). Finally, feed stream is sent to the inlet of the IPOX reactor at the methane light-off temperature. Variation of light-off temperature of methane with the CH_4/O_2 ratio is presented in Table 2.3 (Ma *et al.*, 1996). The light-off temperature of methane at CH_4/O_2 ratios of 2.24 and 1.89 is obtained by linear interpolation between the values given in Table 2.3 and is found as 620 K and 627 K for CH_4/O_2 ratios of 2.24 and 1.89, respectively.

Table 3.1. Output data for autothermal methane conversion in mixed-bed system (Ma and Trimm, 1996)

Feed conditions		T_{max} (K)	CH_4 converted (mol per cent)	Product Yields (mol/100 mol CH_4 admitted)		
CH_4/O_2	H_2O/CH_4			H_2	CO_2	CO
2.24	0	855	38.1	37.9	25.7	12.1
2.24	1.17	839	39.5	47.8	33.3	6.3
1.89	1.17	888	53.3	74.9	41.6	11.7
1.89	1.56	889	53.8	76.4	41.3	12.5
1.89	2.34	851	54.9	82.9	45.0	9.9
1.55	1.56	931	69.1	105.7	54.2	15.0
1.55	2.34	908	70.1	107.1	50.5	19.6
1.35	2.34	953	83.6	119.5	53.3	30.3
1.16	2.34	1007	91.7	120.6	55.8	35.9

After the total oxidation, steam reforming and water-gas shift reactions (IPOX process) which can increase catalyst bed temperature up to ca. 1100 K (Ma, 1995), effluent stream of the IPOX reactor is cooled via heat exchange with the feed stream through the first heat exchanger (Figure 3.1). Cooled stream is then sent to the water-gas shift converter to decrease the carbon monoxide level via Reaction (2.4) down to approximately 2 mol per cent at around 473 K which is a typical operating temperature for the low-temperature water-gas shift reaction (Amadeo and Laborde, 1995; Sun *et al.*, 2005).

PEMFCs operate typically between 343 and 363 K; this also dictates the operating temperature range of the selective CO oxidation unit: the inlet temperature of this unit should be around 353 K (Sedmak *et al.*, 2003; Santarelli and Torchio, 2007). Therefore, due to the slight exothermicity of the water-gas shift reaction (Reaction 2.4), which is around ca. 30-50 K, a cooler is placed between two reactors.

3.1.2. Material Balance Calculations

Fuel processor system is projected for autothermal hydrogen production from methane; inlet temperatures of reactors and feed composition ratios are decided by the investigation through the literature so far. In order to determine the size of the IPOX, WGS and CO oxidation reactors, a complete mass balance of the fuel processor system (Figure 3.1) should be done. Resulting values will give the boundary conditions that describe flow rate values of components that will be used in sizing the reactors through the reactor models. Building of complete mole balance for the whole system necessitates firstly the consideration of each part of the system as control volume. Balance equations for each unit of the fuel processor unit are presented below.

Assuming that the methane feed flow is specified, flow rates of oxygen and water in the feed can be calculated by the pre-determined CH_4/O_2 and H_2O/CH_4 ratios. In addition, amount of oxygen dictates the amount of nitrogen, since their composition in the air is known. If CH_4/O_2 and H_2O/CH_4 ratios are taken as *a* and *b* respectively, then the molar flow rates in the feed becomes:

$$F_{1,O_2} = F_{1,CH_4} / a \tag{3.3}$$

$$F_{1,H_{2O}} = F_{1,CH_4} \times b \tag{3.4}$$

$$F_{1,N_2} = {}^{79}\!/_{21} F_{1,O_2} \tag{3.5}$$

In Equations (3.3)-(3.5), F_{1,CH_4} is the molar flow rate of CH_4 in the feed, $F_{1,H_{2O}}$, F_{1,O_2} and F_{1,N_2} are that of H_2O, O_2 and N_2, respectively. Conversion value for total oxidation (TOX) (Reaction 2.5) has to be assumed to calculate the molar flow rates of components after total oxidation during the IPOX process. At this stage, it is assumed that TOX and SR+WGS reactions occur sequentially. This assumption is quite realistic, since it is reported that TOX reaction is much faster than SR and WGS reactions (Avcı *et al.*, 2003). Therefore, if a degree of conversion of X_{TOX} (for methane) is assigned for total oxidation, molar flow rates of components after total oxidation becomes:

$$F_{2,CH_4} = F_{1,CH_4}(1 - X_{TOX}) \tag{3.6}$$

$$F_{2,O_2} = F_{1,O2} - 2F_{1,CH_4} X_{TOX} \tag{3.7}$$

$$F_{2,H_2O} = F_{1,H_2O} + 2F_{1,CH_4} X_{TOX} \tag{3.8}$$

$$F_{2,CO_2} = F_{1,CH_4} X_{TOX} \tag{3.9}$$

$$F_{2,N_2} = F_{1,N_2} \tag{3.10}$$

where $F_{2,j}$ is the molar flow rate of component *j* in IPOX reactor after total oxidation, before steam reforming and water-gas shift.

Hydrogen generation step in the IPOX reactor occurs via methane steam reforming and water-gas shift reactions. Conversion values for steam reforming and water-gas shift reaction have to be assumed to estimate the molar flow rates of components at the exit of IPOX reactor. If X_{SR} (for methane) and X_{WGS1} (for CO) are assumed as degree of

conversion of steam reforming and water-gas shift respectively, then the molar flow rates of components can be calculated as follows:

$$F_{3,CH_4} = F_{2,CH_4}(1 - X_{SR}) \tag{3.11}$$

$$F_{3,H_2O} = F_{2,H_2O} - (F_{2,CH_4} X_{SR}) - (F_{2,CH_4} X_{SR} X_{WGS1}) \tag{3.12}$$

$$F_{3,CO} = (F_{2,CH_4} X_{SR}) - (F_{2,CH_4} X_{SR} X_{WGS1}) \tag{3.13}$$

$$F_{3,CO_2} = F_{2,CO_2} + (F_{2,CH_4} X_{SR} X_{WGS1}) \tag{3.14}$$

$$F_{3,H_2} = (3F_{2,CH_4} X_{SR}) + (F_{2,CH_4} X_{SR} X_{WGS1}) \tag{3.15}$$

$$F_{3,N_2} = F_{2,N_2} \tag{3.16}$$

In Equations (3.11)-(3.16), $F_{3,j}$ is the molar flow rate of component *j* at the exit of IPOX reactor. Molar flow rate of nitrogen does not change through the IPOX reactor since it is neither consumed nor generated in any of the reactions.

Estimated molar flow rate values at the exit of the IPOX reactor are also the molar flow rates of components at the inlet of WGS converter. If a conversion value of X_{WGS2} (for CO) is assumed for water-gas shift reaction in WGS converter, then the molar flow rates of components at the exit of the WGS converter will be:

$$F_{4,CH_4} = F_{3,CH_4} \tag{3.17}$$

$$F_{4,H_2O} = F_{3,H_2O} - (F_{3,CO} X_{WGS2}) \tag{3.18}$$

$$F_{4,CO} = F_{3,CO}(1 - X_{WGS2}) \tag{3.19}$$

$$F_{4,CO_2} = F_{3,CO_2} + F_{3,CO} X_{WGS2} \tag{3.20}$$

$$F_{4,H_2} = F_{3,H_2} + F_{3,CO} X_{WGS2} \tag{3.21}$$

$$F_{4,N_2} = F_{3,N_2} \tag{3.22}$$

where $F_{4,j}$ denotes the molar flow rate of component *j* at the exit of the WGS converter.

In CO oxidation unit, carbon monoxide oxidation is accompanied by undesired hydrogen oxidation. However, by selecting an appropriate catalyst such as the one mentioned in Chapter 2 that has 100 per cent selectivity for CO ($Cu_{0.1}Ce_{0.9}O_{2-y}$) (Sedmak *et al.* 2003), only carbon monoxide oxidation can be considered to take place in CO oxidation reactor. Additional air is introduced to CO oxidation unit to meet the oxygen demand for oxidation. Therefore, if X_{PROX} (for CO) is assumed as conversion value for preferential oxidation of CO, the molar flow rates at the air inlet stream and exit of the CO oxidation reactor will be:

$$F_{5,O_2} = F_{4,CO} X_{PROX} / 2 \tag{3.23}$$

$$F_{5,N_2} = {}^{79}\!/\!_{21} F_{5,O_2} \tag{3.24}$$

$$F_{6,CH_4} = F_{4,CH_4} \tag{3.25}$$

$$F_{6,H_2O} = F_{4,H_2O} \tag{3.26}$$

$$F_{6,CO} = F_{4,CO}(1 - X_{PROX}) \tag{3.27}$$

$$F_{6,CO_2} = F_{4,CO_2} + F_{4,CO} X_{PROX} \tag{3.28}$$

$$F_{6,H_2} = F_{4,H_2} \tag{3.29}$$

$$F_{6,N_2} = F_{4,N_2} + F_{5,N_2} \tag{3.30}$$

In Equations (3.23)-(3.30), $F_{5,j}$ is the molar flow rate of component *j* at the air inlet stream and $F_{6,j}$ is the molar flow rate of component *j* at the exit of the CO oxidation unit. The changes are only in CO, CO_2 and N_2 molar flow rates since others do not react in the CO oxidation unit.

Although component mole balance is formulated for the whole system as explained above, parameters such as degree of conversion of reactions and required hydrogen production rate should be specified. In addition, a value for methane flow rate in the feed stream will be assumed and will be taken as the basis. Once values of these parameters are fixed and inlet methane flow rate is assigned, mole balance calculations can be executed via equations (3.3)-(3.30). Calculated hydrogen throughput rate will then be compared with the required hydrogen production rate. Using this comparison, inlet methane flow rate will be changed, reassigned and same set of calculations will be re-executed until calculated and required hydrogen production rates are equal. Outcomes of the final calculation will give flow rates that will be used in reactor design/sizing calculations.

In this study, hydrogen production rates corresponding to 500, 1000 and 1500 W of PEMFC power outputs are of interest. The hydrogen flow rate required for a PEMFC is reported as 37-40 mol h^{-1} kW^{-1} in the literature (Brown, 2001; Zalc and Löffler, 2002). It is also reported that a 27 L min^{-1} H_2 at standard temperature and pressure can operate a 1.5 kW PEMFC (Karakaya, 2006). Using this set of information, molar hydrogen flows are selected as given in Table 3.2 for the three power sizes of PEMFC investigated.

Table 3.2. Required hydrogen production rate for PEMFC types

PEMFC power size (W)	Required hydrogen production rate (mol h^{-1})
500	20.35
1000	40.70
1500	61.03

After assuming methane feed flow rate as the basis value and assigning feed composition ratios (Ma and Trimm, 1996), some further assumptions have to be made in order to proceed with the mass balance calculations. These assumptions are given below:

- To estimate the total oxidation conversion, consumption of all oxygen fed within the feed stream is considered. By a simple calculation from stoichiometric ratios, conversion of total oxidation of methane, X_{TOX}, is calculated as:

$$X_{TOX} = \frac{F_{1,O_2}}{2F_{1,CH_4}} \tag{3.31}$$

  where F_{1,O_2} is determined from methane:oxygen ratio in the feed stream.

- In order to assign approximate values for steam reforming and water-gas shift conversions during IPOX, studies involving similar reactor/catalyst combinations were investigated in detail. As a result, an average value of 60 per cent conversion is assumed for steam reforming of methane (Ma, 1995; Ma and Trimm, 1996; Avcı *et al.*, 2002; Rakass *et al.*, 2006; Comas *et al.*, 2006). Similarly, an average conversion value of 75 per cent is assumed for water-gas shift as a side reaction in the IPOX reactor (Lee *et al.*, 2005; De Smet *et al.*, 2001, Hoang and Chan, 2004).

- Conversion of CO in WGS reactor and in CO oxidation unit is also approximated using data in the literature. An average value of 60 per cent conversion is assumed for the WGS reaction (Amadeo and Laborde, 1995; Kamarudin *et al.*, 2004; Sun *et al.*, 2005; Choi and Stenger, 2003) and 99 per cent conversion is assumed for the CO oxidation (Sedmak *et al.*, 2003; Lin *et al.*, 2005; Choi and Stenger, 2004; Kahlich *et al.*, 1997).

- Carbon monoxide concentration at exit stream of water-gas shift converter has to be below ca. 2 mol per cent (Avcı *et al.*, 2002).

- CO concentration has to be reduced down to 10 ppm at the exit of CO oxidation unit and so at the inlet of PEMFC (Cheng *et al.*, 2007).

- Steam to carbon ratio that is given in Equation (2.16) has to be around 2.5 for preventing carbon formation (Rostrup-Nielsen, 1984; Trimm and Önsan, 2001).

In the light of the assumptions stated above, a complete mole balance study has been done for the fuel processor system. The set of information explained above is formulated into MS Excel to execute a trial-and-error solution for figuring out the methane feed flow rate and, therefore, the component and stream flow rate values that would end up with the desired hydrogen production rates given in Table 3.2. Outcomes of the balance calculations are given in Section 4.1.

3.2. Modeling of Catalytic Reactors in the Fuel Processor System

Determination of the flow rates of the components in each stream via material balances provides the boundary conditions needed for designing, i.e. sizing the three main reactors of the fuel processor system – indirect partial oxidation reactor, water-gas shift converter and carbon monoxide oxidation reactor (Figure 3.1). Reactor sizes, i.e. catalyst weights and reactor volumes can therefore be computed using appropriate mathematical models. In this study, all of the reactors are considered to be tubular, packed-bed type and steady state, adiabatic operation is assumed. Therefore, one-dimensional pseudo-homogeneous reactor model, involving a set of differential equations that describe flow and temperature behaviors through the reactors are employed (Avcı *et al.*, 2000; Fogler, 1999). These equations include a reaction rate term in order to take the effect of reaction kinetics into account. Reaction rate expressions reported for the catalysts of interest are obtained from literature and are presented in Tables 2.4, 2.5, 2.6 and Equations 2.27 and 2.33 in Chapter 2 and used in the solution of the model equations. As mentioned above, the equations are differential in nature and solved using a stiff, variable order ODE solver, the "ode15s" function of the MATLAB^{TM} numerical computation software.

These equations are initial value type, i.e. solved by providing entrance conditions (feed conditions) and by defining an integration limit, which is the catalyst weight in this

study. Once a solution is completed, i.e. reactor simulation is executed, the output, which is the exit flow rate of the reactor, is compared with the value obtained from the material balance. Different values of catalyst weight are tried systematically until the simulation output is in accordance with the material balance calculations.

The calculations explained briefly above gives the design catalyst weight and therefore the reactor volume, provided that the catalyst bed-density is known. Reactor dimensions and catalyst particle diameter are then figured out such that interfacial (bulk fluid-catalyst surface) and intraparticle transport resistances and flow non-uniformities such as axial dispersion are minimized. This is achieved using the relevant criteria that take properties such as reaction rate, physical properties of the bulk fluid into account and indicate the significance of the transport resistance of interest. This is explained in Section 3.2.2 in detail.

3.2.1. Mathematical Models

3.2.1.1. Indirect Partial Oxidation. Total oxidation of methane (Reaction 2.5) takes place mainly over Pt/δ-Al_2O_3 catalyst in indirect partial oxidation reactor. A power-law type rate equation is used for describing the kinetics of methane total oxidation (Ma, 1995):

$$-r_{TOX} = 1.57*10^5 * \exp\left(\frac{-21068}{1.987*T}\right) * (P_{CH_4})^{0.95} * (P_{O_2})^{-0.17} \qquad (2.11)$$

In Equation (2.11), T is the reaction temperature (K), P_{CH_4} and P_{O_2} are the partial pressures of methane and oxygen, respectively (bar).

Another reaction taking place in IPOX reactor is the hydrogen producing steam reforming reaction (Reaction 2.15). This reaction occurs on mainly Ni/MgO-Al_2O_3 catalyst and favored thermodynamically at high temperatures. Rate equation suggested by Xu and Froment (1989) for a Ni/$MgAl_2O_4$ catalyst is taken to quantify the kinetics of steam reforming reaction:

$$-r_{SR} = \frac{k_{SR} / P_{H_2}^{2.5} (P_{CH_4} P_{H_2O} - P_{H_2}^3 P_{CO} / K_{eq}^{SR})}{(1 + K_{CO} P_{CO} + K_{H_2} P_{H_2} + K_{CH_4} P_{CH_4} + K_{H_2O} P_{H_2O} / P_{H_2})^2} \qquad (2.17)$$

In Equation (2.17), k_{SR} is the rate constant (kmol kgcat^{-1} h^{-1}), K_{eq}^{SR} is the equilibrium constant for steam reforming reaction in (bar^2), K_{CO}, K_{H_2}, K_{CH_4} and K_{H_2O} are the adsorption constants for indexed species in (bar^{-1}), P_{CH_4}, P_{CO}, P_{H_2O} and P_{H_2} are the partial pressures of indexed species (bar). The temperature dependence of rate and adsorption constants is expressed by Arrhenius and van't Hoff type equations respectively, whose parameters given in Table 2.7.

Water-gas shift reaction also takes place as a side reaction during indirect partial oxidation, at same temperature interval and over the same catalyst mixture. Xu and Froment (1989) also proposed a rate equation for the water-gas shift side reaction over a $Ni/MgAl_2O_4$ catalyst, which is also used in this study:

$$-r_{WGS1} = \frac{k_{WGS1} / P_{H_2} (P_{CO} P_{H_2O} - P_{H_2} P_{CO2} / K_{eq}^{WGS1})}{(1 + K_{CO} P_{CO} + K_{H_2} P_{H_2} + K_{CH_4} P_{CH_4} + K_{H_2O} P_{H_2O} / P_{H_2})^2} \qquad (2.20)$$

In Equation (2.20), K_{eq}^{WGS1} is the equilibrium constant for water-gas shift side reaction (bar^2), k_{WGS1} is the rate constant (kmol kgcat^{-1} h^{-1}) and other variables are defined to be the same with those of steam reforming given above.

As mentioned above, a one-dimensional pseudohomogeneous reactor model is employed for simulating and sizing the packed-bed reactors. The model equations employed for simulation of IPOX reactor given below describe the flow rate variation of species along catalyst weight (Avcı *et al.*, 2000):

$$\frac{dF_{CH_4}}{dW} = r_{TOX} + r_{SR} \qquad (3.32)$$

$$\frac{dF_{CO}}{dW} = -r_{SR} + r_{WGS1} \tag{3.33}$$

$$\frac{dF_{CO_2}}{dW} = -r_{TOX} - r_{WGS1} \tag{3.34}$$

$$\frac{dF_{H_2}}{dW} = -3r_{SR} - r_{WGS1} \tag{3.35}$$

$$\frac{dF_{H_2O}}{dW} = -2r_{TOX} + r_{SR} + r_{WGS1} \tag{3.36}$$

$$\frac{dF_{O_2}}{dW} = 2r_{TOX} \tag{3.37}$$

The differential energy balance for the adiabatically operating fixed-bed reactor gives the temperature variation along the catalyst weight (Fogler, 1999):

$$\frac{dT}{dW} = \frac{\sum_{i=1}^{3}\left((-\Delta H_i)(-r_i)\right)}{\sum_j F_j c_{p,j}} \tag{3.38}$$

$$\text{at } W = 0, \quad F_j = F_{1,j}; \quad T = T_1^{in} \tag{3.39}$$

Equation (3.39) is the set of initial conditions defined for the solving Equations (3.32)-(3.38). This set of non-linear differential equations is solved using stiff, variable order ODE solver, the “ode15s” function in MATLAB environment. In Equations (3.38) and (3.39), i is the reaction index and j designates the component. ΔH_i is the heat of reaction i at temperature T (kJ kmol^{-1}), $-r_i$ the rate of reaction i (kmol kgcat^{-1} h^{-1}), F_j the molar flow rate of component j along the IPOX reactor (kmol h^{-1}), $c_{p,j}$ the temperature-dependent gas-phase heat capacity of component j (kJ kmol^{-1} K^{-1}), $F_{1,j}$ is the flow rate of component j at the inlet of the IPOX reactor (kmol h^{-1}) and T_1^{in} the temperature of the inlet

stream of IPOX reactor (K). The parameters needed to calculate the temperature-dependent heat capacities are presented in Appendix A.

3.2.1.2. Water-gas Shift. After the IPOX process, CO content is reduced and hydrogen content is increased in the water-gas shift reactor. Water-gas shift reaction (Reaction 2.4) runs over a $Cu/ZnO/Al_2O_3$ catalyst at a temperature range of 393 and 523 K (Choi and Stenger, 2003). In order to quantify the kinetics of this reaction, a power law type rate expression proposed by Choi and Stenger (2003) is used due to its convenience in terms of temperature interval and catalyst:

$$r_{WGS2} = 2.96x10^5 \exp\left(-\frac{47{,}400}{RT}\right)\left(P_{CO}P_{H_2O} - \frac{P_{CO_2}P_{H_2}}{K_{eq}^{WGS2}}\right) \tag{2.27}$$

In Equation (2.27), K_{eq}^{WGS2} is the equilibrium constant for water-gas shift reaction, R is the gas constant (8.3144 kJ $kmol^{-1}$ K^{-1}), P_{CO_2}, P_{CO}, P_{H_2O} and P_{H_2} are the partial pressures of the indexed species (bar).

The model equations that describe flow behavior of the species, temperature variation along the catalyst weight and initial conditions for water-gas shift reactor are as follows:

$$\frac{dF_{CO}}{dW} = -r_{WGS2} \tag{3.40}$$

$$\frac{dF_{H_2O}}{dW} = -r_{WGS2} \tag{3.41}$$

$$\frac{dF_{CO_2}}{dW} = r_{WGS2} \tag{3.42}$$

$$\frac{dF_{H_2}}{dW} = r_{WGS2} \tag{3.43}$$

$$\frac{dT}{dW} = \frac{-\Delta H_{WGS2} r_{WGS2}}{\sum_j F_j c_{p,j}} \tag{3.44}$$

$$\text{at } W = 0, \quad F_j = F_{3,j}; \quad T = T_2^{in} \tag{3.45}$$

In Equations (3.40)-(3.45), j designates the component, ΔH_{WGS2} is the heat of water-gas shift reaction at temperature T (kJ kmol^{-1}), r_{WGS2} the rate of water-gas shift reaction (kmol kgcat^{-1} h^{-1}), F_j the molar flow rate of component j along the WGS converter (kmol h^{-1}), $F_{3,j}$ is the flow rate of component j at the inlet of the WGS converter (kmol h^{-1}) and T_2^{in} the temperature of the inlet stream of WGS converter (K).

3.2.1.3. Preferential CO Oxidation. Since carbon monoxide oxidation is accompanied by undesired hydrogen oxidation reaction in the CO oxidation unit, it is important to select a catalyst that has a high selectivity to carbon monoxide. It is reported that carbon monoxide can be oxidized at 353 K over a $Cu_{0.1}Ce_{0.9}O_{2-y}$ nanostructured catalyst at 100 per cent selectivity (Sedmak *et al.*, 2003). Sedmak *et al.* (2003) have also studied the kinetics of CO oxidation over this catalyst in the temperature range from 318 to 363 K by considering two different kinetic models and they observed that Mars and van Krevelen type kinetic model which has been derived on the basis of a redox mechanism is the best alternative to describe the rate of carbon monoxide oxidation:

$$r_{PROX} = \frac{k_{CO} k_{O_2} P_{CO} P_{O_2}^n}{0.5 k_{CO} P_{CO} + k_{O_2} P_{O_2}^n} \tag{2.33}$$

In Equation (2.33), k_{CO} is the rate constant for the reduction of surface by CO (kmol kgcat^{-1} h^{-1} bar^{-1}) and k_{O_2} is the rate constant for the re-oxidation of surface by O_2 (kmol kgcat^{-1} h^{-1} bar^{-n}), P_{CO} and $P_{O_2}^n$ are the partial pressures of indexed species (bar). Temperature dependence of rate constants according to carbon monoxide and oxygen are expressed by Arrhenius type equation whose parameters given in Table 2.15.

Variation of flow rates of species and temperature along the CO oxidation reactor are expressed differentially by the model equations as follows:

$$\frac{dF_{CO}}{dW} = r_{PROX} \tag{3.46}$$

$$\frac{dF_{O_2}}{dW} = 0.5 r_{PROX} \tag{3.47}$$

$$\frac{dF_{CO_2}}{dW} = -r_{PROX} \tag{3.48}$$

$$\frac{dT}{dW} = \frac{(-\Delta H_{PROX})(-r_{PROX})}{\sum_j F_j c_{p,j}} \tag{3.49}$$

$$\text{at } W = 0, \quad F_j = F_{4,j}; \quad T = T_3^{in} \tag{3.50}$$

In Equations (3.58)-(3.62), ΔH_{PROX} the heat of CO oxidation reaction at temperature T (kJ kmol^{-1}), r_{PROX} the rate of CO oxidation reaction (kmol kgcat^{-1} h^{-1}), F_j the molar flow rate of component *j* along the CO oxidation unit (kmol h^{-1}), $F_{4,j}$ is the flow rate of component *j* at the inlet of the CO oxidation unit (kmol h^{-1}) and T_3^{in} the temperature of the inlet stream of CO oxidation unit (K).

3.2.2. Equations for Heat and Mass Transfer Criteria

Apart from the model equations that define component flow and temperature variations along the reactor, phenomena that limit heat and mass transfer between bulk fluid and catalyst particle and within the catalyst particle have to be considered. In this study, criteria that indicate interfacial gradients defined by resistances between catalyst exterior-bulk fluid and intraparticle gradients defined by resistances inside the catalyst particle are taken into account to come up with reactor and catalyst particle dimensions that

prevent existence of these resistances and allow intrinsic kinetics to define reactor temperature and species flow. Moreover, pressure drop along the reactor length and criteria that indicate the flow non-uniformities such as axial dispersion have also been considered in the sizing and design of the reactors.

One dimensional model accounting for interfacial and intraparticle gradients is conducted for modeling of fuel processor reactors; however, mass transfer between bulk fluid-catalyst pellet and heat transfer inside the catalyst assumed to be negligible. It is assumed that catalyst particle is practically isothermal; thus, intraparticle heat transfer is neglected and it is supposed that the main resistance inside the particle is to mass transfer. Besides, interfacial mass transfer is neglected since reactants are assumed to diffuse in the bulk sufficiently rapidly. Therefore, heat transfer between the bulk and catalyst is assumed as the main resistance (Fogler, 1999).

Mears' criterion uses the measured rate of reaction to understand the significance of heat and mass transfer from bulk fluid to the catalyst pellet surface (Fogler, 1999). Modified version of Mears' criterion for the multiple reaction case for heat transfer form bulk fluid to catalyst surface is as follows (Rase, 1990):

$$\left| \frac{\sum_i (-\Delta H_i)(-r_i)\rho_p D_p E_A}{h_s T^2 R} \right| < 0.3 \qquad (3.51)$$

In Equation (3.51), ρ_p is the particle density of the catalyst (kg m^{-3}), D_p the particle diameter (m), E_A the activation energy (kJ $kmol^{-1}$), h_s particle-to-fluid heat transfer coefficient (kJ m^{-2} h^{-1} K^{-1}). It is proposed that if criterion given in Equation (3.63) is satisfied, then external heat transfer effects can be neglected (Fogler, 1999).

Particle density of the catalyst ρ_p can be estimated by considering the known properties of the catalyst such as bulk density and void fraction with the following equations (Fogler, 1999; Bird *et al.*, 2002):

$$\rho_b = \frac{m_{cat}}{V_{particle} + V_{void}} \tag{3.52}$$

$$\rho_p = \frac{m_{cat}}{V_{particle}} \tag{3.53}$$

$$V_{total} = V_{particle} + V_{void} \tag{3.54}$$

$$V_{void} = \varepsilon_f V_{total} \tag{3.55}$$

In Equations (3.52)-(3.55) ρ_b is the bulk density of the catalyst (kg m^{-3}), m_{cat} the catalyst weight (kg), $V_{particle}$ particle volume of the catalyst (m^3), V_{void} void volume of the catalyst (m^3), V_{total} total volume of the catalyst (m^3) and ε_f the void fraction.

Particle-to-fluid heat transfer coefficient, h_s, can be evaluated using the following correlation (Rase, 1990):

$$\frac{h_s D_p}{\lambda_f} = 2 + 1.1 \mathrm{Pr}^{1/3}\, \mathrm{Re}^{0.6} \tag{3.56}$$

In Equation (3.56), λ_f is the thermal conductivity of the bulk fluid (kJ m^{-1} h^{-1} K^{-1}), Pr the Prandtl number and Re the Reynolds number. Prandtl number can be estimated from Perry (1997) for nitrogen as 0.7 and Reynolds number can be evaluated from the well-known relationship:

$$\mathrm{Re} = \frac{D_t \rho_m v}{\mu} \tag{3.57}$$

In Equation (3.57), D_t is the tube diameter (m), ρ_m the density of the gas mixture (kg m^{-3}), v the velocity of the gas mixture (m s^{-1}) and μ viscosity of the mixture (kg m^{-1} s^{-}

[1]). The gas mixture is assumed to behave like nitrogen in evaluating its physical properties, since the gas mixture contains mostly nitrogen (~ 35 per cent by volume).

Temperature dependence of nitrogen thermal conductivity, representing that of the bulk fluid, can be expressed as follows (Avcı, 2003):

$$\lambda_{N_2} = 1.295 * 10^{-2} + 5.223 * 10^{-5} * T \tag{3.58}$$

where T is in K and λ_{N_2} is in W m^{-1} K^{-1}.

Weisz-Prater criterion for intraparticle diffusion is used to quantify the significance of intraparticle diffusion. This criterion, formulated for multiple reaction cases, is given as follows (Avcı *et al.*, 2001b):

$$\frac{\sum_i (\nu_{ij})(r_i)\rho_c D_p}{4 D_e C_{sj}} << 1 \tag{3.59}$$

In Equation (3.59), ν_{ij} is stoichiometric coefficient of species j in reaction i, ρ_c the solid density of the catalyst (kg m^{-3}), D_e effective diffusivity inside catalyst (m^2 h^{-1}) and C_{sj} surface concentration of j (kmol m^{-3}). It is stated that there are no diffusion limitations and no concentration gradients exist within the catalyst pellet if criterion given above is satisfied (Fogler, 1999).

Solid density of the catalyst, ρ_c, can be calculated by the equations:

$$\rho_c = \frac{m_{cat}}{V_{particle,ex}} \tag{3.60}$$

$$V_{particle} = V_{particle,ex} + V_{pore} \tag{3.61}$$

$$V_{pore} = \varepsilon_p V_{particle} \tag{3.62}$$

In Equations (3.60)-(3.62), $V_{particle,ex}$ is the particle volume of the catalyst excluded pores (m^3), V_{pore} pore volume of the catalyst (m^3) and ε_p the pellet porosity.

Effective diffusivity is defined to describe the average diffusion taking place at any position in the catalyst pellet since it would not be feasible to describe diffusion within each pore due to the fact that the pores are not straight and cylindrical, the diffusion paths are tortuous and all the area normal to direction of flux is not available for molecular diffusion. Equation that formulates effective diffusivity is given as follows (Fogler, 1999):

$$D_e = \frac{D_{km}\varepsilon_p\sigma}{\tau} \tag{3.63}$$

In Equation (3.63), τ is tortuosity which is defined as the ratio of actual distance a molecule travels between two points to shortest distance between those two points, σ the constriction factor which is equal to unity if the cross-section area of the reactor tube remains constant and D_{km} the multicomponent gas mixture diffusivity which is defined by Rase (1990) as follows:

$$D_{km} = \left(\sum_{j=1}^{n} \frac{Y_j}{D_{kj}} \right)^{-1} \tag{3.64}$$

In Equation (3.64), D_{km} is the diffusivity of component *k* diffusing into a homogeneous gas mixture ($m^2\ h^{-1}$), D_{kj} is the binary diffusivity of component *k* into component *j* ($m^2\ h^{-1}$) and Y_j is the mole fraction of component *j*.

Binary diffusivity of component *k* into component *j* can be estimated by the following correlation (Rase, 1990):

$$D_{kj} = \frac{0.00143T^{1.75}}{P_T M_{kj}^{0.5}\left[(\sum v_a)_k^{1/3} + (\sum v_a)_j^{1/3}\right]^2} \tag{3.65}$$

In Equation (3.65), D_{kj} is the diffusivity for *k* diffusing into *j* ($cm^2\ sec^{-1}$), P_T is total pressure (atm), $M_{kj} = 2\left[(1/M_k) + (1/M_j)\right]^{-1}$, M_k and M_j are molecular weights of *k* and *j* respectively (g mol^{-1}), v_a is atomic diffusion volume to be summed over atoms, groups and structural features of diffusing compound values presented in Table 3.3.

Table 3.3. Atomic and structural diffusion volume increments (Rase, 1990)

C	15.9	F	14.7
H	2.31	Cl	21.0
O	6.11	Br	21.9
N	4.54	I	20.8
S	22.9	Aromatic or heterocyclic ring	18.3

Change in total pressure is another factor that affects the rate of a reaction. Concentration of reacting components in liquid phase reactions is affected insignificantly by the changes in total pressure; therefore, effect of pressure drop on the rate of reaction can be totally ignored during the reactor sizing. However, in gas phase reactions, the concentration of reactants and consequently the rate of reaction are proportional to the total pressure change and pressure drop may become an important factor that can result a failure in reactor operation if not taken into consideration. Since the reactions in present work occur in gas phase, pressure drop is taken into account in designing the reactors. Ergun equation, which is widely used in estimating pressure drop in packed-beds, is used to obtain the total pressure drop along the catalyst weight (Fogler, 1999; Bird *et al.*, 2002):

$$\frac{dP_T}{dW} = -\frac{G}{\rho_m D_p}\left(\frac{1-\phi}{\phi^3}\right)\left[\frac{150(1-\phi)\mu}{D_p} + 1.75G\right]\frac{1}{A_c \rho_b} \tag{3.66}$$

For each reactor simulation and design calculation, Equation (3.66) is solved simultaneously with the differential mole and energy balances. At the entrance of the each reactor, total pressure is taken as 1.013 bar, i.e. initial condition for Equation (3.66) is at $W = 0,\ P_T = 1.013$.

In Equation (3.66), G is superficial mass velocity (kg m^{-2} s^{-1}) and equals to $\rho_m v$, ϕ the porosity (volume of void / total bed volume = void fraction), A_c the cross-sectional area of the pipe (m^2).

The packed-bed reactor model considered is of plug-flow pseudohomogeneous type in which conditions in the bulk and on the catalyst surface are assumed to be identical in a 'pseudohomogeneous' continuum. In addition, the 'plug-flow' term implies an assumption of fluid flow in the form of a plug. In plug-flow, each differential element of interest is assumed to pass through the system without back-mixing (axial dispersion) and has single uniform temperature and composition at a given axial position throughout the cross-section of reactor tube. Therefore, criteria that provide flat velocity profile and negligible axial dispersion are needed for this model to ensure the quality of operation and design. A reasonably flat velocity profile is assured by the following criterion (Rase, 1990):

$$\frac{D_t}{D_p} \geq 30 \tag{3.67}$$

The equation above implies that the diameter of the reactor tube, D_t, has to be at least 30 times bigger than the diameter of the catalyst pellet, D_p. Axial dispersion has no effect on performance in a packed bed for gases if the following criterion is achieved (Rase, 1990):

$$\frac{L}{D_p} > 50 \tag{3.68}$$

This relationship stipulates that the reactor length, L has to be at least 50 times of diameter of the catalyst pellet, D_p. Different values have been assigned to the particle

diameter, D_p, for minimizing flow non-uniformities, pressure drop and transport resistances. These values are given in Tables 4.16-4.33 for every reactor and power output/ feed ratio combinations.

Parameters used during the calculation of criteria and of total pressure change stated above are given in Table 3.4.

Table 3.4. Parameters used in calculation of criteria

IPOX		WGS		PROX	
ρ_b (kg m^{-3})	1163.7	ρ_b (kg m^{-3})	900	ρ_b (kg m^{-3})	1160
ρ_c (kg m^{-3})	2377	ρ_c (kg m^{-3})	1863	ρ_c (kg m^{-3})	2369
ε_f	0.3	ε_f	0.3	ε_f	0.3
ε_p	0.6	ε_p	0.6	ε_p	0.6
τ	3.3	τ	3.3	τ	3.3

4. RESULTS AND DISCUSSION

Fuel processor system for autothermal hydrogen production from methane is mathematically investigated at steady-state conditions. The main reactors of the fuel processor system, namely indirect partial oxidation reactor, water-gas shift converter and preferential carbon monoxide oxidation reactor are of interest. Steady-state operation, sizing and design of these reactors are conducted via computer simulations using one-dimensional pseudohomogeneous fixed-bed reactor model for two different CH_4/O_2 and H_2O/CH_4 ratios and for three hydrogen throughput rates corresponding to 500, 1000 and 1500 W power outputs of a PEM fuel cell. Appropriate external and internal transport resistance criteria are used as constraints in figuring out reactor dimensions.

Indirect partial oxidation reactor is considered to consist of a physical mixture of an oxidation and a reforming catalyst, $Pt/\delta\text{-}Al_2O_3$ and $Ni/MgO\text{-}Al_2O_3$ respectively (Ma and Trimm, 1996). Water-gas shift converter and CO oxidation reactor are considered to be packed with a $Cu/ZnO/Al_2O_3$ catalyst (Choi and Stenger, 2003) and with a $Cu_{0.1}Ce_{0.9}O_{2-y}$ nano-structured catalyst (Sedmak *et al.*, 2003), respectively. The fuel processor system is presented here again in Figure 4.1 with streams numbered according to the formulation given in Section 3.1.2.

4.1. Preliminary Material Balance Calculations for 500-1000-1500 W Fuel Cell Systems

Flow rate variation of components and temperature distribution in IPOX, WGS and PROX reactors are needed for designing and sizing of reactors by reactor models explained in Section 3.2.1. However, boundary conditions that describe flow rates of components at inlet and outlet of the reactors are needed first for this purpose. These flow rates are determined by material balance calculations. Once the boundary conditions are obtained for each stream of the whole processor system (Figure 4.1), the reactor model can be used in a trial-and-error scheme to figure out the catalyst weight that will give the desired throughput rate defined by the boundary condition at the exit.

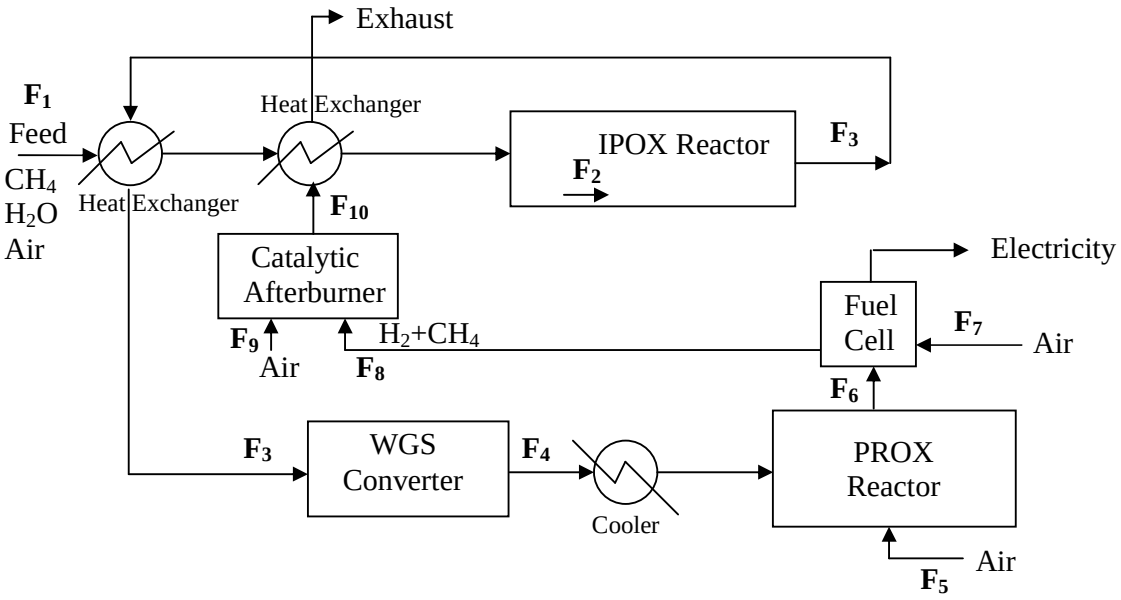

Figure 4.1. Fuel Processor System with stream numbers

A simple and complete material balance is built for processor system by introducing the material balance equations (3.3)-(3.30) and assumptions given in Section 3.1.2 into MS Excel to execute a trial-and-error solution to obtain the flow rates of each species at each stream. Trial-and-error solution procedure is based on assigning a methane feed flow rate and executing material balance calculation and comparing the calculated hydrogen throughput rate with the required hydrogen production rate given in Table 3.2 until they are equal, as explained in Section 3.1.2.

Material balance calculations are executed for six different feed ratios–power output configurations (Feed ratios: (CH_4/O_2, H_2O/CH_4) = (2.24, 1.17), (1.89, 1.56); PEMFC power outputs: 500, 1000 and 1500 W) and the results are presented in Tables 4.1-4.6. As explained above, these results are then used in reactor modeling and simulation calculations as boundary conditions to estimate the size of the reactor in terms of catalyst weight.

Table 4.1. Material Balance Results for 500 W PEMFC system (CH_4/O_2 = 1.89, H_2O/CH_4 = 1.56)

Stream / Component	F_1 (mol/h)	F_2 (mol/h)	F_3 (mol/h)	F_4 (mol/h)	F_5 (mol/h)	F_6 (mol/h)	F_7 (mol/h)	F_8 (mol/h)	F_9 (mol/h)	F_{10} (mol/h)
CH_4	12.36	9.09	3.86	3.86	0.00	3.86	0.00	3.86	0.00	0.00
H_2O	19.28	25.82	16.67	15.93	0.00	15.93	0.00	31.19	0.00	44.00
O_2	6.54	0.00	0.00	0.00	0.28	0.00	7.63	0.00	10.27	0.00
N_2	24.60	24.60	24.60	24.60	1.05	25.65	28.71	54.36	38.64	92.99
CO	0.00	0.00	1.31	0.56	0.00	0.001	0.00	0.00	0.00	0.00
CO_2	0.00	3.27	7.19	7.94	0.00	8.50	0.00	8.50	0.00	12.36
H_2	0.00	0.00	19.60	20.35	0.00	20.35	0.00	5.09	0.00	0.00

Table 4.2. Material Balance Results for 500 W PEMFC system (CH_4/O_2 = 2.24, H_2O/CH_4 = 1.17)

Stream / Component	F_1 (mol/h)	F_2 (mol/h)	F_3 (mol/h)	F_4 (mol/h)	F_5 (mol/h)	F_6 (mol/h)	F_7 (mol/h)	F_8 (mol/h)	F_9 (mol/h)	F_{10} (mol/h)
CH_4	11.70	9.09	3.86	3.86	0.00	3.86	0.00	3.86	0.00	0.00
H_2O	13.69	18.91	9.77	9.02	0.00	9.02	0.00	24.28	0.00	37.09
O_2	5.22	0.00	0.00	0.00	0.28	0.00	7.63	0.00	10.27	0.00
N_2	19.65	19.65	19.65	19.65	1.05	20.70	28.70	49.40	38.63	88.03
CO	0.00	0.00	1.31	0.56	0.00	0.001	0.00	0.00	0.00	0.00
CO_2	0.00	2.61	6.53	7.28	0.00	7.84	0.00	7.84	0.00	11.70
H_2	0.00	0.00	19.60	20.35	0.00	20.35	0.00	5.09	0.00	0.00

Table 4.3. Material Balance Results for 1000 W PEMFC system (CH_4/O_2 = 1.89, H_2O/CH_4 = 1.56)

Stream / Component	F_1 (mol/h)	F_2 (mol/h)	F_3 (mol/h)	F_4 (mol/h)	F_5 (mol/h)	F_6 (mol/h)	F_7 (mol/h)	F_8 (mol/h)	F_9 (mol/h)	F_{10} (mol/h)
CH_4	24.72	18.18	7.73	7.73	0.00	7.73	0.00	7.73	0.00	0.00
H_2O	38.56	51.64	33.35	31.85	0.00	31.85	0.00	62.38	0.00	88.00
O_2	13.08	0.00	0.00	0.00	0.56	0.00	15.26	0.00	20.54	0.00
N_2	49.20	49.20	49.20	49.20	2.10	51.30	57.41	108.72	77.27	185.99
CO	0.00	0.00	2.61	1.12	0.00	0.0019	0.00	0.00	0.00	0.00
CO_2	0.00	6.54	14.38	15.88	0.00	16.99	0.00	16.99	0.00	24.72
H_2	0.00	0.00	39.20	40.70	0.00	40.70	0.00	10.17	0.00	0.00

Table 4.4. Material Balance Results for 1000 W PEMFC system (CH_4/O_2 = 2.24, H_2O/CH_4 = 1.17)

Stream / Component	F_1 (mol/h)	F_2 (mol/h)	F_3 (mol/h)	F_4 (mol/h)	F_5 (mol/h)	F_6 (mol/h)	F_7 (mol/h)	F_8 (mol/h)	F_9 (mol/h)	F_{10} (mol/h)
CH_4	23.40	18.18	7.73	7.73	0.00	7.73	0.00	7.73	0.00	0.00
H_2O	27.38	37.82	19.53	18.04	0.00	18.04	0.00	48.56	0.00	74.18
O_2	10.45	0.00	0.00	0.00	0.56	0.00	15.26	0.00	20.54	0.00
N_2	39.30	39.30	39.30	39.30	2.10	41.40	57.40	98.80	77.26	176.06
CO	0.00	0.00	2.61	1.12	0.00	0.0019	0.00	0.00	0.00	0.00
CO_2	0.00	5.22	13.06	14.56	0.00	15.67	0.00	15.67	0.00	23.40
H_2	0.00	0.00	39.19	40.69	0.00	40.69	0.00	10.17	0.00	0.00

Table 4.5. Material Balance Results for 1500 W PEMFC system (CH_4/O_2 = 1.89, H_2O/CH_4 = 1.56)

Stream / Component	F_1 (mol/h)	F_2 (mol/h)	F_3 (mol/h)	F_4 (mol/h)	F_5 (mol/h)	F_6 (mol/h)	F_7 (mol/h)	F_8 (mol/h)	F_9 (mol/h)	F_{10} (mol/h)
CH_4	37.08	27.27	11.59	11.59	0.00	11.59	0.00	11.59	0.00	0.00
H_2O	57.84	77.46	50.02	47.78	0.00	47.78	0.00	93.56	0.00	132.00
O_2	19.62	0.00	0.00	0.00	0.84	0.00	22.89	0.00	30.81	0.00
N_2	73.80	73.80	73.80	73.80	3.14	76.95	86.12	163.08	115.91	278.98
CO	0.00	0.00	3.92	1.67	0.00	0.0029	0.00	0.00	0.00	0.00
CO_2	0.00	9.81	21.57	23.82	0.00	25.49	0.00	25.49	0.00	37.08
H_2	0.00	0.00	58.80	61.05	0.00	61.05	0.00	15.26	0.00	0.00

Table 4.6. Material Balance Results for 1500 W PEMFC system (CH_4/O_2 = 2.24, H_2O/CH_4 = 1.17)

Stream / Component	F_1 (mol/h)	F_2 (mol/h)	F_3 (mol/h)	F_4 (mol/h)	F_5 (mol/h)	F_6 (mol/h)	F_7 (mol/h)	F_8 (mol/h)	F_9 (mol/h)	F_{10} (mol/h)
CH_4	35.04	27.22	11.57	11.57	0.00	11.57	0.00	11.57	0.00	0.00
H_2O	41.00	56.64	29.02	26.91	0.00	26.91	0.00	72.68	0.00	111.08
O_2	15.64	0.00	0.00	0.00	0.78	0.00	22.89	0.00	30.76	0.00
N_2	58.85	58.85	58.85	58.85	2.95	61.80	86.10	147.90	115.73	263.63
CO	0.00	0.00	3.68	1.57	0.00	0.0029	0.00	0.00	0.00	0.00
CO_2	0.00	7.82	19.79	21.90	0.00	23.47	0.00	23.47	0.00	35.04
H_2	0.00	0.00	58.92	61.03	0.00	61.03	0.00	15.26	0.00	0.00

4.2. Reactor Sizing

Model equations for IPOX reactor (Equations 3.32-3.39 and 3.66), WGS converter (Equations 3.40-3.45 and 3.66) and PROX reactor (Equations 3.46-3.50 and 3.66) are used to size, i.e. determine the amount (weight) of the catalyst packed within these units. This is achieved via a 'trial-and-error' type solution and also by using the results of the material balances presented in Tables 4.1-4.6 as boundary conditions: Flow rates of components from material balances and typical stream temperatures obtained from literature (Ma *et al.*, 1996; Amadeo and Laborde, 1995; Sun *et al.*, 2005; Sedmak *et al.*, 2003; Santarelli and Torchio, 2007) are used as boundary conditions in reactor simulations. An arbitrary catalyst weight value is assigned to determine the integration span for the non-linear differential model equations which are solved using a stiff, variable order ODE solver, the "ode15s" function of the MATLAB^{TM} environment. The simulated exit flow rates from the reactor of interest are then compared with those obtained from the material balance calculations. The comparison is based on the hydrogen flow rates. This procedure is continued until the catalyst weight value, which gives hydrogen exit flow rates in accordance with the ones given in Tables 4.1-4.6, is obtained. Catalyst weight is accepted to be exact, if the difference between the hydrogen production rates obtained from material balance and simulation is below 10 per cent at the end of the simulation.

In consequence, reactor sizing procedure briefly explained above is repeated for two distinct feed ratios and three power type of PEM fuel cell (Feed ratios: (CH_4/O_2, H_2O/CH_4) = (2.24, 1.17), (1.89, 1.56); PEMFC power outputs: 500, 1000 and 1500 W), resulting in six different feed composition/hydrogen throughput rate configurations of the fuel processor system.

4.2.1. 500 W PEMFC Operation

Simulation results for 500 W PEMFC operation are tabulated in Tables 4.7-4.9. Temperature and flow rate variations in IPOX, WGS and PROX are shown in Figures 4.2-4.13 for two distinct feed ratios.

Table 4.7. Simulation results for 500 W PEMFC system

(CH_4/O_2 = 1.89, H_2O/CH_4 = 1.56)

Stream / Component	F_1 (mol/h)	F_3 (mol/h)	F_4 (mol/h)	F_5 (mol/h)	F_6 (mol/h)
CH_4	12.36	4.64	4.64	0.00	4.64
H_2O	19.28	15.09	12.79	0.00	12.8
O_2	6.54	2.3	0.00	0.29	0.00
N_2	24.60	24.60	24.60	1.09	25.7
CO	0.00	2.87	0.58	0.00	0.000334
CO_2	0.00	5.05	7.34	0.00	7.92
H_2	0.00	19.73	22.48	0.00	22.48

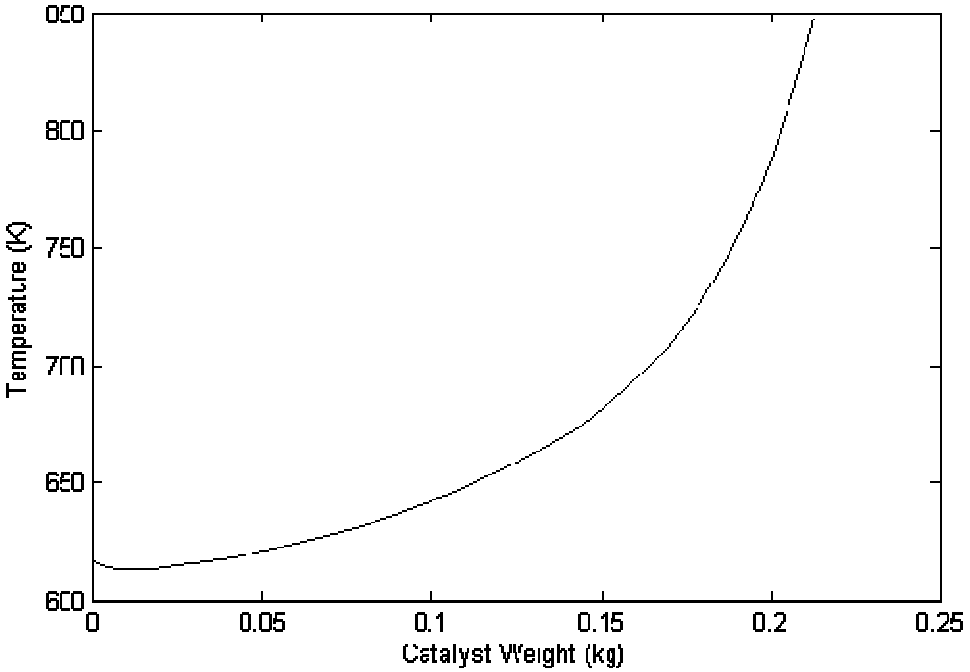

Figure 4.2. Temperature profile in IPOX reactor for 500 W PEMFC operation

(CH_4/O_2 = 1.89, H_2O/CH_4 = 1.56)

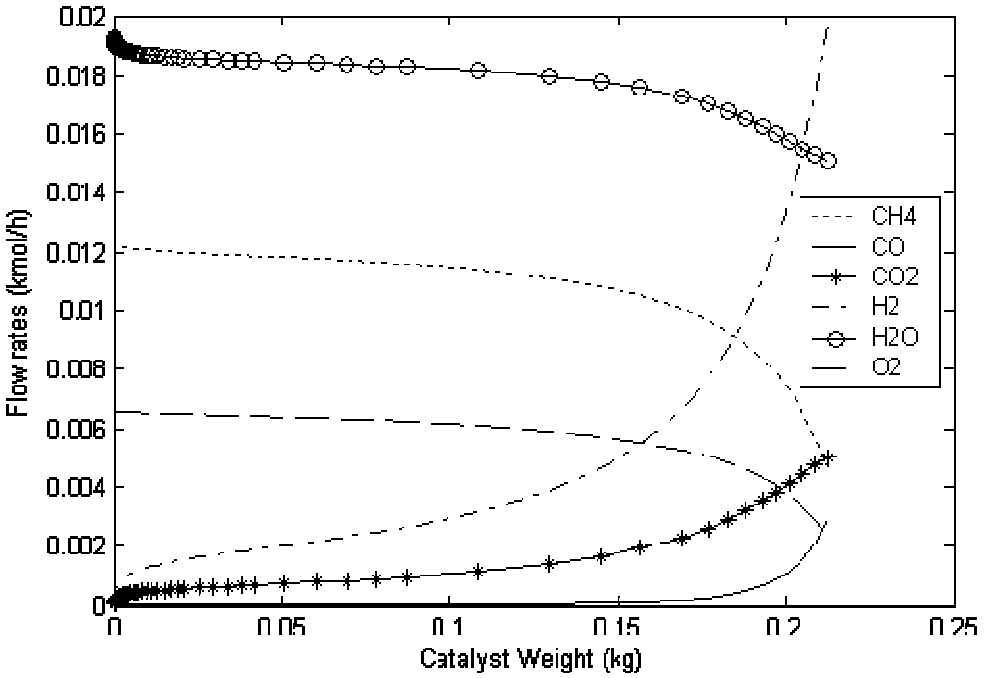

Figure 4.3. Flow rate variations in IPOX reactor for 500 W PEMFC operation (CH_4/O_2 = 1.89, H_2O/CH_4 = 1.56)

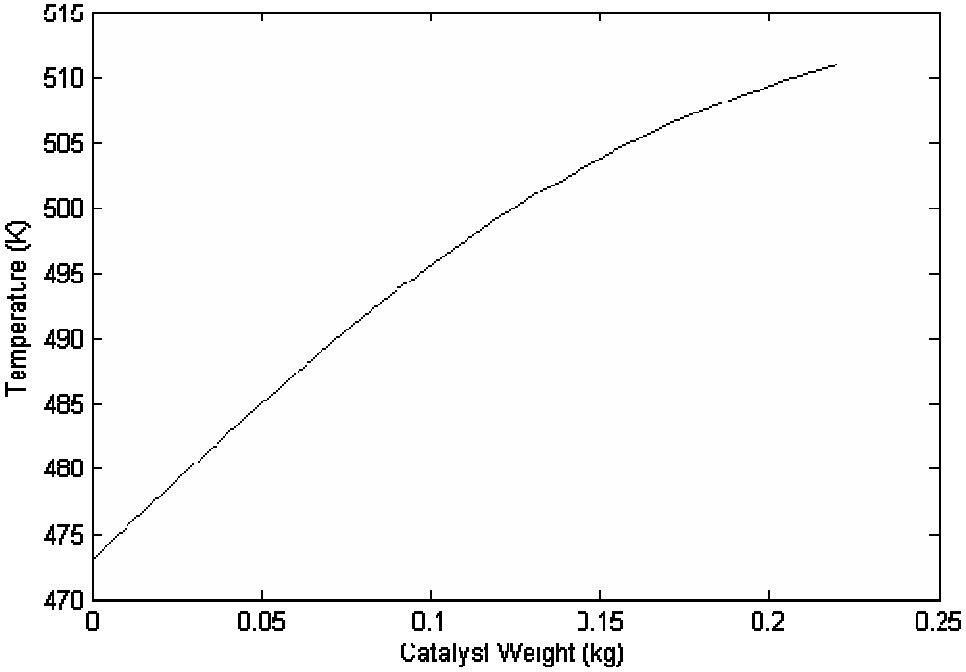

Figure 4.4. Temperature profile in WGS converter for 500 W PEMFC operation (CH_4/O_2 = 1.89, H_2O/CH_4 = 1.56)

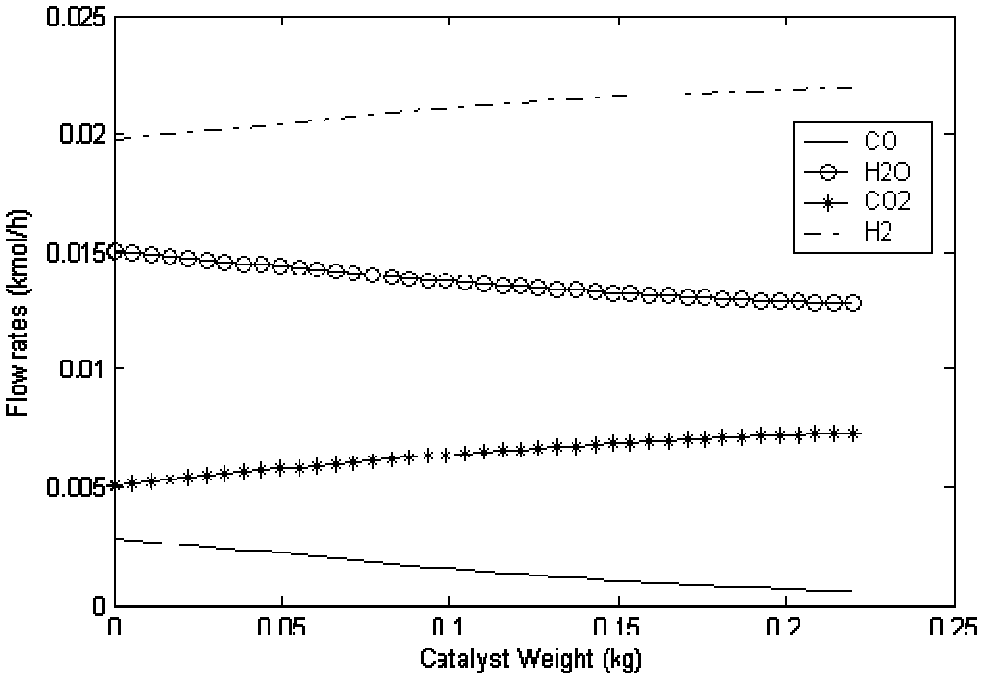

Figure 4.5. Flow rate variations in WGS converter for 500 W PEMFC operation (CH_4/O_2 = 1.89, H_2O/CH_4 = 1.56)

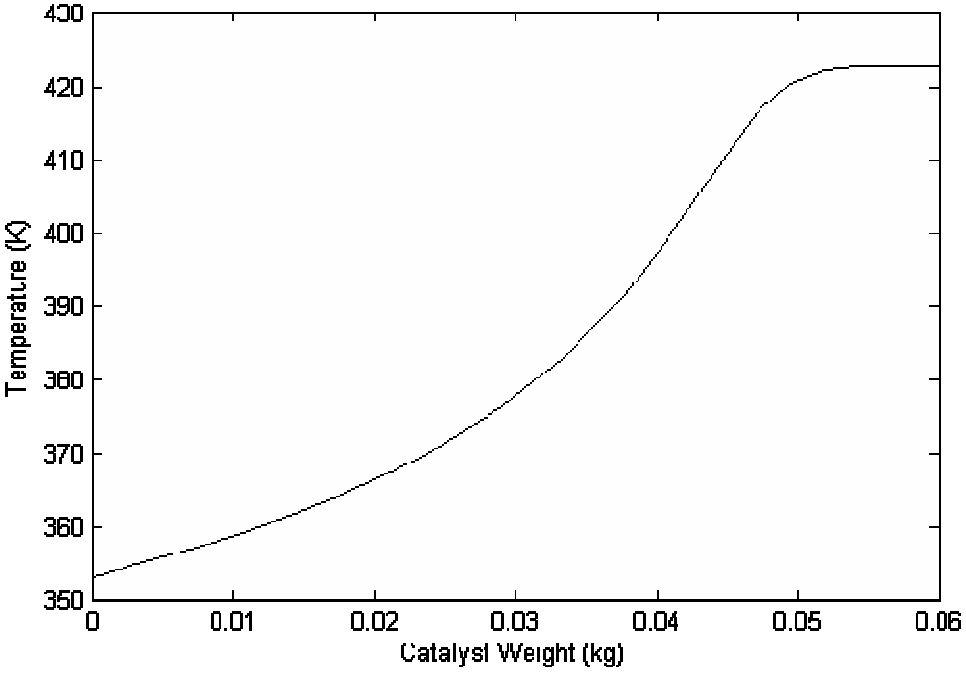

Figure 4.6. Temperature profile in PROX reactor for 500 W PEMFC operation (CH_4/O_2 = 1.89, H_2O/CH_4 = 1.56)

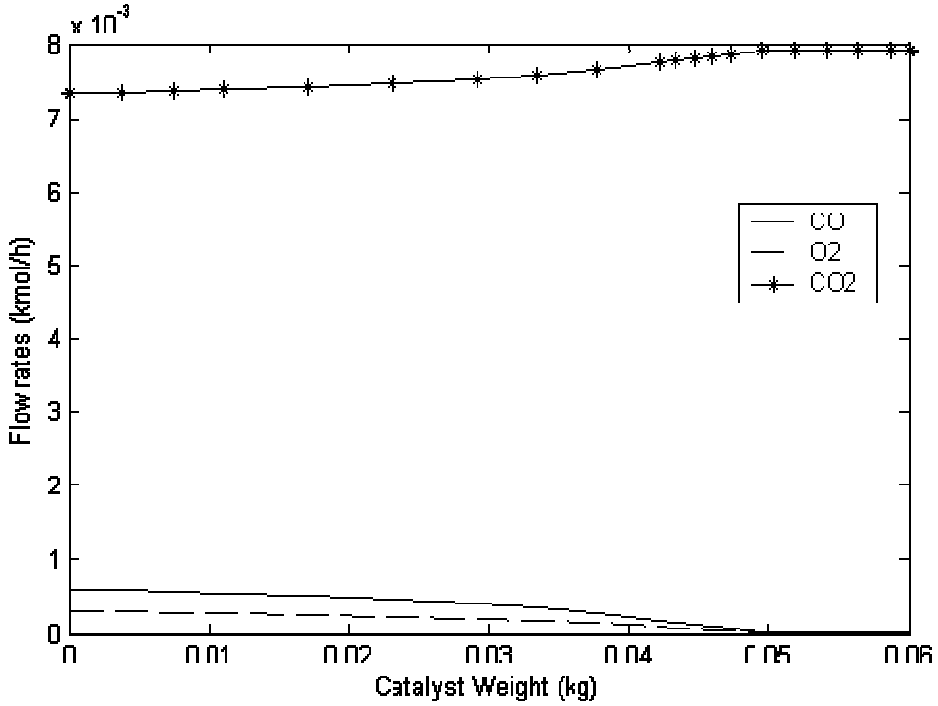

Figure 4.7. Flow rate variations in PROX reactor for 500 W PEMFC operation (CH_4/O_2 = 1.89, H_2O/CH_4 = 1.56)

Table 4.8. Simulation results for 500 W PEMFC system (CH_4/O_2 = 2.24, H_2O/CH_4 = 1.17)

Stream / Component	F_1 (mol/h)	F_3 (mol/h)	F_4 (mol/h)	F_5 (mol/h)	F_6 (mol/h)
CH_4	11.70	3.61	3.61	0.00	3.61
H_2O	13.69	10.43	7.06	0.00	7.06
O_2	5.22	0.76	0.00	0.37	0.00
N_2	19.65	19.65	19.65	1.79	21.44
CO	0.00	4.11	0.74	0.00	0.00057
CO_2	0.00	4.17	7.53	0.00	8.27
H_2	0.00	19.53	22.89	0.00	22.89

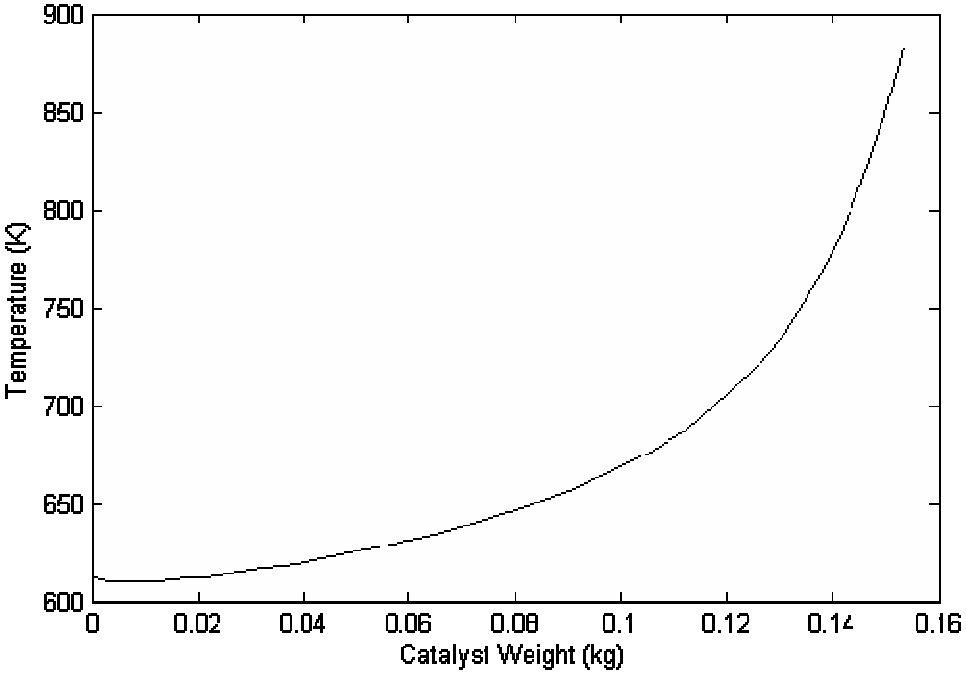

Figure 4.8. Temperature profile in IPOX reactor for 500 W PEMFC operation (CH_4/O_2 = 2.24, H_2O/CH_4 = 1.17)

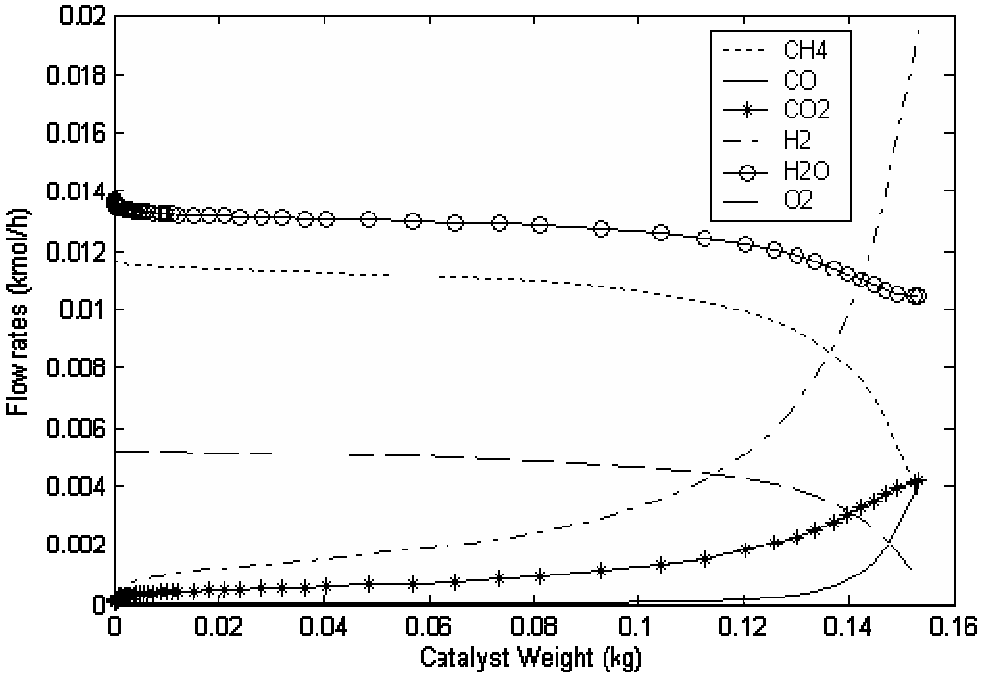

Figure 4.9. Flow rate variations in IPOX reactor for 500 W PEMFC operation (CH_4/O_2 = 2.24, H_2O/CH_4 = 1.17)

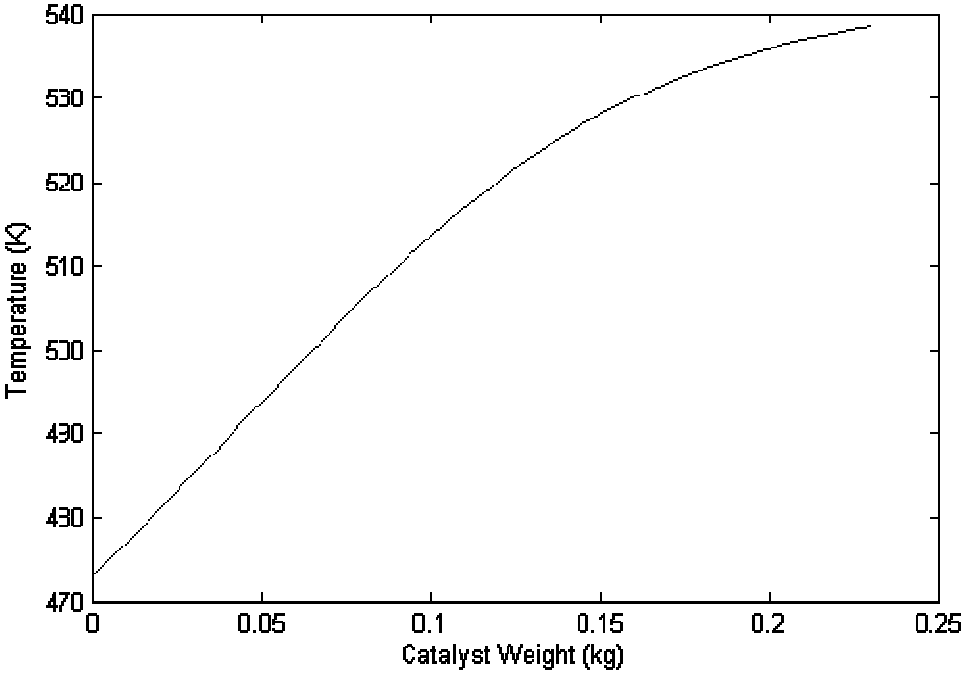

Figure 4.10. Temperature profile in WGS converter for 500 W PEMFC operation (CH_4/O_2 = 2.24, H_2O/CH_4 = 1.17)

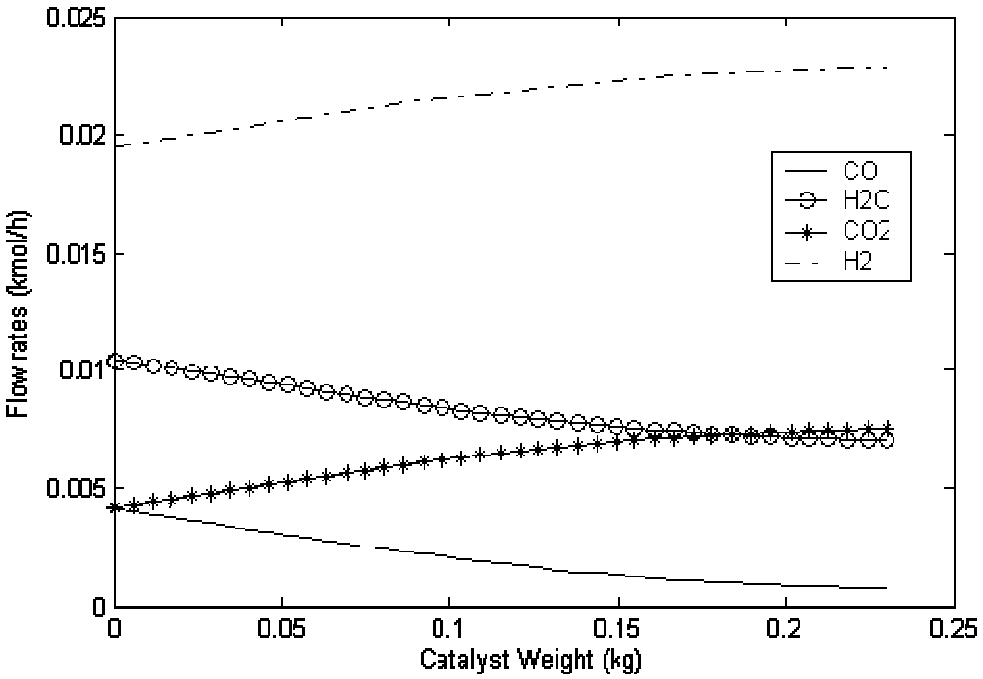

Figure 4.11. Flow rate variations in WGS converter for 500 W PEMFC operation (CH_4/O_2 = 2.24, H_2O/CH_4 = 1.17)

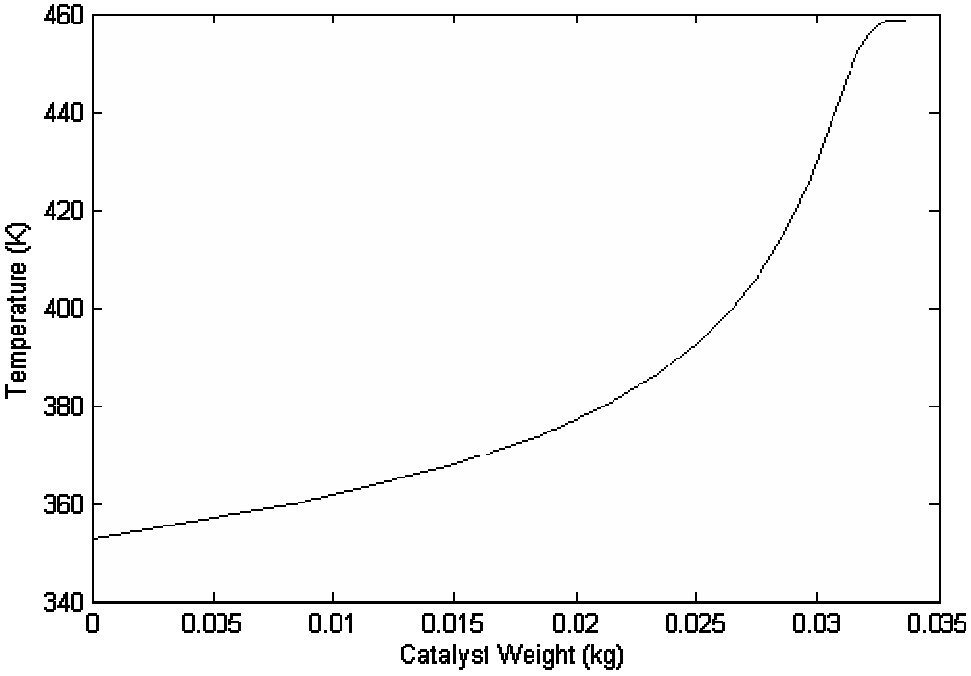

Figure 4.12. Temperature profile in PROX reactor for 500 W PEMFC operation (CH_4/O_2 = 2.24, H_2O/CH_4 = 1.17)

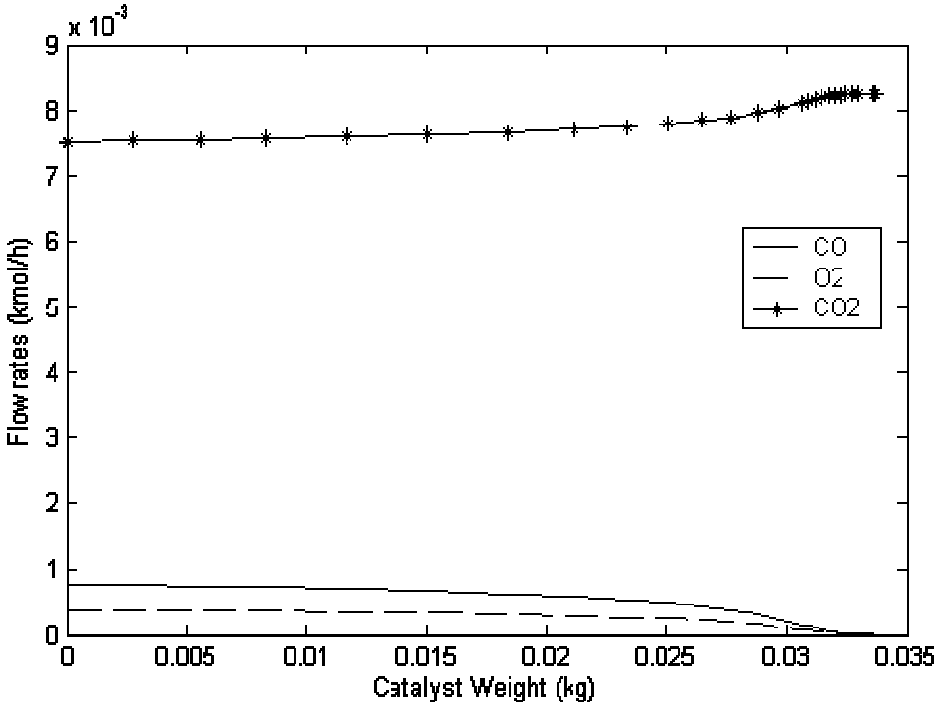

Figure 4.13. Flow rate variations in PROX reactor for 500 W PEMFC operation (CH_4/O_2 = 2.24, H_2O/CH_4 = 1.17)

Inlet and outlet temperatures of each reactor, catalyst quantities packed into the reactors and carbon monoxide levels at exit of WGS and PROX reactors are presented in Table 4.9 for 500 W operation. It is worth noting that, regardless of the feed condition, inlet temperatures for WGS and PROX reactors are at 473 and 353 K, respectively, since these temperatures are assumed to be obtained after cooling via the heat exchangers shown in Figure 4.1. On the other hand, the inlet temperature of the IPOX reactor is assumed to be equal to the light-off temperature of methane, which depends on the CH_4/O_2 ratio. Light-off temperatures of methane as a function of CH_4/O_2 over $Pt/\delta\text{-}Al_2O_3$ catalyst is given in Table 2.3. As a result, 620 and 627 K are determined as inlet temperatures of IPOX reactor for CH_4/O_2 ratios of 2.24 and 1.89 respectively, as explained in Section 3.1.1.

The results in Tables 4.7 and 4.8 show that component flow rates obtained from reactor simulations are in approximate agreement with the preliminary material balance results given in Tables 4.1 and 4.2. The differences come mainly from the oxygen consumption during indirect partial oxidation reaction: in material balance calculations, oxygen is assumed to be consumed completely in IPOX. However, during the simulations, it is aimed to obtain a hydrogen production rate that should be ideally equal to the value calculated from the material balance results. This objective in the calculation scheme has led to some oxygen remaining in the reaction medium. Therefore methane conversion in total oxidation became smaller than predicted in the material balance and, due to higher quantity of remaining methane, steam reforming conversion became higher. The reason of low flow rates of H_2O, CO_2 and high flow rates of CH_4, CO in the exit stream of IPOX reactor (F_3) can therefore be explained by lower amount of oxygen consumption. Flow rate difference at WGS converter exit (F_4) is because of aiming the simulated CO flow rate at effluent stream to be same with material balance results with the constraint that the CO content in WGS exit has to be below 2 mol per cent. Higher conversion of carbon monoxide in water-gas shift reaction causes consumption of more steam and production of more CO_2 and H_2 which is still in the limit that is designated for the difference of hydrogen production rates. CO conversion in preferential oxidation is almost same; however, difference in CO and CO_2 flow rates in exit stream of PROX reactor (F_6) comes from the difference at the inlet stream (F_4). For both feed ratios, hydrogen production rates from reactor simulations and material balance calculations are almost equal to each other, which indicate that the termination criterion for trial and error calculations is satisfied.

Table 4.9. Simulation outputs for CH_4/O_2 = 2.24&H_2O/CH_4 = 1.17 and CH_4/O_2 = 1.89&H_2O/CH_4 = 1.56 at IPOX reactor inlet in 500 W PEMFC operation

	IPOX reactor		WGS converter		PROX reactor	
	1.89&1.56	2.24&1.17	1.89&1.56	2.24&1.17	1.89&1.56	2.24&1.17
Inlet temperature (K)	627	620	473	473	353	353
Exit temperature (K)	848	884	511	539	423	459
Catalyst weight (g)	213	154	220	230	60	34
CO level †	--	--	0.8 *	1.2 *	4.5 **	9.0 **

† CO level at the exit of the reactor, in mol per cent after WGS, in ppm after PROX
* CO level has to be below 2 mol per cent at WGS reactor outlet
** CO level has to be below 10 ppm at PROX reactor outlet.

The results in Table 4.9 also indicate that at both feed ratios, amount of catalyst packed in WGS converter is greater than needed for the other reactors. This is expected since, over a Cu-based catalyst, WGS is a slower reaction than IPOX and PROX (Zalc and Löffler, 2002). In addition, amount of catalyst packed in WGS reactor is higher for 2.24&1.17 than 1.89&1.56 feed ratio because the former has higher carbon monoxide amount entering WGS reactor, i.e. higher catalyst amount is needed to obtain higher carbon monoxide conversion, which also results in elevated exit temperatures due to the exothermicity of the water-gas shift reaction. Furthermore, carbon monoxide concentrations at the exit of WGS and PROX reactors are below the limits of 2 mol per cent and 10 ppm, respectively.

If the two feed ratios are compared, it can be seen that the feed ratio of 2.24&1.17 leads to formation of elevated temperatures at the exit of reactors. This may be because of the higher conversion of exothermic total oxidation reaction at 2.24&1.17, which is inference of higher oxygen conversion (85 per cent in 2.24&1.17, 64 per cent in 1.89&1.56). Possible occurrence of reverse water-gas shift reaction in 1.89&1.56 may be the reason of elevated temperature of 2.24&1.17 at PROX reactor exit. According to the Tables 4.7 and 4.8, 30-40 per cent of the product stream (F_6) is hydrogen for both feed ratios on wet basis. There is also inert nitrogen as much as hydrogen in product stream which requires downstream processing if high purity hydrogen is needed. In such cases, oxygen may also be used as the oxidant rather than air.

4.2.2. 1000 W PEMFC Operation

Simulation results for 1000 W PEMFC operation are presented in Tables 4.10-4.12. Temperature and flow rate profiles in IPOX, WGS and PROX reactors are shown in Figures 4.14-4.25 for two feed ratios.

Table 4.10. Simulation results for 1000 W PEMFC system

(CH_4/O_2 = 1.89, H_2O/CH_4 = 1.56)

Stream / Component	F_1 (mol/h)	F_3 (mol/h)	F_4 (mol/h)	F_5 (mol/h)	F_6 (mol/h)
CH_4	24.72	9.17	9.17	0.00	9.17
H_2O	38.56	30.23	25.60	0.00	25.60
O_2	13.08	4.50	0.00	0.55	0.00
N_2	49.20	49.20	49.20	2.07	51.27
CO	0.00	5.73	1.10	0.00	0.000305
CO_2	0.00	10.02	14.64	0.00	15.74
H_2	0.00	39.53	44.15	0.00	44.15

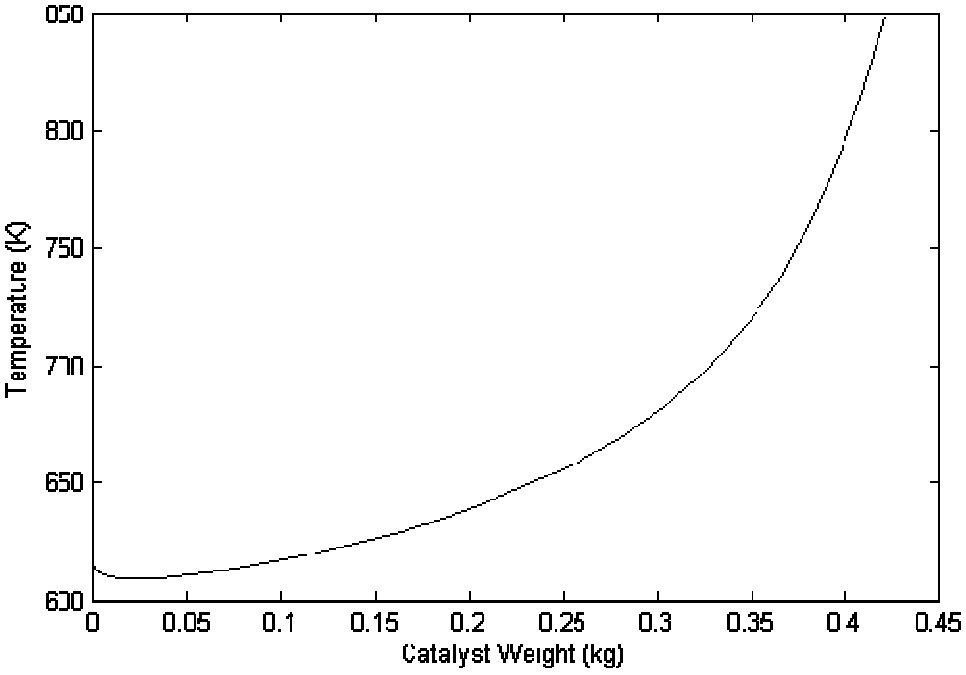

Figure 4.14. Temperature profile in IPOX reactor for 1000 W PEMFC operation

(CH_4/O_2 = 1.89, H_2O/CH_4 = 1.56)

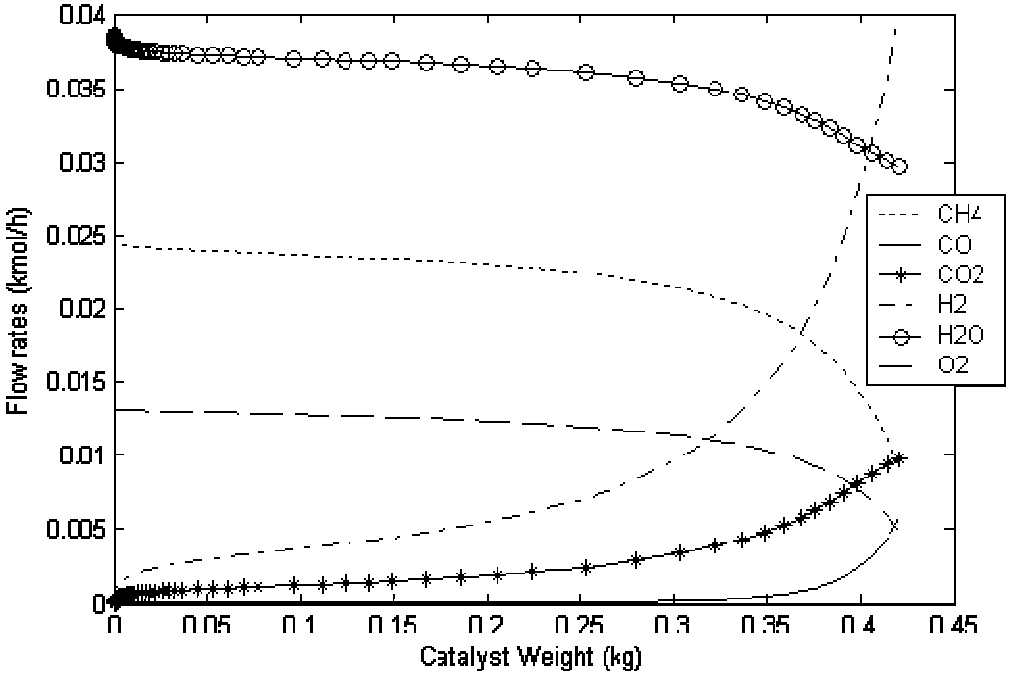

Figure 4.15. Flow rate variations in IPOX reactor for 1000 W PEMFC operation (CH_4/O_2 = 1.89, H_2O/CH_4 = 1.56)

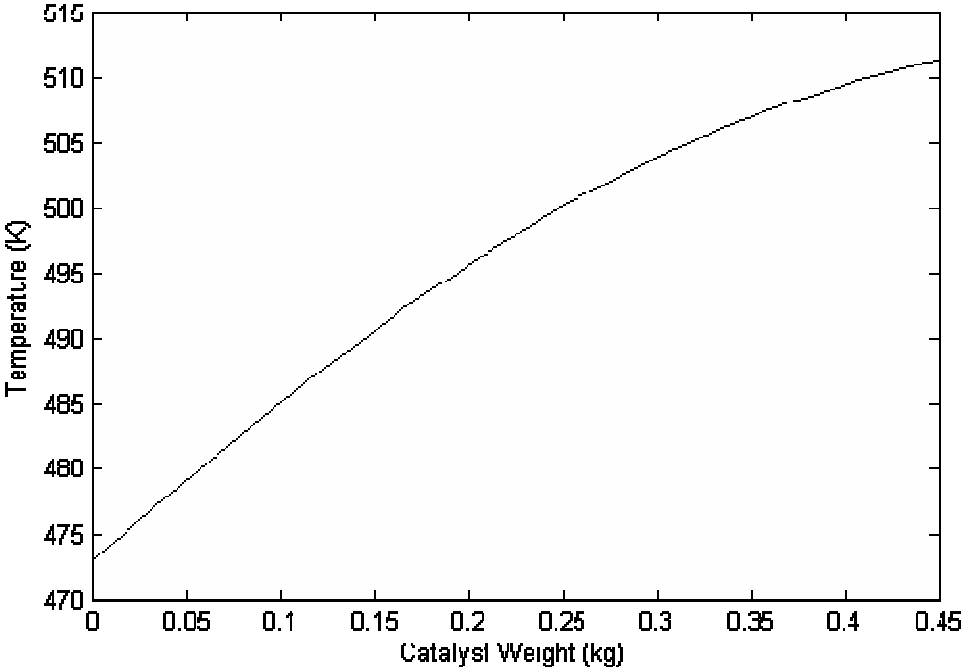

Figure 4.16. Temperature profile in WGS converter for 1000 W PEMFC operation (CH_4/O_2 = 1.89, H_2O/CH_4 = 1.56)

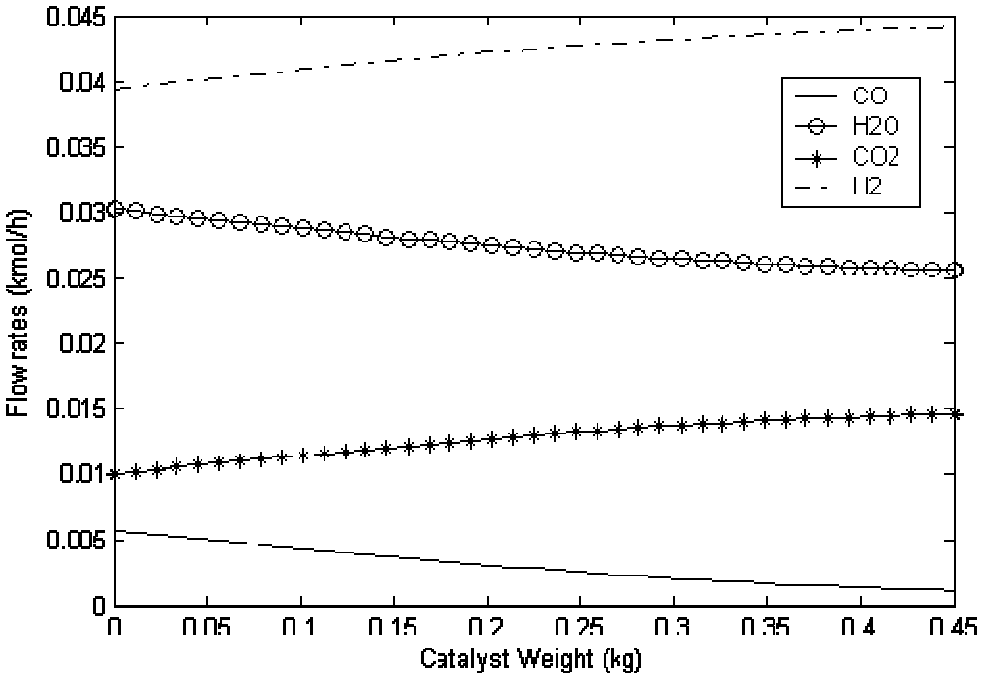

Figure 4.17. Flow rate variations in WGS converter for 1000 W PEMFC operation (CH_4/O_2 = 1.89, H_2O/CH_4 = 1.56)

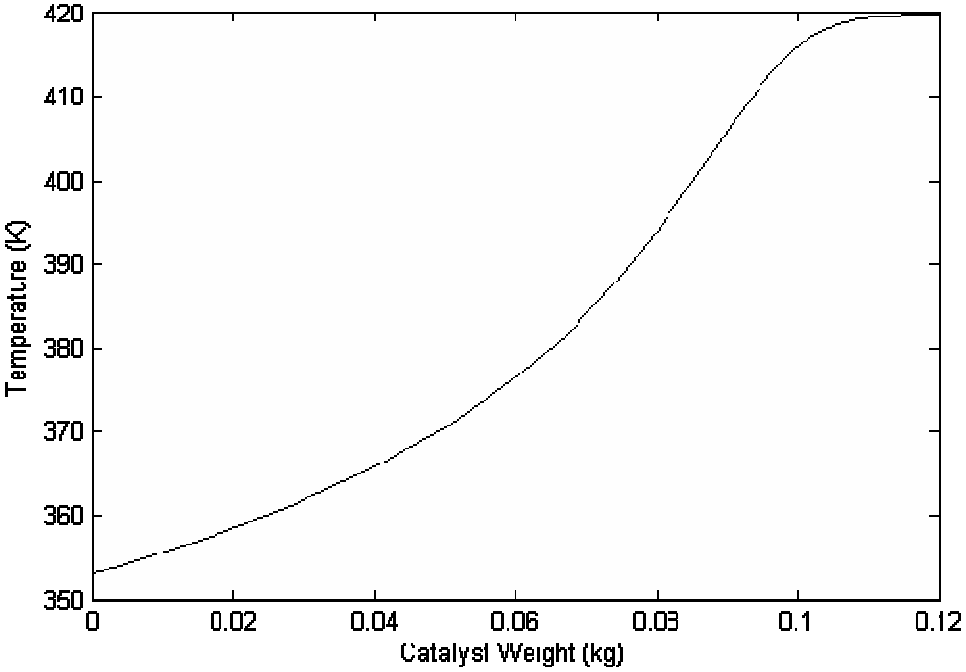

Figure 4.18. Temperature profile in PROX reactor for 1000 W PEMFC operation (CH_4/O_2 = 1.89, H_2O/CH_4 = 1.56)

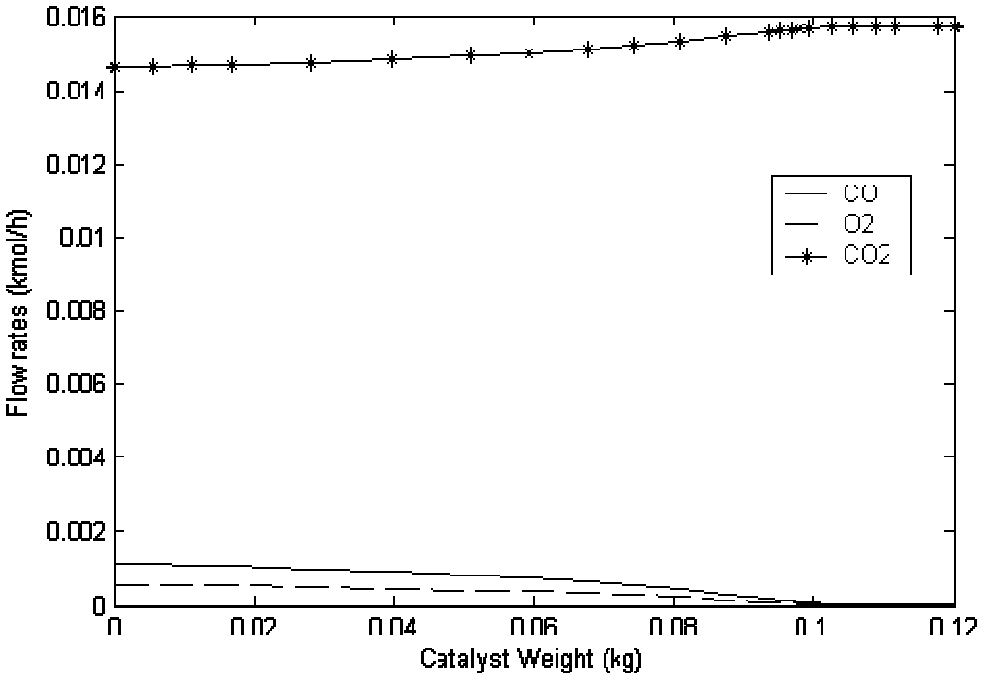

Figure 4.19. Flow rate variations in PROX reactor for 1000 W PEMFC operation (CH_4/O_2 = 1.89, H_2O/CH_4 = 1.56)

Table 4.11. Simulation results for 1000 W PEMFC system (CH_4/O_2 = 2.24, H_2O/CH_4 = 1.17)

Stream / Component	F_1 (mol/h)	F_3 (mol/h)	F_4 (mol/h)	F_5 (mol/h)	F_6 (mol/h)
CH_4	23.40	7.01	7.01	0.00	7.01
H_2O	27.38	20.84	14.03	0.00	14.03
O_2	10.45	1.40	0.00	0.755	0.00
N_2	39.30	39.30	39.30	2.84	42.14
CO	0.00	8.32	1.51	0.00	0.00031
CO_2	0.00	8.27	15.07	0.00	16.58
H_2	0.00	39.42	46.22	0.00	46.22

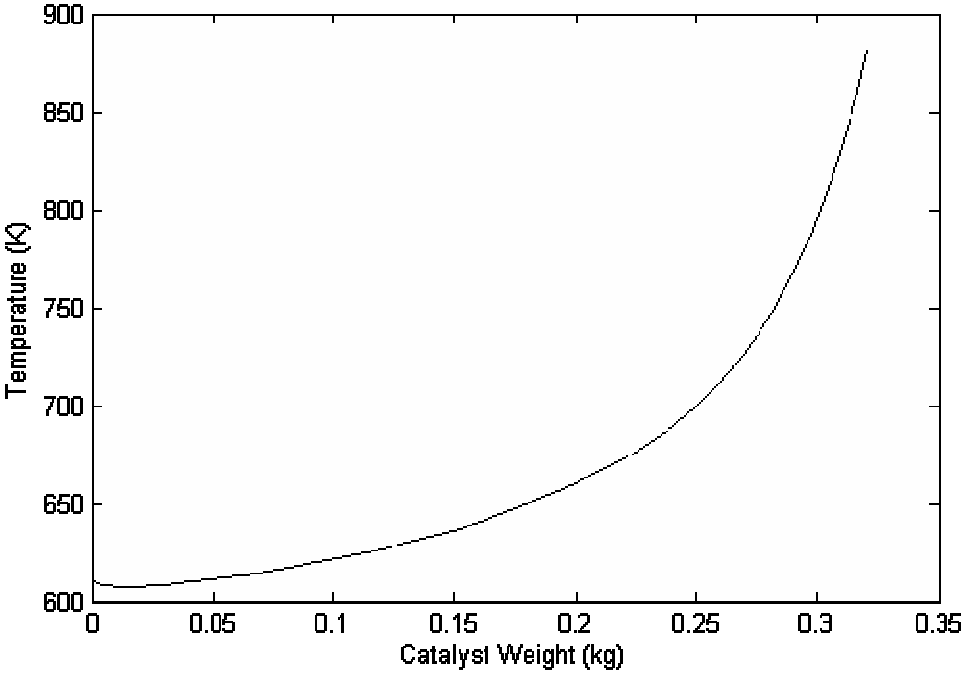

Figure 4.20. Temperature profile in IPOX reactor for 1000 W PEMFC operation (CH_4/O_2 = 2.24, H_2O/CH_4 = 1.17)

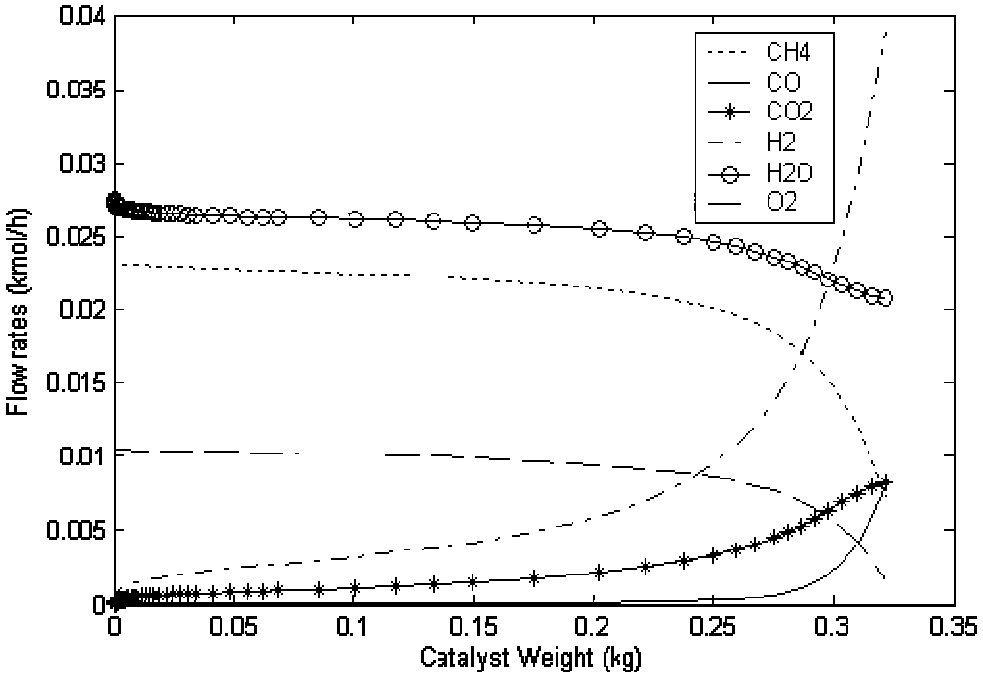

Figure 4.21. Flow rate variations in IPOX reactor for 1000 W PEMFC operation (CH_4/O_2 = 2.24, H_2O/CH_4 = 1.17)

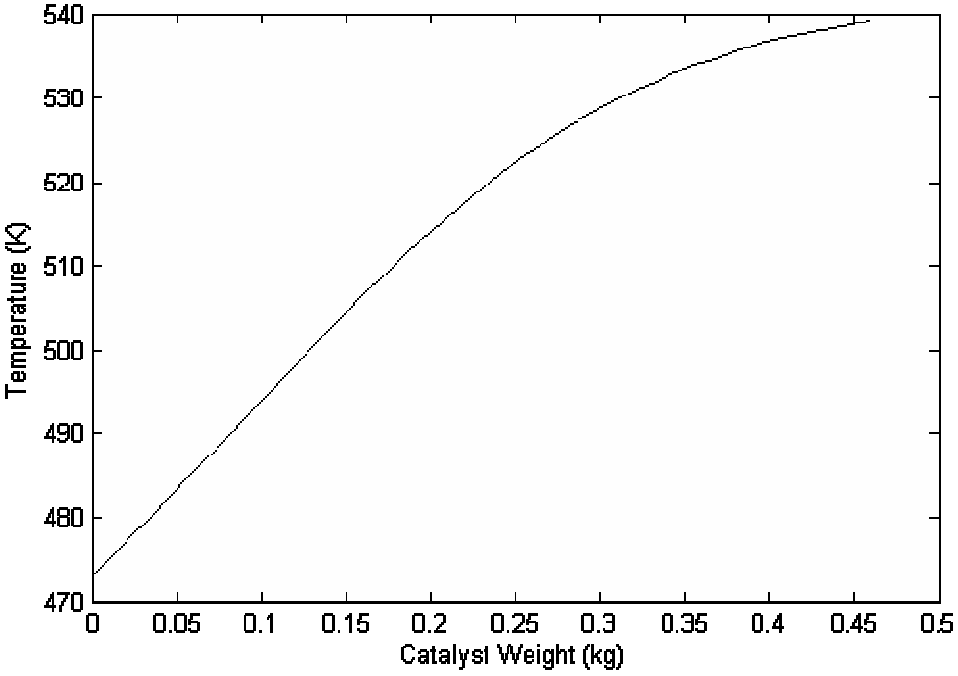

Figure 4.22. Temperature profile in WGS converter for 1000 W PEMFC operation (CH_4/O_2 = 2.24, H_2O/CH_4 = 1.17)

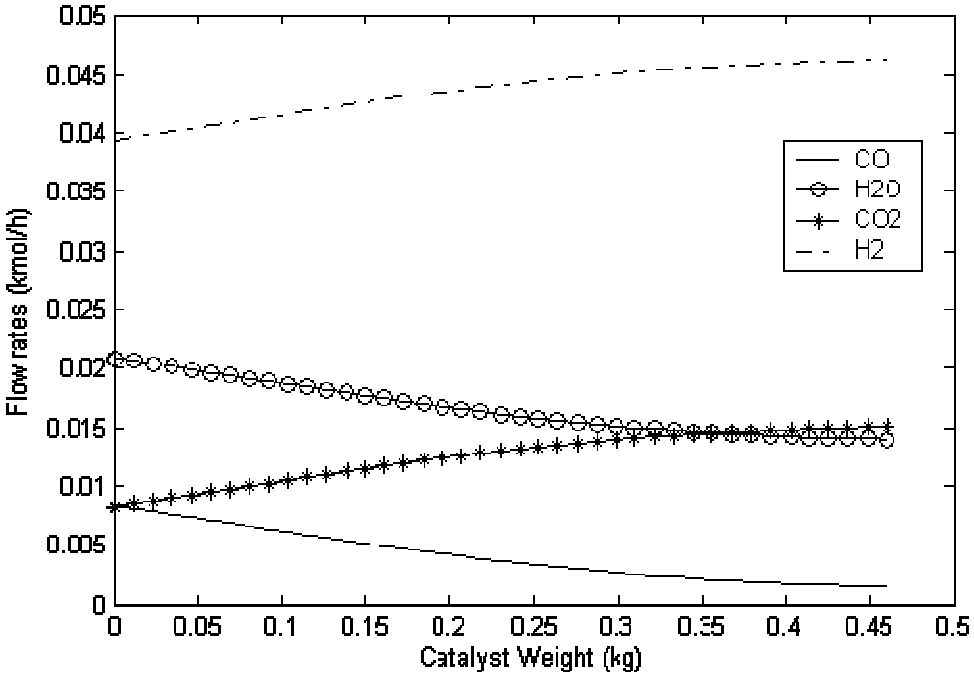

Figure 4.23. Flow rate variations in WGS converter for 1000 W PEMFC operation (CH_4/O_2 = 2.24, H_2O/CH_4 = 1.17)

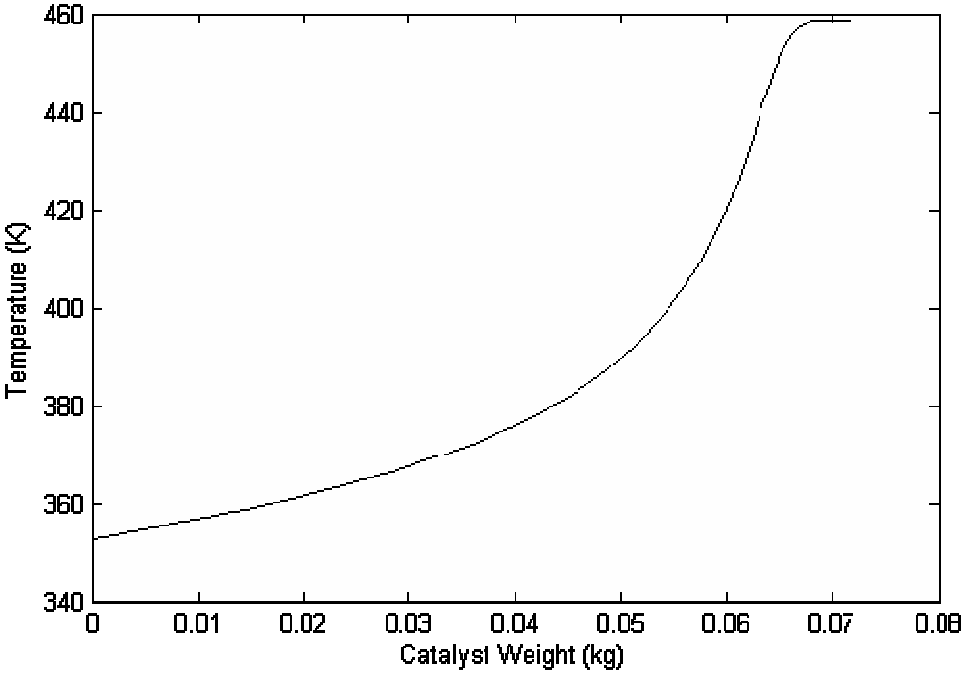

Figure 4.24. Temperature profile in PROX reactor for 1000 W PEMFC operation (CH_4/O_2 = 2.24, H_2O/CH_4 = 1.17)

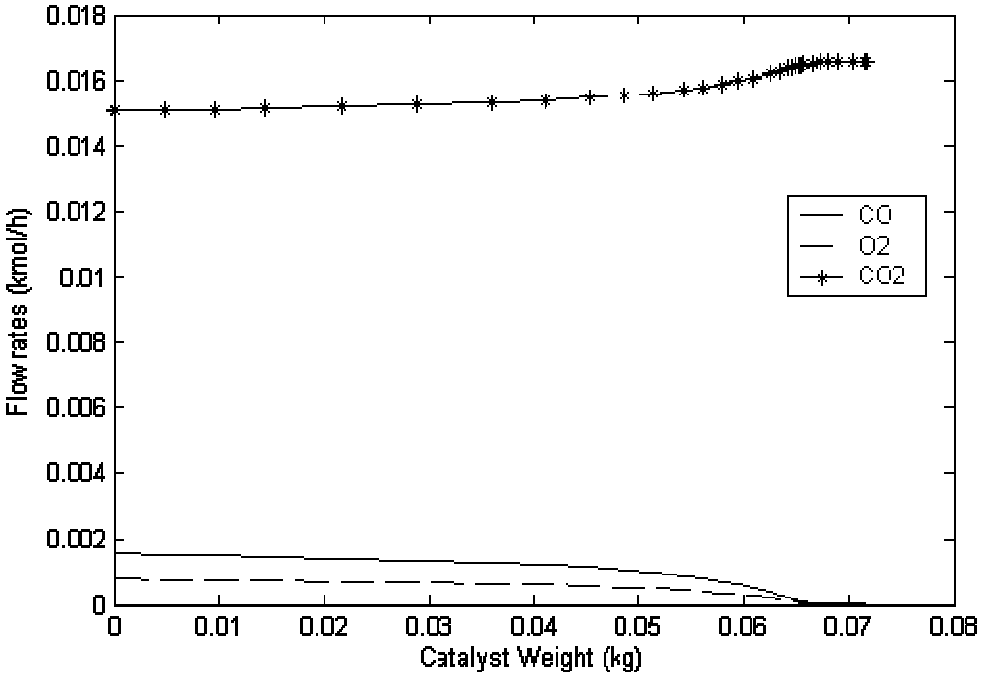

Figure 4.25. Flow rate variations in PROX reactor for 1000 W PEMFC operation (CH_4/O_2 = 2.24, H_2O/CH_4 = 1.17)

Table 4.12 gives the inlet and outlet temperatures of the reactors, catalyst quantities and carbon monoxide levels at WGS converter and PROX reactor exit streams.

It can be seen that the simulation outputs given in Tables 4.10-4.11 and material balance results given in Tables 4.3-4.4 are in general agreement. The differences come mainly from oxygen consumption during IPOX, as explained for 500 W operation in Section 4.2.1.

2.24&1.17 feed ratio needs smaller amount of catalyst for hydrogen production by 1000 W PEMFC operation than 1.89&1.56 in all reactors except WGS converter like in 500 W operation. 1.89&1.56 needs much more IPOX catalyst, which is because 2.24&1.17 has higher total oxidation conversion due to the oxygen consumption and consequently higher steam reforming conversion. The small difference between the catalyst demands for WGS is because 2.24&1.17 operation has more CO amount entering the WGS converter and consequently higher catalyst is needed for higher CO conversion. More PROX catalyst demand for 1.89&1.56 may be because of possible occurrence of reverse water-gas shift reaction, as stated in Section 4.2.1.

As in the case of 500 W operation, CO levels are below the limits of 2 mol per cent and 10 ppm (Table 4.12). Product stream is therefore convenient for PEMFC operation, where also inert nitrogen as much as hydrogen, that requires downstream processing in high purity hydrogen demanding applications, is introduced within.

4.2.3. 1500 W PEMFC Operation

Simulation results are presented in Tables 4.13-4.15. Temperature and flow rate profiles within the reactors are shown in Figures 4.26-4.37.

Table 4.12. Simulation outputs for CH_4/O_2 = 2.24&H_2O/CH_4 = 1.17 and CH_4/O_2 = 1.89&H_2O/CH_4 = 1.56 at IPOX reactor inlet in 1000 W PEMFC operation

	IPOX reactor		WGS converter		PROX reactor	
	1.89&1.56	2.24&1.17	1.89&1.56	2.24&1.17	1.89&1.56	2.24&1.17
Inlet temperature (K)	627	620	473	473	353	353
Exit temperature (K)	849	885	511	539	420	459
Catalyst weight (g)	421	321	450	460	120	72
CO level †	--	--	0.8*	1.2*	2.1**	2.5**

† CO level at the exit of the reactor, in mol per cent after WGS, in ppm after PROX
* CO level has to be below 2 mol per cent at WGS reactor outlet
** CO level has to be below 10 ppm at PROX reactor outlet.

Table 4.13. Simulation results for 1500 W PEMFC system

(CH_4/O_2 = 1.89, H_2O/CH_4 = 1.56)

Stream / Component	F_1 (mol/h)	F_3 (mol/h)	F_4 (mol/h)	F_5 (mol/h)	F_6 (mol/h)
CH_4	37.08	14.20	14.20	0.00	14.20
H_2O	57.84	45.27	38.71	0.00	38.71
O_2	19.62	7.1	0.00	0.84	0.00
N_2	73.80	73.80	73.80	3.16	76.96
CO	0.00	8.23	1.68	0.00	0.000252
CO_2	0.00	14.83	20.78	0.00	22.46
H_2	0.00	58.41	64.96	0.00	64.96

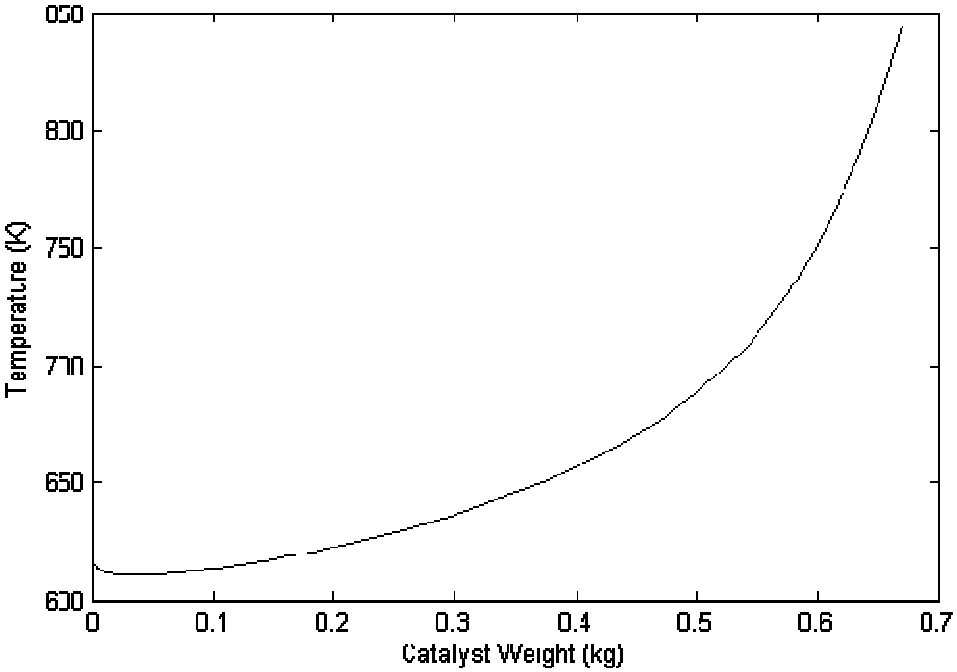

Figure 4.26. Temperature profile in IPOX reactor for 1500 W PEMFC operation

(CH_4/O_2 = 1.89, H_2O/CH_4 = 1.56)

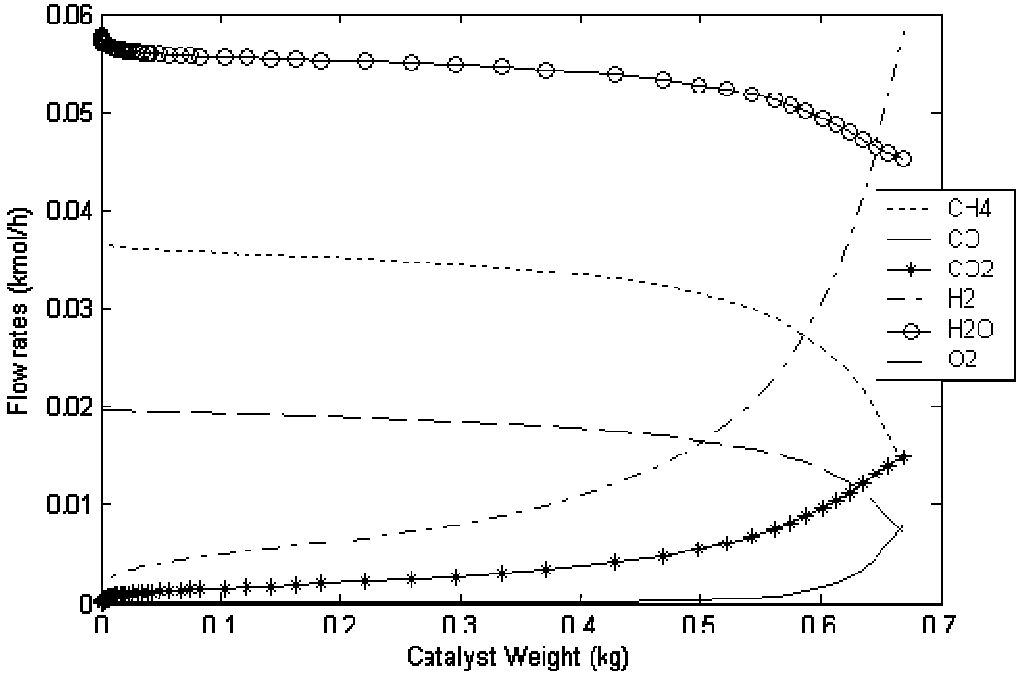

Figure 4.27. Flow rate variations in IPOX reactor for 1500 W PEMFC operation (CH_4/O_2 = 1.89, H_2O/CH_4 = 1.56)

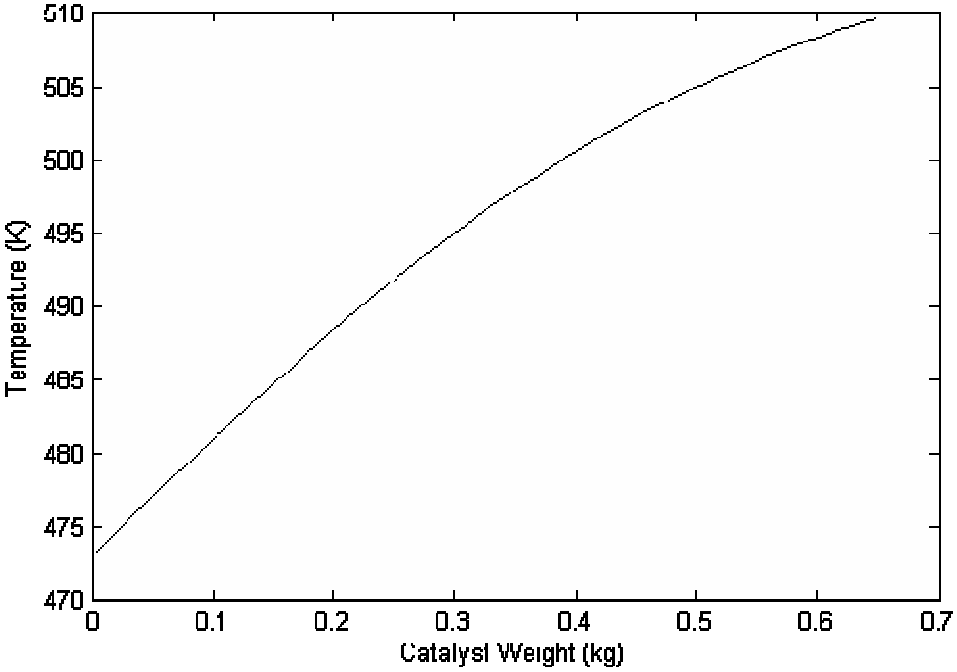

Figure 4.28. Temperature profile in WGS converter for 1500 W PEMFC operation (CH_4/O_2 = 1.89, H_2O/CH_4 = 1.56)

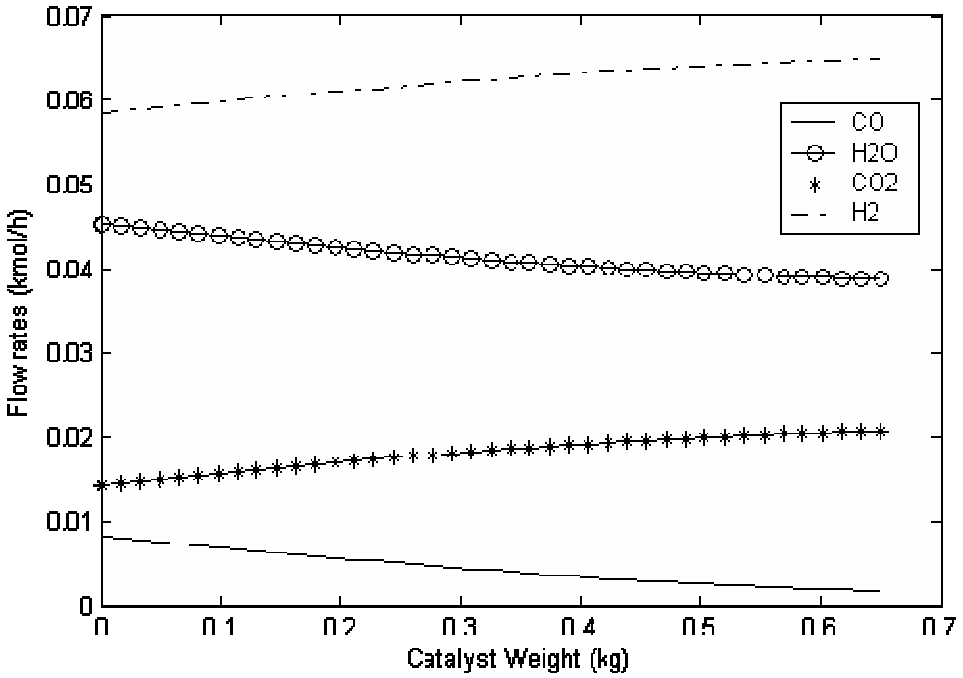

Figure 4.29. Flow rate variations in WGS converter for 1500 W PEMFC operation (CH_4/O_2 = 1.89, H_2O/CH_4 = 1.56)

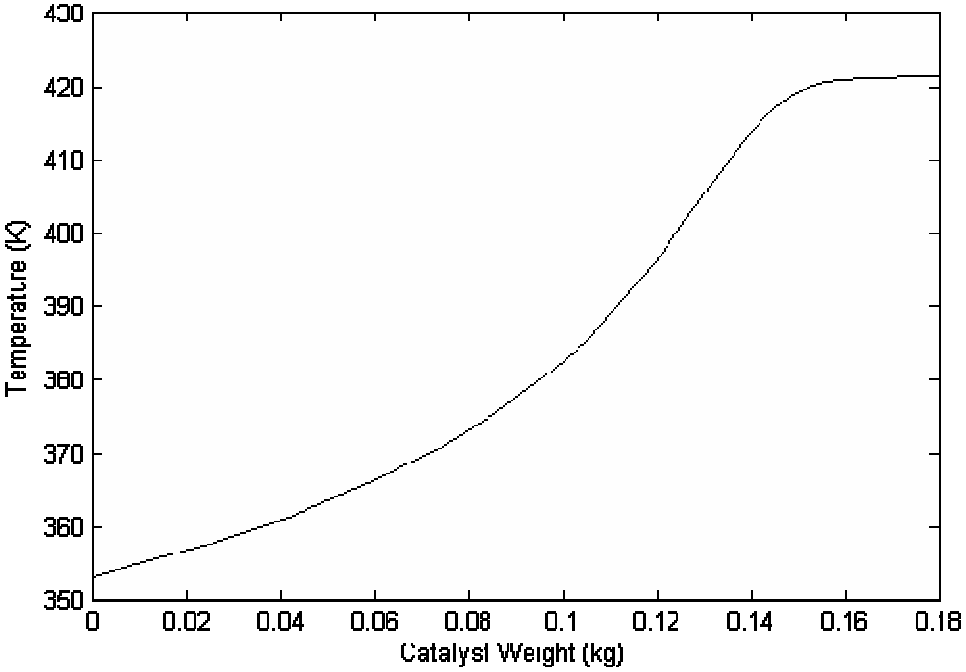

Figure 4.30. Temperature profile in PROX reactor for 1500 W PEMFC operation (CH_4/O_2 = 1.89, H_2O/CH_4 = 1.56)

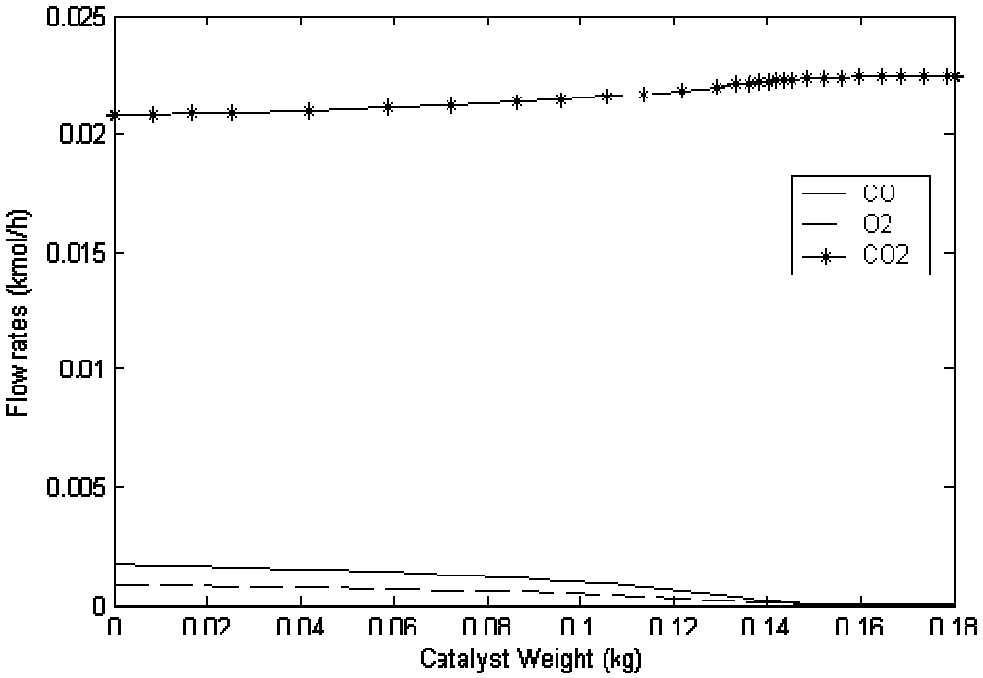

Figure 4.31. Flow rate variations in PROX reactor for 1500 W PEMFC operation (CH_4/O_2 = 1.89, H_2O/CH_4 = 1.56)

Table 4.14. Simulation results for 1500 W PEMFC system (CH_4/O_2 = 2.24, H_2O/CH_4 = 1.17)

Stream / Component	F_1 (mol/h)	F_3 (mol/h)	F_4 (mol/h)	F_5 (mol/h)	F_6 (mol/h)
CH_4	35.04	10.30	10.30	0.00	10.30
H_2O	41.00	31.20	20.9	0.00	20.9
O_2	15.64	2.14	0.00	1.122	0.00
N_2	58.84	58.84	58.84	4.217	63.06
CO	0.00	12.54	2.245	0.00	0.00024
CO_2	0.00	12.34	22.63	0.00	24.87
H_2	0.00	59.20	69.55	0.00	69.55

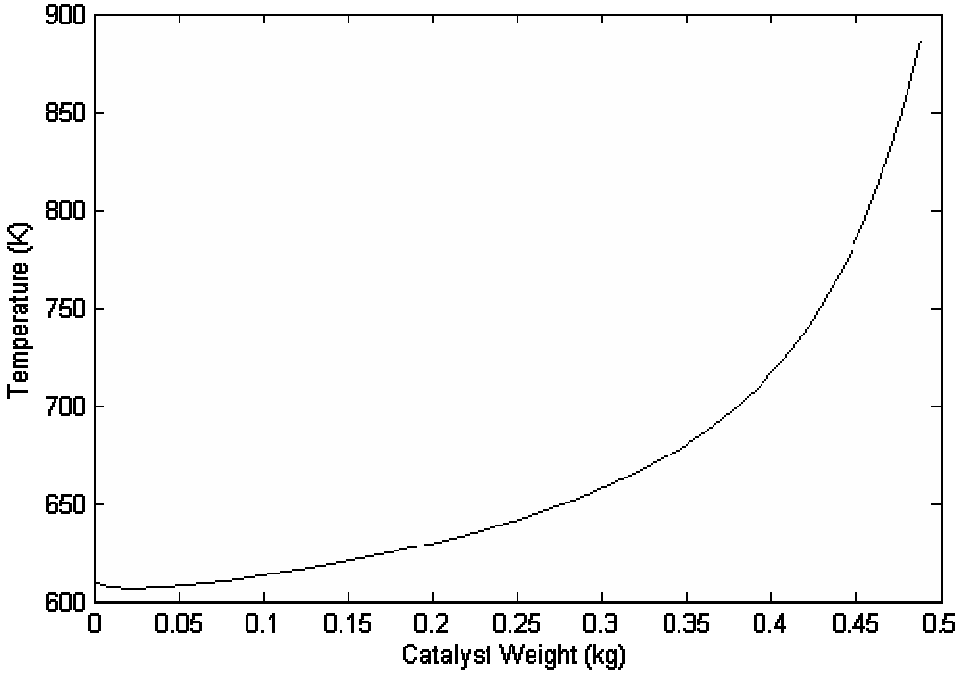

Figure 4.32. Temperature profile in IPOX reactor for 1500 W PEMFC operation (CH_4/O_2 = 2.24, H_2O/CH_4 = 1.17)

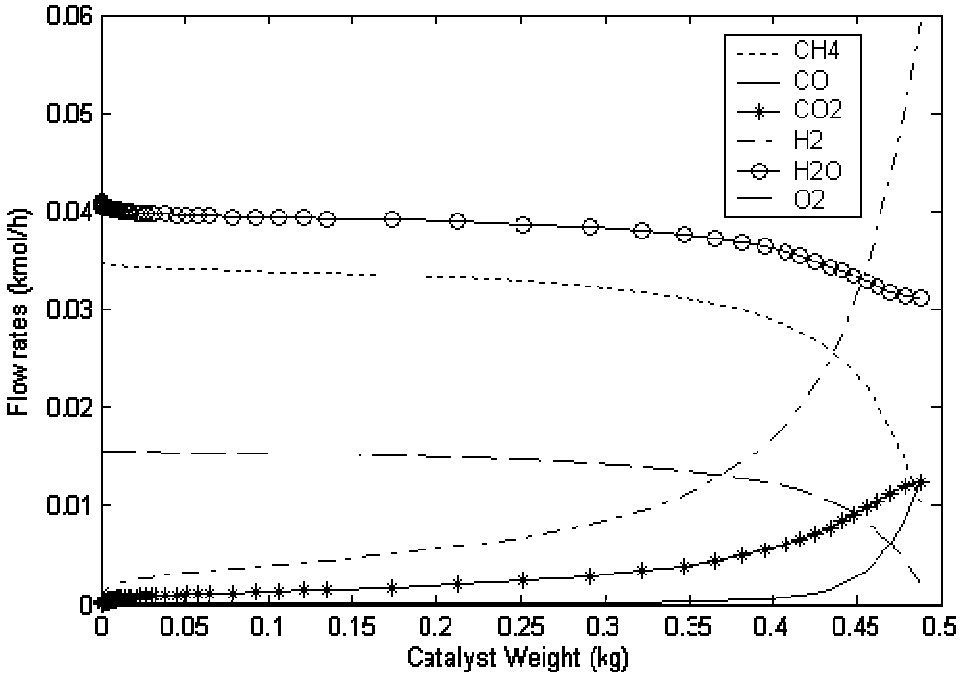

Figure 4.33. Flow rate variations in IPOX reactor for 1500 W PEMFC operation (CH_4/O_2 = 2.24, H_2O/CH_4 = 1.17)

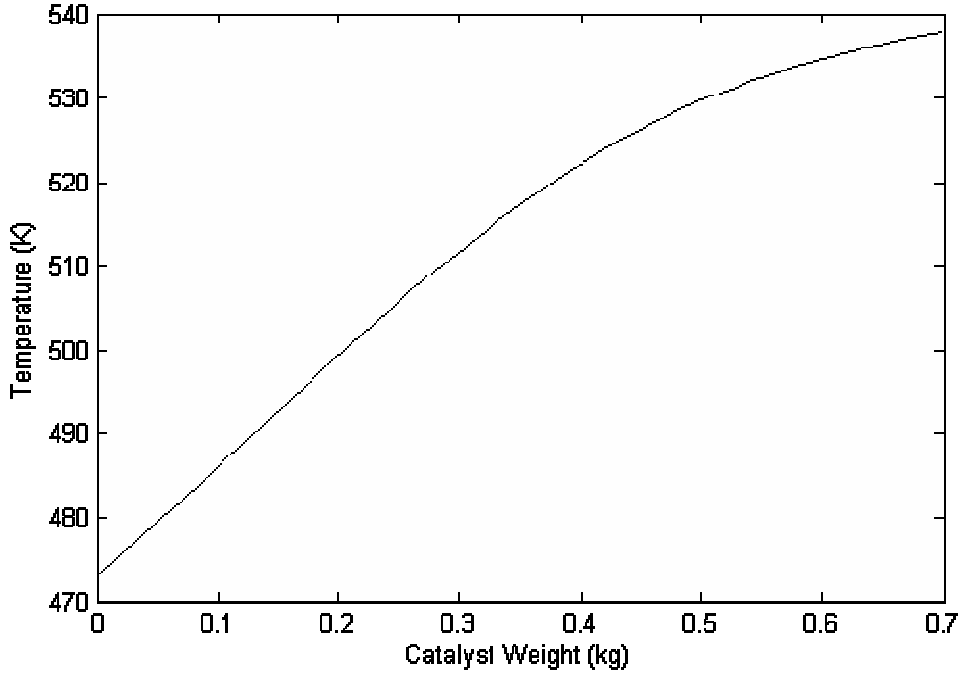

Figure 4.34. Temperature profile in WGS converter for 1500 W PEMFC operation (CH_4/O_2 = 2.24, H_2O/CH_4 = 1.17)

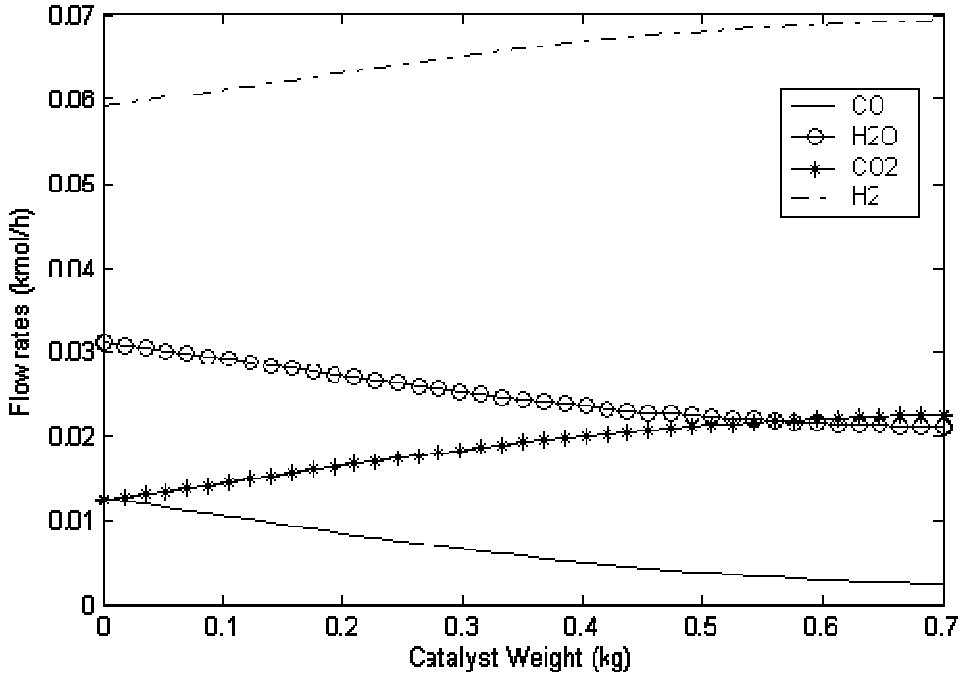

Figure 4.35. Flow rate variations in WGS converter for 1500 W PEMFC operation (CH_4/O_2 = 2.24, H_2O/CH_4 = 1.17)

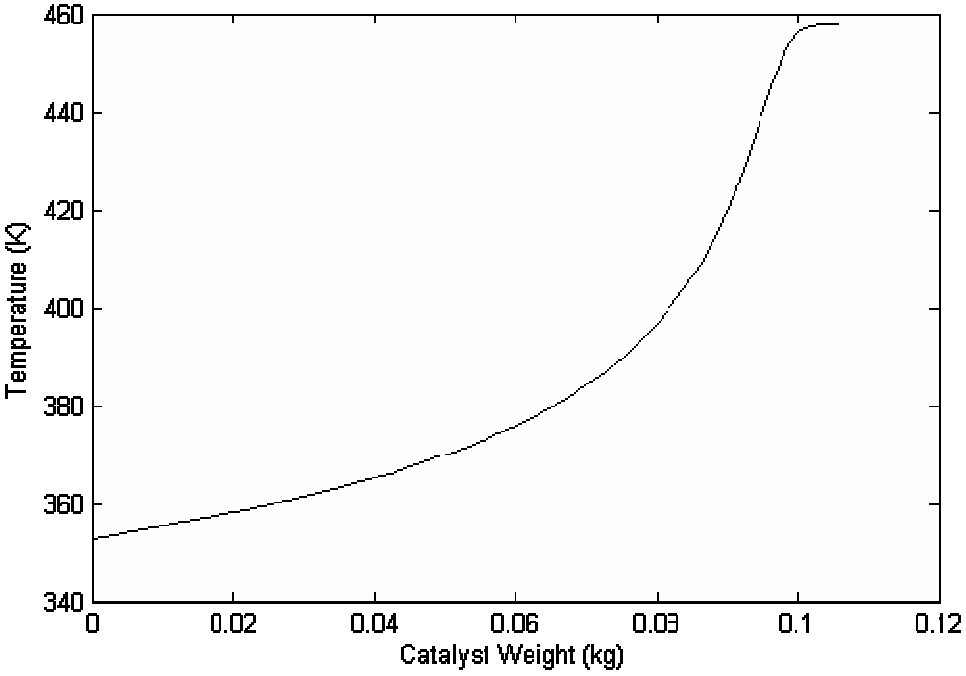

Figure 4.36. Temperature profile in PROX reactor for 1500 W PEMFC operation (CH_4/O_2 = 2.24, H_2O/CH_4 = 1.17)

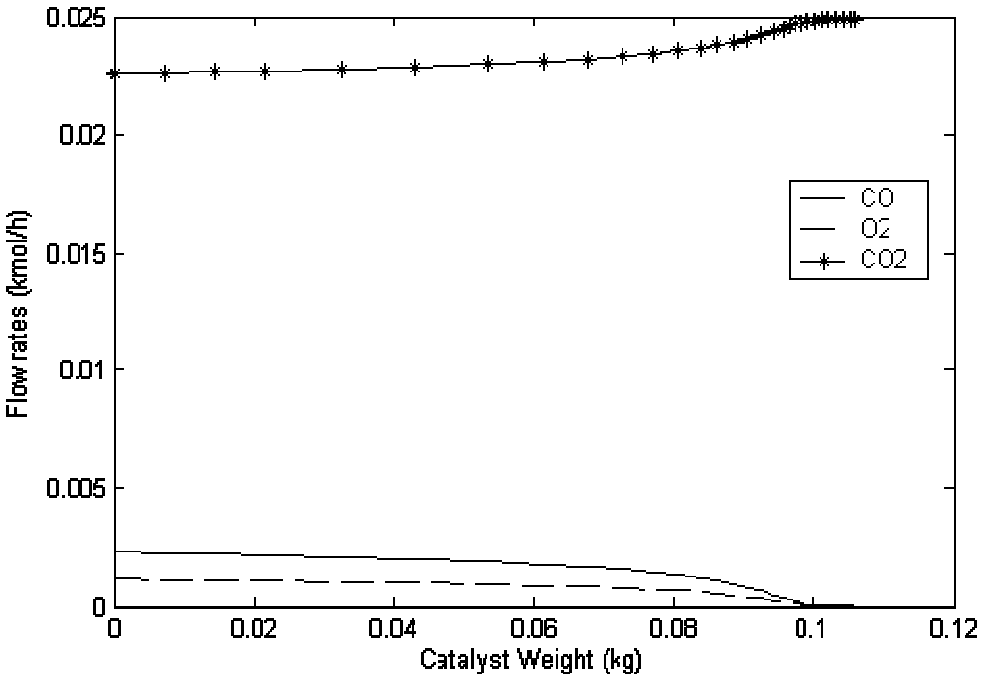

Figure 4.37. Flow rate variations in PROX reactor for 1500 W PEMFC operation (CH_4/O_2 = 2.24, H_2O/CH_4 = 1.17)

Table 4.15. Simulation outputs for CH_4/O_2 = 2.24&H_2O/CH_4 = 1.17 and CH_4/O_2 = 1.89&H_2O/CH_4 = 1.56 at IPOX reactor inlet in 1500 W PEMFC operation

	IPOX reactor		WGS converter		PROX reactor	
	1.89&1.56	2.24&1.17	1.89&1.56	2.24&1.17	1.89&1.56	2.24&1.17
Inlet temperature (K)	627	620	473	473	353	353
Exit temperature (K)	845	886	511	540	421	458
Catalyst weight (g)	669	488	650	700	180	106
CO level †	--	--	0.8	1.2	1.2	1.3

† CO level at the exit of the reactor, in mol per cent after WGS, in ppm after PROX
* CO level has to be below 2 mol per cent at WGS reactor outlet
** CO level has to be below 10 ppm at PROX reactor outlet.

As in the case of calculations for other power outputs, reactor simulations for 1500 W PEMFC operation show that simulated exit flow rates are in agreement with the material balance results (cf. Tables 4.5-4.6 and Tables 4.13-4.14). As seen in Table 4.15, carbon monoxide levels are below their maximum limits. The results in Table 4.15 also indicate that 2.24&1.17 operation has elevated temperatures at the exit of the reactors, because of the reasons explained in Section 4.2.1 and 4.2.2.

If six of the feed composition/power output configurations of the fuel processor system are compared, it can be seen that, for both feed ratios, catalyst quantities increase almost linearly with increasing power output of the PEM fuel cell. Thus, based on the results above, it can be concluded that amount of catalyst used in each reactor of the fuel processor system is directly proportional to the power output of the PEMFC (Tables 4.9, 4.12 and 4.15). Change of amount of catalyst used in each reactor with power output of PEMFC is shown in Figures 4.38 and 4.39 for 1.89&1.56 and 2.24&1.17, respectively. Linearity is observed between the values, while linear regression is performed and regression coefficients of 0.9974, 09984 and 1 is observed for IPOX, WGS and PROX, respectively for 1.89&1.56 operation and 1, 0.9998 and 0.999 is observed for IPOX, WGS and PROX, respectively for 2.24&1.17 operation.

Independent of the feed conditions and power type of PEMFC, a temperature decrease is observed at the IPOX reactor entrance, as seen in Figures 4.2, 4.8, 4.14, 4.20, 4.26 and 4.32. This temperature decrease may be due to model equations, i.e. reforming rate modelled by Xu and Froment (1989) can be said to be comparably faster than oxidation which is modelled by Ma (1995), at least at the entrance of the reactor.

4.3. Reactor Design Calculations

Catalyst weights in IPOX, WGS and PROX reactors have been estimated for six different feed ratio-power output configurations of the fuel processor system by solving model equations simultaneously in MATLAB. However, sizes of the reactors, i.e. their length and diameter, have not been calculated yet.

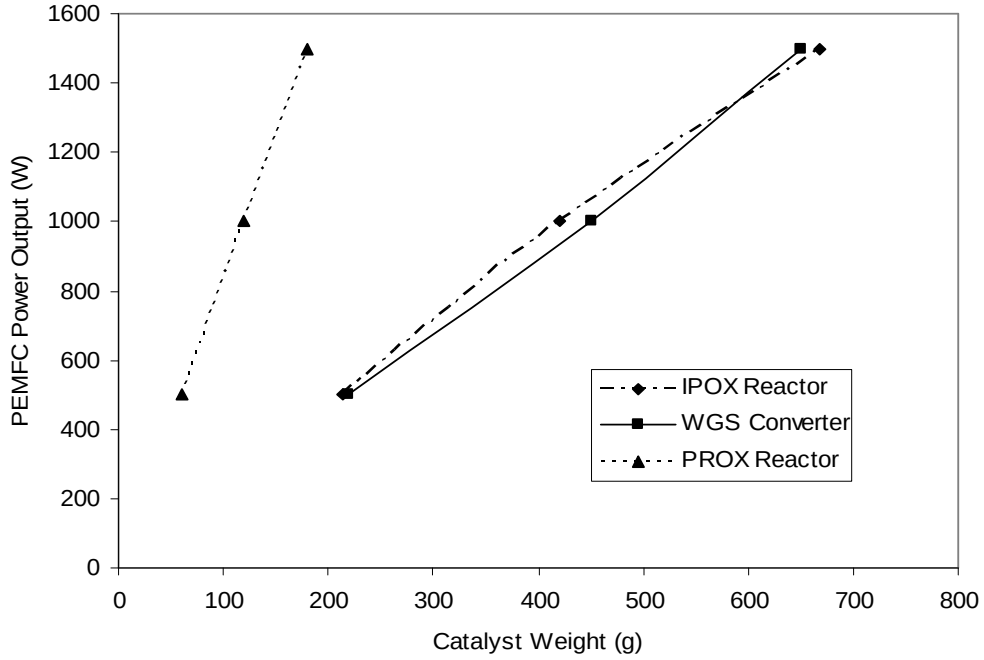

Figure 4.38. Catalyst weight variation with PEMFC power output in IPOX, WGS and PROX reactors (CH_4/O_2 = 1.89, H_2O/CH_4 = 1.56)

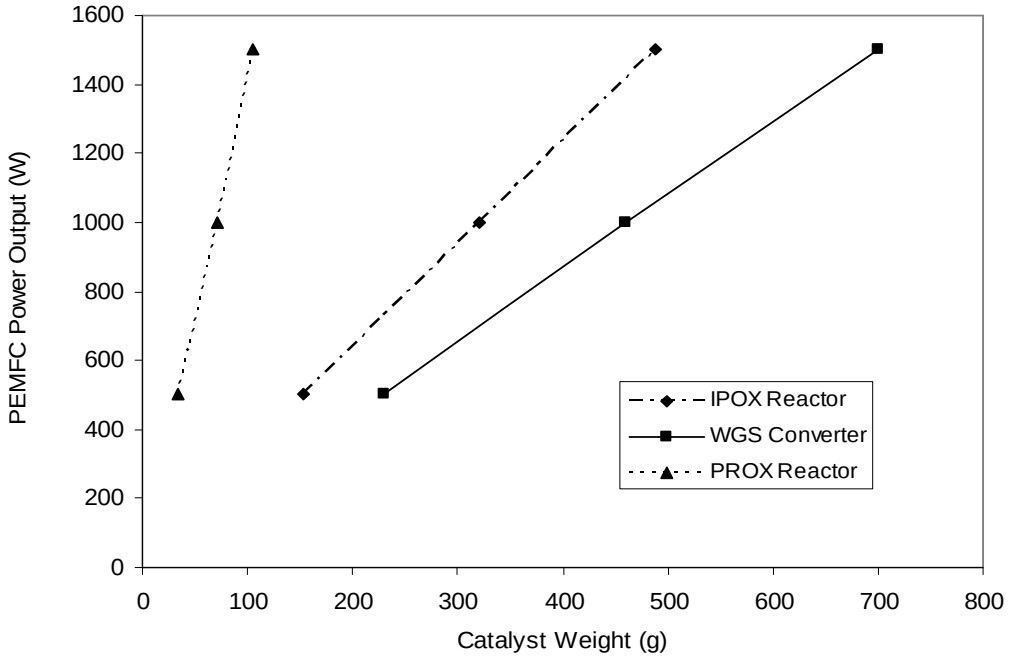

Figure 4.39. Catalyst weight variation with PEMFC power output in IPOX, WGS and PROX reactors (CH_4/O_2 = 2.24, H_2O/CH_4 = 1.17)

Reactor sizing calculations are conducted by using criteria reported to quantify interfacial heat and intraparticle mass transfer resistances and flow behaviour (axial dispersion, radial flow profile) in packed beds (Rase, 1990; Fogler, 1999; Bird *et al.*, 2002; Perry, 1997). These criteria are given in Section 3.2.2, in Equations (3.51)-(3.68). Calculations are carried out for three of the catalytic reactors through a set of catalyst particle size (D_p)-reactor diameter (D_t) configurations. Values of these parameters are assigned such that their ratio, D_t/D_p, is above the threshold value of 30 (Equation 3.67) indicating the validity of plug-flow behaviour (Rase, 1990). Using these values, length of each reactor is estimated via Equation (3.68), such that axial dispersion in each reactor will be insignificant (Rase, 1990). Finally, catalyst particle size, reactor diameter and length values are tested using Mears' and Weisz-Prater criteria (Equations 3.51 and 3.59) to check whether they help in suppressing transport resistances (Avcı *et al.*, 2001; Fogler, 1999; Rase, 1990). In addition, total pressure change along the reactor tube is checked using Equation (3.66), such that the dimensions do not lead to excessive pressure drop. Note that the differential pressure drop equation is solved simultaneously with the differential mole and energy balances given in Section 3.2.1.

4.3.1. 500 W PEMFC Operation

4.3.1.1. IPOX Reactor. Design calculations for IPOX reactor in 500 W PEMFC operation at feed ratios of 1.89&1.56 and 2.24&1.17 are presented in Tables 4.16 and 4.17, respectively.

In Tables 4.16 and 4.17, it can be seen that reactor dimensions and catalyst particle sizes, which are selected to minimize axial dispersion and ensure flat velocity profile, indicate a 'border-line' status for the transport resistances when the limit values of Mears' criterion of max. 0.3 and Weisz-Prater criterion of max. 1 are considered (see Equations 3.51 and 3.59). As a rule of thumb, reactor length is regarded to be approximately five times of the reactor tube diameter in each run, for assuming plug-flow behaviour during the reactor design calculations (Rase, 1990). The tabulated five runs are the optimum results that give acceptable values for criteria; they are selected by the elimination of the runs that give extremely high or low values for any of the criteria.

Table 4.16. Reactor design results for IPOX reactor in 500 W PEMFC operation (CH_4/O_2 = 1.89 & H_2O/CH_4 = 1.56)

Run	1	2	3	4	5
W (g)	213	213	213	213	213
D_p (μm)	700	650	600	600	600
D_t (cm)	3.50	3.50	3.50	3.60	3.40
L (cm)	19.02	19.02	19.02	17.97	20.15
$\frac{L}{D_p}$	271.66	292.56	316.94	299.57	335.85
$\frac{D_t}{D_p}$	50.00	53.85	58.33	60.00	56.67
Mears' criterion	0.46	0.40	0.34	0.34	0.33
Weisz-Prater criterion	0.90	0.78	0.66	0.66	0.67
P_{out} (bar)	0.44	0.35	0.24	0.33	0.14

Effect of pressure drop was mentioned to be an important parameter for design calculations; total pressure change has to be kept low to minimize mechanical energy loss. In Tables 4.16 and 4.17, it can be seen that outlet pressure increases with increasing particle diameter at constant tube diameter and increasing tube diameter at constant particle diameter. For 1.89&1.56 feed ratio, outlet pressure in Run 5 is critically low, while other criteria are in acceptable limits. Similarly, for 2.24&1.17 ratio, Run 1 gives acceptable outlet pressure, while intraparticle and interfacial limitations are off the acceptance. A new run that presents bigger catalyst and tube diameter can be tried for 1.89&1.56 operation, since the runs in both operations are experimented in same catalyst and tube diameter for comparison. However, increment in catalyst particle diameter would lead to the increase in intraparticle and interfacial resistances. Consequently, catalyst with 1 mm diameter and tube with 4 cm diameter, 14.6 cm length gives outlet pressure of 0.85 bar, which seems as a plausible option. Therefore, if Run 1 would be the selection for 2.24&1.17, in comparison, the new run for 1.89&1.56 is the choice for IPOX reactor in 500 W operation.

Table 4.17. Reactor design results for IPOX reactor in 500 W PEMFC operation (CH_4/O_2 = 2.24 & H_2O/CH_4 = 1.17)

Run	1	2	3	4	5
W (g)	154	154	154	154	154
D_p (μm)	700	650	600	600	600
D_t (cm)	3.50	3.50	3.50	3.60	3.40
L (cm)	13.70	13.70	13.70	12.95	14.52
$\frac{L}{D_p}$	195.77	210.83	228.40	215.89	242.04
$\frac{D_t}{D_p}$	50.00	53.85	58.33	60.00	56.67
Mears' criterion	0.85	0.73	0.63	0.62	0.62
Weisz-Prater criterion	1.65	1.42	1.21	1.21	1.21
P_{out} (bar)	0.69	0.64	0.58	0.63	0.52

If the two feed ratios are compared, it is seen that 1.89&1.56 needs longer reactor length; this situation is because of the catalyst amounts packed in the bed, 1.89&1.56 needs much more catalyst than 2.24&1.17, which is because of the reasons explained in Section 4.2. Furthermore, 1.89&1.56 has more convenient responses to the interfacial heat and intraparticle mass transfer limitations, whereas 2.24&1.17 offers higher outlet pressures, i.e. ignorable total pressure drop at the same reactor dimensions and catalyst diameters. This situation is mainly because of the difference in flow rates of the species at different feed ratios; this difference influences reaction rates which is directly related to Mears' and Weisz-Prater criteria (see Equations 3.51 and 3.59) and also influences velocity and density of the gas mixture which are related to the total pressure change (see Equation 3.66); even the particle-to-fluid heat transfer coefficient and surface concentration of species are related to flow rates. Moreover, difference in reaction temperature also affects values of the criteria.

4.3.1.2. WGS Converter. Design calculations for WGS converter in 500 W PEMFC operation at feed ratios of 1.89&1.56 and 2.24&1.17 are presented in Tables 4.18 and 4.19, respectively.

It is seen in Tables 4.18 and 4.19 that when reactor dimensions and catalyst diameter is selected to minimize axial dispersion and ensure flat velocity profile, interfacial heat and intraparticle mass transfer are not serious problems since Mears' and Weisz-Prater criteria are met.

Table 4.18. Reactor design results for WGS converter in 500 W PEMFC operation (CH_4/O_2 = 1.89 & H_2O/CH_4 = 1.56)

Run	1	2	3	4	5
W (g)	220	220	220	200	220
D_p (μm)	800	700	600	600	600
D_t (cm)	4.00	4.00	4.00	4.50	3.50
L (cm)	19.46	19.46	19.46	15.38	25.42
$\frac{L}{D_p}$	243.38	278.03	324.37	256.29	423.67
$\frac{D_t}{D_p}$	50.00	57.14	66.67	75.00	58.33
Mears' criterion	5.5×10^{-4}	4.2×10^{-4}	3.1×10^{-4}	3.3×10^{-4}	2.9×10^{-4}
Weisz-Prater criterion	0.021	0.016	0.012	0.012	0.012
P_{out} (bar)	0.82	0.76	0.69	0.81	0.44

Total pressure was mentioned to change with changing catalyst particle and tube diameter; for both feed ratios, outlet pressure increases with increasing particle diameter at constant tube diameter (cf. Runs 1, 2 and 3) and with increasing tube diameter at constant particle diameter (cf. Runs 3, 4 and 5). Moreover, in comparison of 1.89&1.56 and 2.24&1.17 feed ratios, outlet pressures are nearly identical at each run. Runs 1 and 4 give

the highest outlet pressure among others for both feed ratios. However, Run 1 seems to be the optimal choice since reactor length is close to the rule that implies reactor length has to be approximately five times of reactor tube (Rase, 1990). Consequently, reactor tube with 4 cm diameter and 20.35 cm length and catalyst particle of 800 µm diameter is the choice for WGS converter in 500 W PEMFC operation.

Table 4.19. Reactor design results for WGS converter in 500 W PEMFC operation (CH_4/O_2 = 2.24 & H_2O/CH_4 = 1.17)

Run	1	2	3	4	5
W (g)	230	230	230	230	230
D_p (µm)	800	700	600	600	600
D_t (cm)	4	4	4	4.5	3.5
L (cm)	20.35	20.35	20.35	16.08	26.58
$\frac{L}{D_p}$	254.34	190.70	339.08	267.94	442.98
$\frac{D_t}{D_p}$	50.00	57.14	66.67	75.00	58.33
Mears' criterion	4.0×10^{-4}	4.2×10^{-4}	3.1×10^{-4}	3.3×10^{-4}	2.9×10^{-4}
Weisz-Prater criterion	0.018	0.013	0.010	0.010	0.010
P_{out} (bar)	0.84	0.80	0.72	0.83	0.50

4.3.1.3. PROX Reactor. Tables 4.20 and 4.21 present the design calculation results for PROX reactor in 500 W PEMFC operation at 1.89&1.56 and 2.24&1.17 feed ratios, respectively.

Intraparticle and interfacial criteria are highly satisfied for both of feed ratios, when reactor dimensions and catalyst particle diameter is selected to minimize axial dispersion and ensure flat velocity profile, as seen in Tables 4.20 and 4.21.

Table 4.20. Reactor design results for PROX reactor in 500 W PEMFC operation (CH_4/O_2 = 1.89 & H_2O/CH_4 = 1.56)

Run	1	2	3	4	5
W (g)	60	60	60	60	60
D_p (μm)	800	700	600	600	600
D_t (cm)	2.50	2.50	2.50	3.00	2.25
L (cm)	10.50	10.50	10.50	7.29	12.96
$\frac{L}{D_p}$	131.24	150.02	174.96	121.52	216.03
$\frac{D_t}{D_p}$	31.25	35.71	41.67	50	37.5
Mears' criterion	5.4×10^{-4}	4.2×10^{-4}	3.1×10^{-4}	3.4×10^{-4}	3.4×10^{-4}
Weisz-Prater criterion	11.4×10^{-4}	8.7×10^{-4}	6.4×10^{-4}	6.4×10^{-4}	6.4×10^{-4}
P_{out} (bar)	0.84	0.80	0.74	0.89	0.57

Pressure at the outlet of preferential oxidation reactor, like outlet pressure of IPOX reactor and WGS converter, increases with increasing tube and particle diameter at constant particle and tube diameters, respectively for both feed ratios. Run 5 in 1.89&1.56 operation gives the highest length-to-diameter ratio for tube but low outlet pressure that leads to an evident total pressure drop. Besides, Run 4 in 2.24&1.17 operation represents ignorable pressure change whereas it gives insufficient length for reactor tube as in other runs.

In 500 W PEMFC operation, outlet pressure and reactor length have similar behaviour to the changing tube and catalyst particle diameter in IPOX, WGS and PROX reactors for both of feed ratios. Total pressure change is critically high in IPOX reactor in Run 5 for 1.89&1.56 operation whereas for other reactors, it may be tentatively said that total pressure change would be in ignorable limits.

Table 4.21. Reactor design results for PROX reactor in 500 W PEMFC operation (CH_4/O_2 = 2.24 & H_2O/CH_4 = 1.17)

Run	1	2	3	4	5
W (g)	34	34	34	34	34
D_p (µm)	800	700	600	600	600
D_t (cm)	2.50	2.50	2.50	3.00	2.25
L (cm)	5.91	5.91	5.91	4.10	7.30
$\frac{L}{D_p}$	73.80	84.36	98.38	68.33	121.48
$\frac{D_t}{D_p}$	31.25	35.71	41.67	50	37.5
Mears' criterion	0.003	0.002	0.002	0.002	0.002
Weisz-Prater criterion	0.013	0.010	0.007	0.007	0.007
P_{out} (bar)	0.91	0.88	0.84	0.93	0.73

Run 1 and Run 5 in 1.89&1.56 and 2.24&1.17 seem to be the most reasonable options; consequently, reactor tube with 2.5 cm diameter, 10.5 cm length and catalyst with 800 µm diameter is selected for WGS converter in 500 W PEMFC system.

4.3.2. 1000 W PEMFC Operation

4.3.2.1. IPOX Reactor. Design calculations for IPOX reactor in 1000 W PEMFC operation at feed ratios of 1.89&1.56 and 2.24&1.17 are presented in Tables 4.22 and 4.23, respectively.

It is seen in Tables 4.22 and 4.23 that there are deviations from interfacial heat and intraparticle mass transfer criteria, yet they are approximately within the limits. As stated for 500 W operation, 1.89&1.56 needs more catalyst for indirect partial oxidation reaction than 2.24&1.17, which causes longer reactor lengths for former operation.

Table 4.22. Reactor design results for IPOX reactor in 1000 W PEMFC operation (CH_4/O_2 = 1.89 & H_2O/CH_4 = 1.56)

Run	1	2	3	4	5
W (g)	421	421	421	421	421
D_p (µm)	800	750	700	700	700
D_t (cm)	4.80	4.80	4.80	5.60	4.50
L (cm)	19.98	19.98	19.98	14.68	22.73
$\frac{L}{D_p}$	249.80	266.45	285.50	209.74	324.77
$\frac{D_t}{D_p}$	60.00	64.00	68.57	80	64.29
Mears' criterion	0.59	0.52	0.45	0.49	0.43
Weisz-Prater criterion	0.74	0.65	0.57	0.59	0.57
P_{out} (bar)	0.65	0.60	0.54	0.77	0.40

Pressure drop that affects the rate of reaction decreases with increasing tube diameter and particle diameter when keeping particle diameter and tube diameter constant, respectively. Minimum pressure drop is seen to be in Run 4 for 1.89&1.56 operation; however, length-to-diameter ratio of the reactor seems insufficiently low. Nevertheless, Run 5 gives suitable responses to all of the hindrances except outlet pressure which affects the operation due to high pressure drop. Similarly, for 2.24&1.17 operation, length-to-diameter ratio of reactor tube and outlet pressure is changing reversely, when it is maximum for one, insufficient for other (cf. Runs 4 and 5). Therefore, Run 1 seems to be the optimum choice for both feed ratios due to the consideration of pressure drop firstly. In consequence, reactor tube with 4.80 cm diameter, 19.98 cm length and catalyst pellet with 800 µm diameter is the selected model for IPOX reactor of 1000 W PEMFC system.

If 500 W and 1000 W operation are compared, it is seen that longer reactor lengths and tube diameters are needed for 1000 W operation at both feed ratio operations.

Moreover, diameter of catalyst particle has to be bigger for 1000 W operation, since outlet pressure is getting lower while catalyst particle is getting smaller. Note that the comparison at the same particle and tube diameter is impossible due to the excessive decrease of outlet pressure in 1000 W operation.

Table 4.23. Reactor design results for IPOX reactor in 1000 W PEMFC operation (CH_4/O_2 = 2.24 & H_2O/CH_4 = 1.17)

Run	1	2	3	4	5
W (g)	321	321	321	321	321
D_p (μm)	800	750	700	700	700
D_t (cm)	4.80	4.80	4.80	5.60	4.50
L (cm)	15.24	15.24	15.24	11.19	17.33
$\frac{L}{D_p}$	190.46	203.16	217.68	159.92	247.63
$\frac{D_t}{D_p}$	60.00	64.00	68.57	80	64.29
Mears' criterion	0.90	0.79	0.69	0.75	0.66
Weisz-Prater criterion	2.13	1.87	1.63	1.63	1.63
P_{out} (bar)	0.72	0.68	0.63	0.81	0.51

4.3.2.2. WGS Converter. Design calculations for WGS converter in 1000 W PEMFC operation at feed ratios of 1.89&1.56 and 2.24&1.17 are presented in Tables 4.24 and 4.25, respectively.

As seen in Tables 4.24 and 4.25, interfacial heat and intraparticle mass transfer resistances can be neglected for both feed ratios. Thus, the focus point for the WGS converter is to choose the optimum run that gives highest outlet pressure (i.e. minimum pressure drop) and reactor length/diameter ratio close to 5. Run 1 in both operations gives the highest outlet pressure, whereas Run 4 represents the most suitable choice for

length/diameter ratio. As a result, Run 1 is chosen for WGS reactor for both feed ratio in 1000 W operation; i.e. reactor tube with 5.60 cm diameter, 20.76 cm length and catalyst with 800 µm diameter is the model for WGS reactor of 1000 W operation.

Table 4.24. Reactor design results for WGS converter in 1000 W PEMFC operation (CH_4/O_2 = 1.89 & H_2O/CH_4 = 1.56)

Run	1	2	3	4	5
W (g)	450	450	450	450	450
D_p (µm)	800	700	600	600	600
D_t (cm)	5.60	5.60	5.60	5.0	5.8
L (cm)	20.31	20.31	20.31	25.48	18.93
$\frac{L}{D_p}$	253.87	290.16	338.52	424.63	315.55
$\frac{D_t}{D_p}$	70.00	80.00	93.33	83.33	96.67
Mears' criterion	4.2×10^{-4}	3.2×10^{-4}	2.4×10^{-4}	2.2×10^{-4}	2.4×10^{-4}
Weisz-Prater criterion	0.020	0.016	0.011	0.011	0.011
P_{out} (bar)	0.81	0.75	0.66	0.45	0.71

Reactor lengths estimated for 1000 W operation is seen to be nearly the same with that of 500 W operation, provided that the catalyst particle diameters are identical. Therefore, reactor tube diameter is bigger for 1000 W operation at both feed ratios, as expected.

4.3.2.3. PROX Reactor. Preferential oxidation reactor sizing calculation results are tabulated for 1000 W PEMFC operation at 1.89&1.56 and 2.24&1.17 feed ratios in Tables 4.26 and 4.27, respectively.

Table 4.25. Reactor design results for WGS converter in 1000 W PEMFC operation (CH_4/O_2 = 2.24 & H_2O/CH_4 = 1.17)

Run	1	2	3	4	5
W (g)	460	460	460	460	460
D_p (µm)	800	700	600	600	600
D_t (cm)	5.60	5.60	5.60	5.0	5.8
L (cm)	20.76	20.76	20.76	26.04	19.35
$\frac{L}{D_p}$	259.53	296.60	346.04	434.07	322.56
$\frac{D_t}{D_p}$	70.00	80.00	93.33	83.33	96.67
Mears' criterion	3.1×10^{-4}	2.4×10^{-4}	1.8×10^{-4}	1.7×10^{-4}	1.8×10^{-4}
Weisz-Prater criterion	0.016	0.012	0.009	0.009	0.009
P_{out} (bar)	0.84	0.79	0.71	0.52	0.75

It can be seen in Tables 4.26 and 4.27 that interfacial mass and intraparticle heat transfer can totally be neglected along the reactor. Length of the reactor is longer for 1.89&1.56 operation because of the need of more catalyst weight and 2.24&1.17 operation represents higher outlet pressures in each run. Run 4 and Run 5 give the highest outlet pressure and length/diameter ratio, respectively. However, Run 5 in 1.89&1.56 and Run 4 in 2.24&1.17 are off the acceptance due to very low outlet pressure and insufficient length-to-diameter ratio. In consequence, reactor tube with 3 cm diameter, 14.58 cm length and catalyst pellet with 900 µm diameter is the model for PROX reactor of 1000 W PEMFC system.

Preferential oxidation reactor needs higher amount of catalyst for 1000 W than needed in 500 W operation. Consequently, longer reactor lengths and diameters, i.e. larger reactor volume are needed for 1000 W operation. In addition, when compared with 500 W operation, pressure drop is greater in 1000 W operation due to the higher amount.

Table 4.26. Reactor design results for PROX reactor in 1000 W PEMFC operation (CH_4/O_2 = 1.89 & H_2O/CH_4 = 1.56)

Run	1	2	3	4	5
W (g)	120	120	120	120	120
D_p (μm)	900	800	700	700	700
D_t (cm)	3.00	3.00	3.00	3.50	2.80
L (cm)	14.58	14.58	14.58	10.71	16.74
$\frac{L}{D_p}$	162.02	182.28	208.29	153.05	239.14
$\frac{D_t}{D_p}$	33.33	37.5	42.86	50	40
Mears' criterion	2.2×10^{-4}	1.8×10^{-4}	1.4×10^{-4}	1.5×10^{-4}	1.3×10^{-4}
Weisz-Prater criterion	6.0×10^{-4}	4.8×10^{-4}	3.6×10^{-4}	3.6×10^{-4}	3.6×10^{-4}
P_{out} (bar)	0.68	0.61	0.51	0.77	0.32

4.3.3. 1500 W PEMFC Operation

4.3.3.1. IPOX Reactor. Design calculations for IPOX reactor in 1500 W PEMFC operation at feed ratios of 1.89&1.56 and 2.24&1.17 are presented in Tables 4.28 and 4.29, respectively.

Compared with 500 and 1000 W operations, Mears' and Weisz-Prater criteria tends to indicate the significance of transport resistances (Tables 4.28 and 4.29) in 1500 W operation. This outcome can be observed in its most pronounced form in Table 4.29, where the limit values of both criteria are exceeded in all runs. This situation can be based on higher reactor dimensions and catalyst particle diameters which are related to the Mears' and Weisz-Prater criteria (see Equations 3.51 and 3.59).

Table 4.27. Reactor design results for PROX reactor in 1000 W PEMFC operation (CH_4/O_2 = 2.24 & H_2O/CH_4 = 1.17)

Run	1	2	3	4	5
W (g)	72	72	72	72	72
D_p (μm)	900	800	700	700	700
D_t (cm)	3.00	3.00	3.00	3.50	2.80
L (cm)	8.71	8.71	8.71	6.4	10.00
$\frac{L}{D_p}$	96.81	108.91	124.45	91.45	142.88
$\frac{D_t}{D_p}$	33.33	37.5	42.86	50	40
Mears' criterion	8.2×10^{-4}	6.5×10^{-4}	5.0×10^{-4}	5.4×10^{-4}	4.8×10^{-4}
Weisz-Prater criterion	0.004	0.003	0.002	0.002	0.002
P_{out} (bar)	0.84	0.81	0.75	0.88	0.66

As in the case of 500 and 1000 W operations, 1500 W PEMFC operation suffers from the relationship between pressure drop and length-to-diameter ratio. When this ratio reaches its highest value, outlet pressure takes its lowest value (Run 5), since reactor dimensions are related to the total pressure change given in equation (3.66), i.e. velocity of the gas mixture and cross-sectional area of the reactor tube is affected by the change in reactor length and diameter. Therefore, intraparticle and interfacial resistances are at their minimum. On the contrary, if the total pressure drop decreases, other hindrances, i.e. Mears' and Weisz-Prater criteria, become critical (cf. Runs 1 and 2). Runs 1 and 5 seem to be plausible options for IPOX reactor in 1500 W system. Consequently, reactor tube with 5.80 cm diameter, 21.75 cm length and catalyst pellet with 1 mm diameter is the choice, which in fact gives more feasible values to the external and internal criteria and reasonable length-to-diameter ratio.

Table 4.28. Reactor design results for IPOX reactor in 1500 W PEMFC operation (CH_4/O_2 = 1.89 & H_2O/CH_4 = 1.56)

Run	1	2	3	4	5
W (g)	669	669	669	669	669
D_p (μm)	1000	900	800	800	800
D_t (cm)	5.80	5.80	5.80	6.00	5.60
L (cm)	21.75	21.75	21.75	20.32	23.33
$\frac{L}{D_p}$	217.50	241.66	271.87	254.05	291.64
$\frac{D_t}{D_p}$	58.00	64.44	72.5	75	70
Mears' criterion	0.67	0.54	0.43	0.43	0.42
Weisz-Prater criterion	1.77	1.43	1.13	1.13	1.13
P_{out} (bar)	0.64	0.56	0.46	0.53	0.36

Among all the power types of PEMFC operations, 1500 W operation required the highest quantity of catalyst. Assuming that the reactor volume is kept constant, a change in catalyst particle size would affect the operating characteristics: selection of a bigger catalyst size (with longer particle diameters) would result in lower pressure drop, but would make the transport resistances more significant.

4.3.3.2. WGS Converter. Tabulated WGS converter design calculations in 1500 W PEMFC operation at 1.89&1.56 and 2.24&1.17 feed ratios are given in Tables 4.30 and 4.31, respectively.

Along the length of the water-gas shift reactor in 1500 W operation, negligible axial dispersion, flat velocity profile are amply reached; it can be seen from Tables 4.30 and 4.31 that, under the conditions of negligible axial dispersion and flat velocity profile, intraparticle and interfacial diffusion can totally be neglected for all the runs. Reactor

length-to-diameter ratio and outlet pressure are therefore of main interest for the design of the WGS converter. Reactor length is related to the tube diameter; it is increasing with the decreasing tube diameter. Run 1 in both operation gives the highest outlet pressure but the reactor length/diameter ratio in Run 5 is the highest. This repeating sequence for all operations leads to the selection of the optimum choice. Hence, Run 1 in both operation seems to be the plausible option, since much higher outlet pressure is represented. Consequently, reactor tube with 6 cm diameter, 27.52 cm length and catalyst pellet of 1 mm diameter is the choice for WGS reactor of 1500 W system.

Table 4.29. Reactor design results for IPOX reactor in 1500 W PEMFC operation (CH_4/O_2 = 2.24 & H_2O/CH_4 = 1.17)

Run	1	2	3	4	5
W (g)	488	488	488	488	488
D_p (µm)	1000	900	800	800	800
D_t (cm)	5.80	5.80	5.80	6.00	5.60
L (cm)	15.87	15.87	15.87	14.83	17.02
$\frac{L}{D_p}$	158.65	176.28	198.31	185.31	212.73
$\frac{D_t}{D_p}$	58.00	64.44	72.5	75	70
Mears' criterion	1.26	1.03	0.81	0.83	0.79
Weisz-Prater criterion	3.62	2.93	2.32	2.32	2.32
P_{out} (bar)	0.80	0.76	0.70	0.74	0.65

4.3.3.3. PROX Reactor. Preferential oxidation reactor design calculations in 1500 W PEMFC operation at 1.89&1.56 and 2.24&1.17 feed ratios are given in Tables 4.32 and 4.33, respectively.

Table 4.30. Reactor design results for WGS converter in 1500 W PEMFC operation (CH_4/O_2 = 1.89 & H_2O/CH_4 = 1.56)

Run	1	2	3	4	5
W (g)	650	650	650	650	650
D_p (μm)	1000	900	800	800	800
D_t (cm)	6.00	6.00	6.00	6.2	5.8
L (cm)	25.56	25.56	25.56	23.93	27.35
$\frac{L}{D_p}$	255.57	283.96	319.46	299.18	341.87
$\frac{D_t}{D_p}$	60.00	66.67	75	77.5	72.5
Mears' criterion	5.8×10^{-4}	4.7×10^{-4}	3.7×10^{-4}	3.8×10^{-4}	3.6×10^{-4}
Weisz-Prater criterion	0.032	0.026	0.021	0.021	0.021
P_{out} (bar)	0.79	0.74	0.67	0.72	0.62

Major problem in designing preferential oxidation reactor is selecting the optimum values for outlet pressure and reactor length-to-diameter ratio, since other criterions do not suffer from exceeding the limits for all runs at both feed ratio. As in 500 and 1000 W operations, outlet pressure and length-to-diameter ratio change reversely with each other. Run 5 in both 1.89&1.56 and 2.24&1.17 operations offers highest length-to-diameter ratio but the lowest outlet pressure. Runs 1 and 4 give similarly high outlet pressures; but Run 1 offers higher length-to-diameter ratio. Hence, due to higher length-to-diameter ratio and particle diameter, Run 1 seems as a plausible selection; i.e. reactor tube with 3.5 cm diameter, 16.07 cm length and catalyst particle with diameter of 1 mm is the model for the PROX reactor in 1500 W PEMFC operation.

Table 4.31. Reactor design results for WGS converter in 1500 W PEMFC operation (CH_4/O_2 = 2.24 & H_2O/CH_4 = 1.17)

Run	1	2	3	4	5
W (g)	700	700	700	700	700
D_p (μm)	1000	900	800	800	800
D_t (cm)	6.00	6.00	6.00	6.2	5.8
L (cm)	27.52	27.52	27.52	25.78	29.45
$\frac{L}{D_p}$	275.23	305.81	344.03	322.19	368.17
$\frac{D_t}{D_p}$	60.00	66.67	75	77.5	72.5
Mears' criterion	4.5×10^{-4}	3.6×10^{-4}	2.9×10^{-4}	2.9×10^{-4}	2.8×10^{-4}
Weisz-Prater criterion	0.029	0.024	0.019	0.019	0.019
P_{out} (bar)	0.80	0.75	0.69	0.73	0.64

In comparison of 500, 1000 and 1500 W operation, reactors with bigger volume were needed for 1500 W PEMFC system, since highest amount of catalyst was needed for 1500 W operation. Besides, catalyst particle diameter between 0.8 and 1 mm was the optimal range for use in all feed ratio/power output configurations. Variation of outlet pressure reversely with reactor length-to-diameter ratio was the main problem for WGS and PROX reactors, while for IPOX reactors, existence of external heat and internal mass transfer resistances significantly was another hindrance. However, since the effectiveness factors are likely to be smaller in large reactor volumes with larger particles, the external and internal transport criteria were taken into consideration after total pressure drop and length-to-diameter ratio considerations.

Table 4.32. Reactor design results for PROX reactor in 1500 W PEMFC operation (CH_4/O_2 = 1.89 & H_2O/CH_4 = 1.56)

Run	1	2	3	4	5
W (g)	180	180	180	180	180
D_p (μm)	1000	900	800	800	800
D_t (cm)	3.50	3.50	3.50	3.80	3.20
L (cm)	16.07	16.07	16.07	13.63	19.22
$\frac{L}{D_p}$	160.70	178.55	200.88	170.41	240.30
$\frac{D_t}{D_p}$	35	38.89	43.75	47.5	40
Mears' criterion	1.4×10^{-4}	1.1×10^{-4}	8.8×10^{-5}	9.2×10^{-5}	8.3×10^{-5}
Weisz-Prater criterion	1.5×10^{-3}	1.2×10^{-3}	9.6×10^{-4}	9.6×10^{-4}	9.6×10^{-4}
P_{out} (bar)	0.67	0.60	0.52	0.68	0.25

Table 4.33. Reactor design results for PROX reactor in 1500 W PEMFC operation (CH_4/O_2 = 2.24 & H_2O/CH_4 = 1.17)

Run	1	2	3	4	5
W (g)	106	106	106	106	106
D_p (μm)	1000	900	800	800	800
D_t (cm)	3.50	3.50	3.50	3.80	3.20
L (cm)	9.46	9.46	9.46	8.03	11.32
$\frac{L}{D_p}$	94.63	105.14	118.29	100.35	141.51
$\frac{D_t}{D_p}$	35	38.89	43.75	47.5	40
Mears' criterion	5.6×10^{-4}	4.5×10^{-4}	3.6×10^{-4}	3.8×10^{-4}	3.4×10^{-4}
Weisz-Prater criterion	2.8×10^{-3}	2.3×10^{-3}	1.8×10^{-3}	1.8×10^{-3}	1.8×10^{-3}
P_{out} (bar)	0.84	0.80	0.76	0.84	0.62

5. PROPOSAL FOR THE INTEGRATION OF FUEL PROCESSING REACTORS VIA PROCESS INTENSIFICATION TECHNIQUES

The reactor sizes and catalyst amounts calculated in previous sections indicate that even small power sizes of PEM fuel cells necessitate considerable catalyst volumes, e.g. 0.49 L, 0.98 L and 1.51 L for 0.5, 1.0 and 1.5 kW PEMFC operation, respectively. These volumes do not include the space requirements of auxiliary equipment that have to be used for heat exchange, pumping etc. The practical application of PEMFC power systems, especially at higher power sizes, calls for more compact devices which integrate reaction and heat exchange functions while also taking up less space. It is, therefore, relevant to propose that process intensification techniques be used to design integrated fuel processors.

Small and medium scale fuel processing systems offering high energy densities with compact sizes have received great attention in hydrogen production for on-board vehicular and for small scale stationary applications (Chan and Ding, 2005, Qi *et al.*, 2007). As a result, process intensification techniques that maximize efficiency and compactness of the fuel processor systems have evolved.

Zalc and Löffler (2002) investigated the transport and kinetic issues of a fuel processor system design. They considered the system to consist of a methane steam reformer, a water-gas shift unit and a preferential oxidation reactor and simulated the operation of this system to deliver 50 kW of electric power, since fuel processors for automotive applications are usually rated for producing 50 kW of electric output (Zalc and Löffler, 2002). It is reported that ca. 31 mol/min hydrogen production is needed to drive a 50 kW PEM fuel cell (Zalc and Löffler, 2002). Based on this hydrogen production demand, they estimated the approximate size of each reactor and found that 10.8, 17 and 5 kg of catalyst are needed for SR (fixed-bed tubular reformer of which volume based on chemical reaction rate), WGS and PROX reactors, respectively. When downscaled to the power requirements considered in this study (500, 1000 and 1500 W), it is observed that catalyst quantities reported above are comparable with the ones calculated in this study (Table 4.9). The difference in hydrogen production reactors is due to the difference in the

fuel conversion process: in this study, autothermal reforming (ATR) is considered instead of steam reforming, which is reported by Zalc and Löffler (2002). They also concluded that the minimum total bed volume of the process stream reactors in a 50 kW fuel processor is 22 l (which is calculated with the assumption of 1.5 kg/l bulk density for each catalyst), excluding heat exchangers, pumps and injectors.

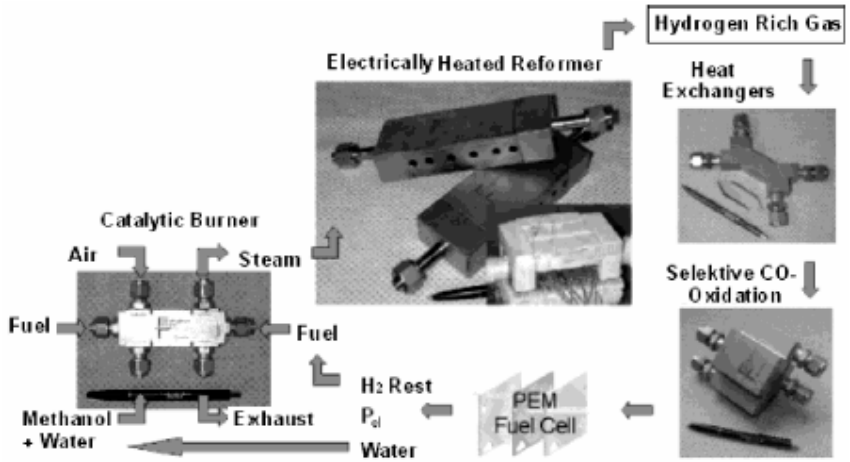

Figure 5.1. Methanol processing system intensification design (Holladay *et al.*, 2004a)

Large volume requirement of the fuel processing reactors of a 50 kW device, as observed in the results stated above, is an important challenge for automotive applications. At this point, process intensification techniques can play an important role in reducing the size of the fuel processor system. Several studies report the major benefits of the intensified processes and units such as enhancement of heat and mass transfer characteristics and increased accuracy in the control of reaction rates (Qi *et al.*, 2007; Holladay *et al.*, 2004). This concept is implemented in every stage of the fuel processor system such as the hydrogen generation step including autothermal reforming, steam reforming or partial oxidation (Johnson *et al.*, 2007; Ji *et al.*, 2003; Prabhu *et al.*, 2000; Holladay *et al.*, 2002; Holladay *et al.*, 2004b; Seo *et al.*, 2004; Ryi *et al.*, 2005; InnovaTek, 2007), carbon monoxide abatement process and hydrogen purification (Ruettinger and Farrauto, 2004; Sirijaruphan *et al.*, 2005a; Sirijaruphan *et al.*, 2005b; Tonkovich *et al.*, 1999; Lattner and Harold, 2004; Chen *et al.*, 2004). One example of process intensification is demonstrated in Figure 5.1 where a methanol processing system based on steam reforming for meeting 200 W PEMFC power output is developed; this is based on

intensification of each part of processor which consists of methanol reformer reactors, heat exchangers, combustors and preferential oxidation reactors (Holladay *et al.*, 2004a).

Process intensification can be implemented mainly by three methods: by engineered catalysts, by membrane-assisted reactors and by micro-technologies (Qi *et al.*, 2007).

5.1. Engineered Catalysts

The conventional catalysts that are considered for use in fuel processing face with some challenges when their use at the commercial scale is considered. For example, conventional Ni-based steam reforming catalysts have tendencies to be deactivated by several mechanisms such as coke formation and sulphur poisoning. Besides, Fe/Cr-based high temperature water-gas shift and Cu-based low temperature water-gas shift catalysts are pyrophoric in character. Thus, robust and non-pyrophoric catalysts (catalysts that have autoignition temperatures above the room temperature) are highly needed (Qi *et al.*, 2007; Tabakova *et al.*, 2000). In addition, carbon monoxide selectivity of the preferential oxidation catalysts have to be improved and the parasitic consumption of hydrogen have to be suppressed (Qi *et al.*, 2007). Hence, development of new and highly effective catalysts such as ceramic/metallic monolith/foam catalysts (Sirijaruphan *et al.*, 2005a; Sirijaruphan *et al.*, 2005b), wall-coated catalysts (Bravo *et al.*, 2004; Fukuhara *et al.*, 2005) and micro-structured catalysts (Horny *et al.*, 2005) became essential for an efficiently operating compact fuel processor system and are being investigated by numerous research groups.

Noble metal-based catalyst and perovskites (calcium titanium oxide, $CaTiO_3$) are developed in both pellet form and in monolithic/foam substrates for driving the reforming reaction (Qi *et al.*, 2007). In addition, in their patent, Ruettinger and Farrauto (2004) presented that they used oxides of tin, gallium and combinations thereof to modify the precious metal catalyst on an inorganic support for suppression of methanation activity of platinum group metal water-gas shift catalysts. Furthermore, plate-type copper-based catalysts are developed for low-temperature water-gas shift reaction. Engineered catalysts such as metal foam supported platinum catalysts are also developed for the selective carbon monoxide oxidation (Sirijaruphan *et al.*, 2005a; Sirijaruphan *et al.*, 2005b).

Among the other process intensification techniques, development of engineered catalysts has received increasing attention (Qi *et al.*, 2005). Catalyst supported on the metallic/cordierite (magnesium iron aluminium cyclosilicate) monolith is reported to have a diffusion length for the reactants one to two orders of magnitude shorter than that of the conventional catalyst (Qi *et al.*, 2007) (Figure 5.2). This configuration allows almost the entire catalyst surface to participate in the reaction due to improved mass and heat transfer characteristics and can therefore catalyze high temperature reactions at short residence times. As an example, Tonkovich *et al.* (1999) developed a Ru/ZrO_2 engineered-monolithic catalyst for the water-gas shift reaction and decreased contact time from 1 s to 50 ms, while achieving carbon monoxide conversion and selectivity of 99.8 per cent and 100 per cent, respectively. Moreover, Johnson *et al.* (2007) reported high performance, coke-resistant, methane steam reforming activity over the Rh-based engineered catalyst supported on the engineered, tape cast, porous, alumina shims. Nevertheless, new reactor configurations based on micro-technologies are needed with the progress of engineered catalysts.

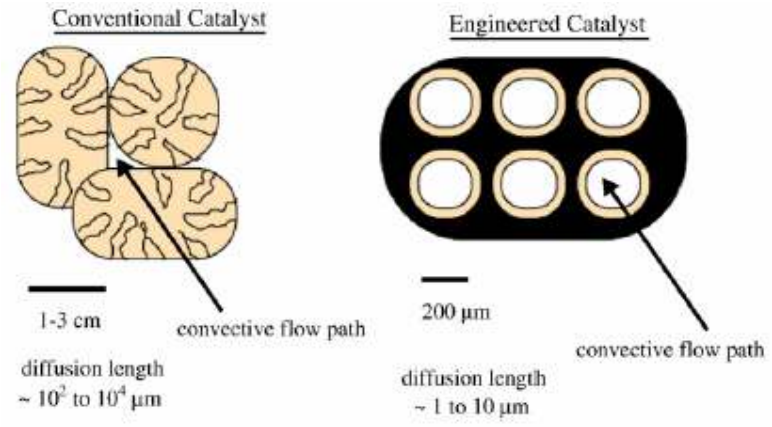

Figure 5.2. Comparison of conventional and engineered catalysts (Qi *et al.*, 2007)

5.2. Membrane-Assisted Reactors

Membrane reactors have been drawing considerable attention since they have the ability to attain separation and reaction simultaneously (Qi *et al.*, 2007). For fuel processing applications, two types of membranes are considered: oxygen transport membranes (OTM) and hydrogen transport membranes (HTM) (Qi *et al.*, 2007).

OTM configuration provides controlled supply of pure oxygen into the reactor and has many advantages over conventional reforming reactors. Figure 5.3 shows the conceptual scheme of the OTM process. In principle, oxygen ions from low-pressure air permeate the OTM and are consumed during the chemical reactions. This configuration creates a driving force that pulls oxygen ions across the membrane at high rates (Qi *et al.*, 2007). Therefore, this scheme helps in avoiding the premixing of oxygen and fuel at the feed zone, eliminating downstream removal of oxygen and formation of NO_x emissions and allows accurate control of the hotspot temperature (Ji *et al.*, 2003). It is reported that OTM configuration offers a potential savings of over 30 per cent in the capital cost of natural gas conversion to hydrogen process by combining air separation and natural gas partial oxidation or autothermal reforming in a single-step ceramic membrane reactor (Qi *et al.*, 2007).

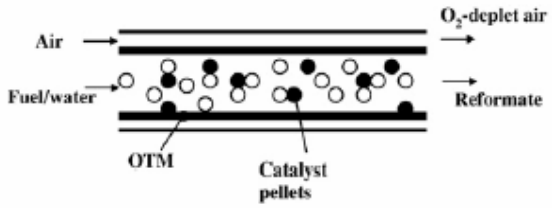

Figure 5.3. Conceptual OTM process (Qi *et al.*, 2007)

Another type of membrane, hydrogen transport membrane (HTM), has some advantages such as enabling hydrogen production at high purity, favoring the equilibrium in the direction of hydrogen production and compactness (Lattner and Harold, 2004). Three types of HTM have been reported: proton transport separation systems, atomic transport/dense metallic separation systems and molecular transport/micro-porous separation systems (Qi *et al.*, 2007). Operating scheme of a HTM reactor is schematically demonstrated in Figure 5.4.

Oyama and his co-workers developed Nanosil which is a silica hydrogen transport membrane with silica layer supported on porous glass or alumina and obtained high hydrogen separation performance and selectivity (100 per cent with respect to CH_4, CO and CO_2). They also utilized this membrane in a reactor configuration (Figure 5.5) for methane steam reforming successfully (Prabhu and Oyama, 2000; Prabhu *et al.*, 2000; Lee and Oyama, 2002; Oyama *et al.*, 2004). The dark region in Figure 5.5 shows the annular

zone where the catalyst is packed between the membrane and the outer tube. The membrane section is 4 cm long.

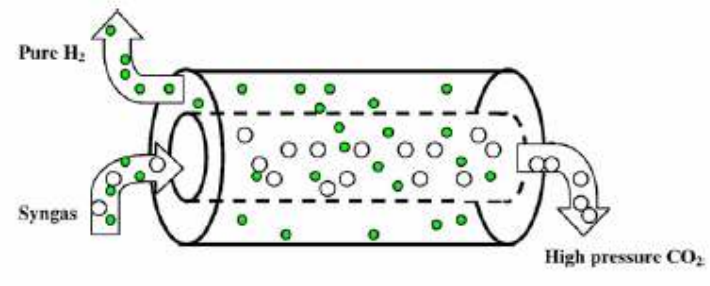

Figure 5.4. HTM reactor concept (Qi *et al.*, 2007)

The coupling of OTM and HTM is presented in Qi *et al.* (2007) and is held as a brand new respective for hydrogen production, which is shown in Figure 5.6. It combines the advantages of HTM and OTM; hotspot temperature can be effectively controlled by the transportation of oxygen through the membrane and high concentration of hydrogen can be produced. However, because the separation is driven by the partial pressure differential across the membrane, heavy-duty air compressors are needed. Typically, an operating pressure of 5 atm is needed for the fuel processor in order to produce hydrogen steam above 2 atm assuming hydrogen composition in the reformate is 40 mol per cent (Qi *et al.*, 2007). Due to the high pressure drop in the whole system, pressure above 10 atm is adopted in practice (Qi *et al.*, 2007).

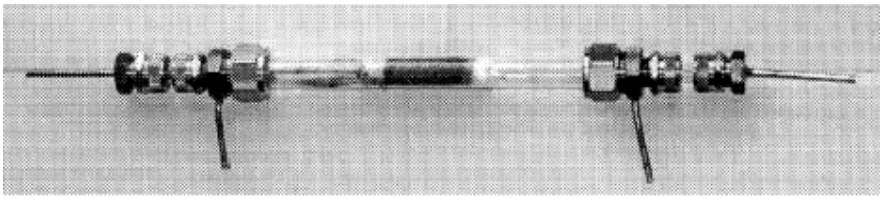

Figure 5.5. Photograph of the HTM reactor assembly (Prabhu *et al.*, 2000)

5.3. Micro-Technologies

Microchannel/microstructured reactor (MCR) technology has been proposed as a promising solution to the challenges associated with the size issues of the complete fuel processor/fuel cell assemblies considered for use in on-board hydrogen production

(Holladay *et al.*, 2004a; Ryi *et al.*, 2005; Qi *et al.*, 2007). Micro-processing techniques offer the size of each separate part of the fuel processor to be reduced significantly, hence making their integration easier and more efficient. Microchannel reactors are particularly useful when improved heat and mass transfer are needed for improved temperature control, such as in highly exothermic reactions, and for achieving increased conversion levels, product yields and selectivities (Holladay *et al.*, 2004a).

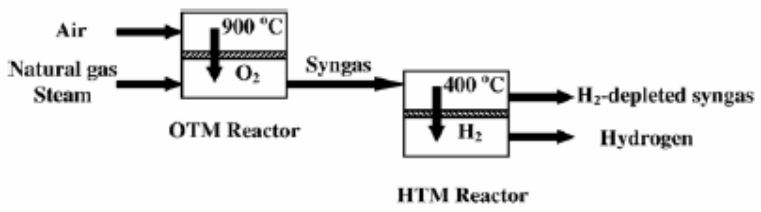

Figure 5.6. The coupling of OTM with HTM (Qi *et al.*, 2007)

MCR has many advantages such as enhanced heat and mass transfer characteristics, high specific-surface area, flow uniformity, safe operation in explosive regimes and easier scale-up without geometry changes (Veser, 2001; Kolb and Hessel, 2004). High heat and mass transfer rates favor overall kinetics and enable reactions to be performed under more aggressive conditions such as short contact times (Jensen, 2001). For the reactions that operate at transport-limited regimes, microstructured reactors offer volumes significantly smaller than their conventional counterparts at the same throughput rates. However, the possibility of heat loss by conduction through the relatively large tubing and piping connected to the miniature microstructured reactors has to be taken into account as a watch-out (Holladay *et al.*, 2004a).

Numerous studies have been reported for the development of microreactors for hydrogen production. Microchannel fuel processors containing catalytic combustion or external (electric) heating combined with reforming reaction (Polman *et al.*, 1999; Holladay *et al.*, 2002; Holladay *et al.*, 2004b; Men *et al.*, 2004; Reuse *et al.*, 2004; Aartun *et al.*, 2004; Seo *et al.*, 2004) and also with CO oxidation or hydrogen separation (Ryi *et al.*, 2005; InnovaTek, 2007) have been reported recently.

An example for an integrated fuel processor is the one developed by Holladay and co-workers for use in meeting sub-watt power requirements (Holladay *et al.*, 2002;

Holladay *et al.*, 2004b). The complete system incorporates two vaporizers/pre-heaters, a heat exchanger, a catalytic combustor and a catalytic methanol reformer in a volume less than 0.25 cm^3 and a weight less than 1 g. It was fabricated of stainless steel and was originally designed to operate within high-temperature fuel cells. These devices which are intended for use in microsensors, are designed to provide power outputs less than 1 W. Second-generation designs, which are shown in Figure 5.7, focused on high efficiency and on addition of a methanation reactor for CO clean-up, in addition to the original first-generation design (Holladay *et al.*, 2004b).

Figure 5.7. Second generation high efficiency micro-scale fuel processor, original (left) and with CO removal reactor (right) (Holladay *et al.*, 2004b)

Seo *et al.* (2004) investigated methanol steam reforming in a prototype microreactor in which a vaporizer and a reformer are connected in series. The dimensions of the vaporizer and reformer unit excluding fittings are about 70 mm x 40 mm x 30 mm. They used stainless steel metal sheets to construct the structure of microreactor and deposited catalyst inside the microchannels of the reformer unit. Rod-type electrical heaters are inserted in the holes of both sides of the end plates to provide heat for the endothermic reforming reaction and for the vaporization of the liquid fuel. The developed fuel processor generates hydrogen for driving a PEMFC of a power output of 10 W (Figure 5.8).

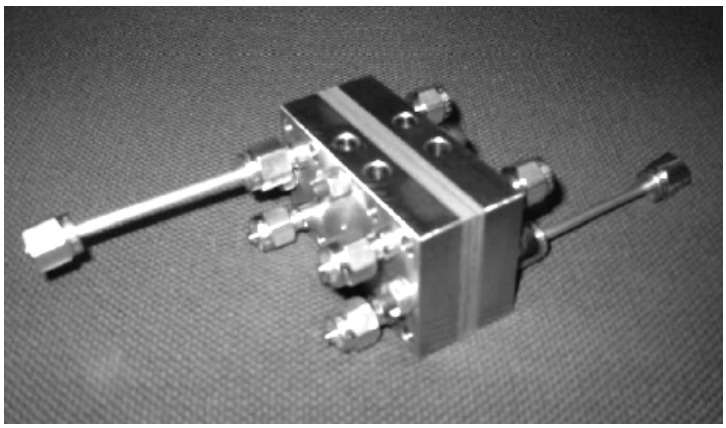

Figure 5.8. Photograph of the assembled reformer (Seo *et al.*, 2004)

Methane steam reforming coupled with hydrogen catalytic combustion is investigated in a microreactor shown in Figure 5.9 (Ryi *et al.*, 2005). The designed MCR consists of a cover plate, a base plate and 25 sets of microchannel sheets, where a set of microchannel sheet includes a hydrogen combustion sheet and a methane reforming sheet. The reactor is designed to introduce fuel and air separately and stainless steel is used for cover and base plates, while Inconel plate is used to fabricate the microchannel sheets. Pt-Sn/Al_2O_3 and Rh-Mg/Al_2O_3 catalysts are impregnated in combustion and reforming sides, respectively. The dimension of the MCR excluding fittings is about 40 mm x 40 mm x 30 mm. Novel flow channels on reformer sheets and microholes on combustor sheet is designed to inhibit the hotspot problem, which takes place in front of the reactor. This configuration is reported to deliver a power output of 26 W.

Figure 5.9. Photograph of assembled catalytic combustor/reformer (Ryi *et al.*, 2005).

InnovaTek Incorporation developed a fuel processor called InnovaGen®5, which includes integrated components in a rack mounted framework, as shown in Figure 5.10. This fuel processor includes a reformer, a fuel injector, heat exchangers, a condenser, an optional hydrogen separation membrane and the required insulation. Physical dimensions of the rack-mounted system are 36.8 cm x 20.3 cm x 31.7 cm (length x width x height) and total volume and weight of the system is 24 l and 18.1 kg, respectively. The InnovaGen®5 fuel processor is capable of reforming biodiesel, low sulphur biodiesel and other liquid fuels and generates enough hydrogen for operating a 1 kW PEMFC. Furthermore, the processor can be readily configured for processing gaseous fuels such as propane and natural gas (InnovaTek, 2007).

Figure 5.10. InnovaGen®5 fuel processor (InnovaTek, 2007)

Researchers at Battelle, Pacific Northwest Laboratories have also been developing fuel processors providing 15 W to 100 W equivalents of hydrogen from methanol fuel. The processors consist of fuel vaporizers and preheaters, a combustor, a steam reformer, heat exchangers and recuperators. Figure 5.11 shows the designed fuel processors of 25-50 W and 50-100 W, which have the weight less than 150 g and 200 g, respectively. However, the fuel processor systems require additional carbon monoxide clean-up systems in order to be used in fuel cells, although the carbon monoxide levels are significantly low (around 5 per cent) (Holladay *et al.*, 2004a).

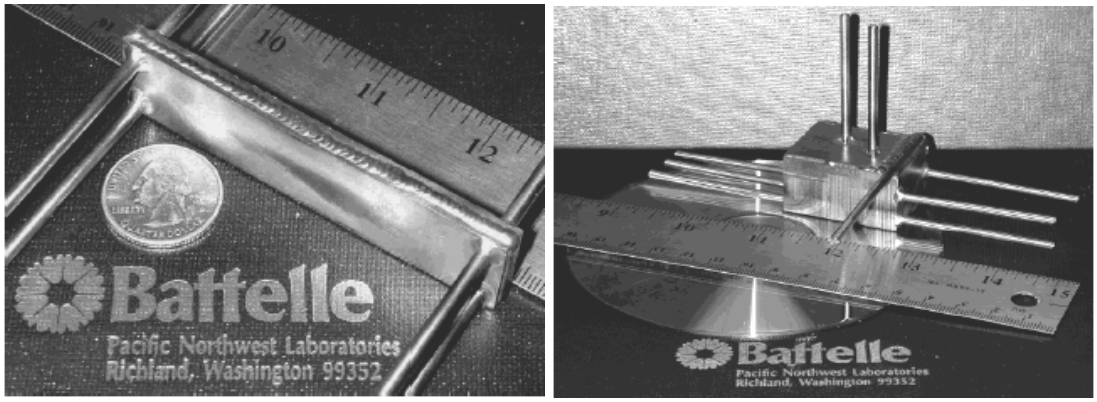

Figure 5.11. Integrated fuel processors by Battelle, 25-50 W (left) and 50-100 W (right) (Holladay *et al.*, 2004a)

The use of microreactor construction techniques to build a gradient-temperature WGS reactor has also been demonstrated (Qi *et al.*, 2007). In the reported WGS reactor design, the high-temperature water-gas shift, heat exchanger and low-temperature water-gas shift sections, a combination used industrially, is collapsed into a single unit, which is highly compact as seen in Figure 5.12. This design reduces the catalyst loading up to 50 per cent compared to the conventional method for powering units of 2-3 kW (Qi *et al.*, 2007).

Figure 5.12. Micro-scale differential temperature water-gas shift reactor (Qi *et al.*, 2007)

A microchannel reactor is developed by Chen *et al.* (2004) for running preferential oxidation of carbon monoxide in a PEM fuel cell system of 0.25 kW power output (Figure 5.13). They used stainless steel microsheets on which potassium promoted Rh metal catalyst is impregnated. Stainless steel microchannel reactor with four sheets is reported to have the potential ability to reduce the CO concentration down to 10 ppm in the H_2-rich gas at a temperature range of 443-523 K.

Figure 5.13. Microchannel preferential oxidation reactor (Chen *et al.* 2004)

6. CONCLUSIONS AND RECOMMENDATIONS

6.1. Conclusions

The objective of this study was to develop a mathematical model for simulating and designing a methane processing system that produces hydrogen for a PEMFC. It is aimed to design, i.e. size the three reactors of the fuel processor system, IPOX, WGS and PROX reactors, such that they deliver hydrogen throughput rates corresponding to 500, 1000 and 1500 W of electrical power. The major conclusions that can be drawn from this study indicate that the objectives were satisfied. These conclusions can be outlined as follows:

- Design and sizing of the reactors are carried out using a one-dimensional pseudohomogeneous reactor model. In this model, kinetics of total oxidation of methane and water-gas shift are expressed by power-law type rate equation (Ma, 1995, Choi and Stenger, 2003), steam-reforming and water-gas shift in IPOX by Langmuir-Hinshelwood-Hougen-Watson-type rate laws (Xu and Froment, 1989) and preferential oxidation of carbon monoxide by a Mars and van Krevelen type rate equation (Sedmak *et al.*, 2003). Comparison of component flow rates obtained from reactor simulations and obtained from material balance results indicates a fair level of agreement.

- Catalyst quantity in each reactor increase almost linearly with the power output of the PEMFC at both feed compositions ((methane/oxygen, steam/methane) = (2.24, 1.17), (1.89, 1.56)).

- For CH_4/O_2 = 1.89 and H_2O/CH_4 = 1.56 and for IPOX, WGS and PROX reactors, estimated catalyst quantities are 213, 220 and 60 g for 500 W, 421, 450 and 120 g for 1000 W and 669, 650 and 180 g for 1500 W PEMFC operation.

- For CH_4/O_2 = 2.24 and H_2O/CH_4 = 1.17 and for IPOX, WGS and PROX reactors, estimated catalyst quantities are 154, 230 and 34 g for 500 W, 321, 460 and 72 g. for 1000 W and 488, 700 and 106 g for 1500 W PEMFC operation.

- 2.24&1.17 feed ratio needs smaller amount of catalyst than 1.89&1.56 in all reactors except WGS converter. The small difference of WGS catalyst demands is because of difference in conversions (82 and 80 per cent for 2.24&1.17 and 1.89&1.56, respectively). More catalyst demand of 1.89&1.56 in IPOX and PROX is because of high steam reforming and water-gas shift conversion in IPOX and occurrence of reverse water-gas shift reaction in PROX.

- Operation at the feed composition of (methane/oxygen, steam/methane) = (2.24, 1.17) leads to formation of elevated reactor exit temperatures, when compared with the 1.89&1.56 operation. This is mainly due to higher TOX conversion of 2.24&1.17 in IPOX, higher catalyst need in WGS and occurrence of endothermic reverse water-gas shift reaction in PROX.

- Similar to the catalyst quantities, lengths and diameters estimated for IPOX, WGS and PROX reactors increase with increasing PEMFC power output. 1.89&1.56 operation offered longer reactor lengths, i.e. higher length-to-diameter ratios than 2.24&1.17 operation except the WGS reactor for which similar reactor lengths are observed at both feed ratios. This is due to the catalyst needs; 1.89&1.56 needs higher catalyst amounts to be packed in all reactors except WGS in which similar catalyst quantities are needed for both ratios.

- Using the criteria to minimize transport resistances, length and diameter are estimated to vary between 14.6 – 21.75 cm and 4 – 5.8 cm, respectively for the IPOX reactor, 20.35 – 27.52 and 4 – 6 cm, respectively for the WGS reactor and 10.5 – 16.07 and 2.5 – 3.5 cm, respectively for the PROX reactor for the power output range of 500-1500 W. For all three reactors, catalyst particle diameter is estimated to vary between 0.8 – 1 mm.

- Total system volume, excluding the piping, pumping and heat exchange units, is estimated to be 0.491, 0.976 and 1.508 l for 500, 1000 and 1500 W of PEMFC power outputs.

6.2. Recommendations

The following studies are recommended to improve the content of this study and to obtain further useful results:

- Different CH_4/O_2 and H_2O/CH_4 ratios can be investigated to understand the effect of feed composition on the estimated catalyst weights. This would give a more reliable idea about the size of the fuel processor system.

- Conversion of hydrocarbons other than methane to hydrogen can be investigated using the same method to compare the differences in the size of the fuel processing system.

- Simulation and design calculations can be done using a dynamic model to analyze the process regarding to its start-up and to its response against changes. Alternatively, a heterogeneous model can be developed and its outcomes can be compared with the existing results based on a pseudohomogeneous model to evaluate the validity of the criteria used to quantify the significance of transport resistances.

- Inclusion of the peripheral units such as heat exchangers and coolers into the mathematical model would provide more realistic results in terms of catalyst weight requirements.

- Validity of the existing results can be tested through setting-up an experimental system and testing the conditions simulated in this study. The outcomes can then be used to refine the mathematical model.

APPENDIX A: TEMPERATURE-DEPENDENT HEAT CAPACITIES OF THE SPECIES

Table A.1. Constants of the heat capacity equation (Sinnot, 1993)

Species	α_j	β_j (x 10^2)	γ_j (x 10^5)	δ_j (x 10^9)
CH_4	19.251	5.2126	1.1974	-11.32
H_2O	32.243	0.19238	1.0555	-3.596
CO	30.869	-1.285	2.7892	-12.72
CO_2	19.795	7.3436	-5.602	17.153
H_2	27.143	0.92738	-1.381	7.6451
O_2	28.106	-0.00037	1.7459	-10.65
N_2	31.15	-1.357	2.6796	-11.68

$$c_{p,j} = \alpha_j + \beta_j T + \gamma_j T^2 + \delta_j T^3 \qquad [\text{kJ kmol}^{-1}\ \text{K}^{-1}] \qquad \text{(A.1)}$$

REFERENCES

Aartun, I., T. Gjervan, H. Venvik, O. Görke, P. Pfeifer, M. Fathi, A. Holmen and K. Schubert, 2004, "Catalytic Conversion of Propane to Hydrogen in Microstructured Reactors", *Chemical Engineering Journal*, Vol. 101, pp. 93-99.

Ahmed S. and M. Krumpelt, 2001, "Hydrogen from Hydrocarbon Fuels for Fuel Cells", *International Journal of Hydrogen Energy*, Vol. 26, pp. 291-301.

Amadeo, N. E. and M. A. Laborde, 1995, "Hydrogen Production from the Low-Temperature Water-Gas Shift Reaction: Kinetics and Simulation of the Industrial Reactor", *International Journal of Hydrogen Energy*, Vol. 20, pp. 949-956.

Andreeva, D., V. Idakiev, T. Tabakova, L. Ilieva, P. Falaras, A. Bourlinos and A. Travlos, 2002, "Low-temperature Water-gas Shift Reaction over Au/CeO_2 Catalysts", *Catalysis Today*, Vol. 72, pp. 51-57.

Armor, J. N., 1999, "The Multiple Roles for Catalysis in the Production of H_2", *Applied Catalysis A: General*, Vol. 176, pp. 159-176.

Aryafar, M. and F. Zaera, 1997, "Kinetic Study of the Catalytic Oxidation of Alkenes over Nickel, Palladium and Platinum Foils", *Catalysis Letters*, Vol. 48, pp. 173-183.

Avcı, A. K., 2003, *Computational and Experimental Investigation of Catalytic Hydrocarbon Fuel Processing for Autothermal Hydrogen Production*, Ph.D. Dissertation, Boğaziçi University.

Avcı, A. K., D. L. Trimm and Z. İ. Önsan, 2000, "Simulation of Alternative Catalyst Bed Configurations in Autothermal Hydrogen Production", *Studies in Surface Science and Catalysis*, Vol. 130, pp. 2753-2758.

Avcı, A. K., Z. İ. Önsan and D. L. Trimm, 2001a, "On-board Fuel Conversion for Hydrogen Fuel Cells: Comparison of Different Fuels by Computer Simulations", *Applied Catalysis A: General*, vol. 216, pp. 243-256.

Avcı, A. K., Z. İ. Önsan and D. L. Trimm, 2001b, "Heterogeneous Reactor Modeling for Simulation of Catalytic Oxidation and Steam Reforming of Methane", *Chemical Engineering Science*, vol.56, pp. 641-649.

Avcı, A. K., D. L. Trimm and Z. İ. Önsan, 2002, "Quantitative Investigation of Catalytic Natural Gas Conversion for Hydrogen Fuel Cell Applications", *Chemical Engineering Journal*, Vol. 90, pp. 77-87.

Avcı, A. K., D. L. Trimm, A. E. Aksoylu and Z. İ. Önsan, 2003, "Ignition Characteristics Pt, Ni and Pt-Ni Catalysts Used for Autothermal Fuel Processing", *Catalysis Letters*, Vol. 88, pp. 17-22.

Barz, D. P. J., U. K. Tragner, V. M. Schmidt and M. Koschowitz, 2003, "Thermodynamics of Hydrogen Generation from Methane for Domestic Polymer Electrolyte Fuel Cell Systems", *Fuel Cells 2003*, Vol. 4, pp. 199-207.

Bharadwaj, S. S. and L. D. Schmidt, 1995, "Catalytic Partial Oxidation of Natural Gas to Syngas", *Fuel Processing Technology*, Vol. 42, pp. 109-127.

Bird, R. B., W. E. Stewart and E. N. Lightfood, 2002, *Transport Phenomena*, 2nd ed., J. Wiley, New York.

Boccuzzi, F., A. Chiorino, M. Manzoli, D. Andreeva and T. Tabakova, 1999, "FTIR Study of the Low-Temperature Water–Gas Shift Reaction on Au/Fe_2O_3 and Au/TiO_2 Catalysts", *Journal of Catalysis*, Vol. 188, pp.176-185.

Bodke, A. S., S. S. Bharadwaj and L. D. Schmidt, 1998, "The Effect of Ceramic Supports on Partial Oxidation of Hydrocarbons over Noble Metal Coated Monoliths", *Journal of Catalysis*, Vol. 179, pp. 138-149.

Boucouvalas, Y., Z. L. Zhang and X. E. Verykios, 1996, "Partial Oxidation of Methane to Synthesis Gas via the Direct Reaction Scheme over Ru/TiO_2 Catalyst", *Catalysis Letters*, Vol. 40, pp. 189-195.

Bradford, M. C. J. and M. A. Vannice, 1996, "Catalytic Reforming of Methane with Carbon Dioxide over Nickel Catalysts II. Reaction Kinetics", *Applied Catalysis A: General*, Vol. 142, pp. 97-122.

Bravo, J., A. Karim, T. Conant, G. P. Lopez and A. Datye, 2004, "Wall Coating of a $CuO/ZnO/Al_2O_3$ Methanol Steam Reforming Catalyst for Micro-Channel Reformers", *Chemical Engineering Journal*, Vol. 101, pp. 113-121.

Brown, L. F., 2001, "A Comparative Study of Fuels for On-board Hydrogen Production for Fuel-Cell-Powered Automobiles", *International Journal of Hydrogen Energy*, Vol. 26, pp. 381-397.

Bui, P.A., D. G. Vlachos and P.R. Westmoreland, 1997, "Catalytic Ignition of Methane/Oxygen Mixtures over Platinum Surfaces: Comparison of Detailed Simulations and Experiments", *Surface Science*, Vol. 385, pp. 1029-1034.

Burch, R., D. J. Crittle and M. J. Hayes, 1999, "C-H Bond Activation in Hydrocarbon Oxidation on Heterogeneous Catalysts", *Catalysis Today*, Vol. 47, pp. 229-234.

Cameron, D., R. Holliday and D. Thompson, 2003, "Gold's Future Role in Fuel Cell Systems", *Journal of Power Sources*, Vol. 118, pp. 298-303.

Cha, S. Y. and W. M. Lee, 1999, "Performance of Proton Exchange Membrane Fuel Cell Electrodes Prepared by Direct Decomposition of Ultrathin Platinum on the Membrane Surface", *Journal of Electrochemical Society*, Vol. 146, pp. 4055-4060.

Chan, S. H. and O. L. Ding, 2005, "Simulation of a Solid Oxide Fuel Cell Power System Fed by Methane", *International Journal of Hydrogen Energy*, Vol. 30, pp. 167-179.

Cheekatamarla, P. K. and A. M. Lane, 2005, "Catalytic Autothermal Reforming of Diesel Fuel for Hydrogen Generation in Fuel Cells I. Activity Tests and Sulphur Poisoning", *Journal of Power Sources*, Vol. 152, pp. 256-263.

Chen, G., Q. Yuan, H. Li and S. Li, 2004, "CO Selective Oxidation in a Microchannel Reactor for PEM Fuel Cell", *Chemical Engineering Journal*, Vol. 101, pp. 101-106.

Cheng, X., Z. Shi, N. Glass, L. Zhang, J. Zhang, D. Song, Z. S. Liu, H. Wang and J. Shen, 2007, "A Review of PEM Hydrogen Fuel Cell Contamination: Impacts, Mechanisms, and Mitigation", *Journal of Power Sources*, Vol. 165, pp. 739-756.

Chin, S. Y., O. S. Alexeev and M. D. Amiridis, 2005, "Preferential Oxidation of CO under Excess H_2 Conditions over Ru Catalysts", *Applied Catalysis A: General*, Vol. 286, pp.157-166.

Choi, Y. and H. G. Stenger, 2003, "Water Gas Shift Reaction Kinetics and Reactor Modeling for Fuel Cell Grade Hydrogen", *Journal of Power Sources*, Vol. 124, pp. 432-439.

Choi, Y. and H. G. Stenger, 2004, "Kinetics, Simulation and Insights for CO Selective Oxidation in Fuel Cell Applications", *Journal of Power Sources*, Vol. 129, pp. 246-254.

Choudhary, V. R., A. M. Rajput and A. S. Mamman, 1998a, "NiO-Alkaline Earth Oxide Catalysts for Oxidative Methane-to-Syngas Conversion: Influence of Alkaline Earth Oxide on the Surface Properties and Temperature-Programmed Reduction/Reaction by H_2 and Methane", *Journal of Catalysis*, Vol. 178, pp. 576-585.

Choudhary, V. R., B. S. Uphade and A. S. Mamman, 1998b, "Partial Oxidation of Methane to Syngas with or without Simultaneous CO_2 and Steam Reforming Reactions over Ni/$AlPO_4$", *Microporous and Mesoporous Materials*, Vol. 23, pp. 61-66.

Choudhary, V. R., B. S. Uphade and A. S. Mamman, 1997, "Oxidative Conversion of Methane to Syngas over Nickel Supported on Commercial Low Surface Area Porous Catalyst Carriers Precoated with Alkaline and Rare Earth Oxides", *Journal of Catalysis*, Vol. 172, pp. 281-293.

Ciaparu, D. and L. Pfefferle, 2001, "Methane Combustion Activity of Supported Palladium Catalyts After Partial Reduction", *Applied Catalysis A: General*, Vol. 218, pp. 197-209.

Cipiti, F., V. Recupero, L. Pino, A. Vita and M. Lagana, 2006, "Experimental Analysis of a 2kWe LPG-Based Fuel Processor for Polymer Electrolyte Fuel Cells", *Journal of Power Sources*, Vol. 157, pp. 914-920.

Comas, J., M. L. Dieuzeide, G. Baronetti, M. Laborde and N. Amadeo, 2006, "Methane Steam Reforming and Ethanol Steam Reforming Using a Ni(II)-Al(III) Catalyst Prepared from Lamellar Double Hydroxides", *Chemical Engineering Journal*, Vol.118, pp. 11-15.

De Smet, C. R. H., M. H. J. M. de Croon, R. J. Berger, G. B. Marin and J. C. Schouten, 2001, "Design of Adiabatic Fixed-Bed Reactors for the Partial Oxidation of Methane to Synthesis Gas. Application to Production of Methanol and Hydrogen-for-fuel-cells", *Chemical Engineering Science*, Vol. 56, pp. 4849-4861.

Dicks, A. L., 1996, "Hydrogen Generation from Natural Gas for the Fuel Cell Systems of Tomorrow", *Journal of Power Sources*, Vol. 61, pp. 113-124.

Dietz, A. G. III., A. F. Carlsson and L. D. Schmidt, 1998, "Partial Oxidation of C_5 and C_6 Alkanes over Monolith Catalysts at Short Contact Times", *Journal of Catalysis*, Vol. 176, pp. 459-473.

Elnashaie, S. S. E. H., A. M. Adris, A. S. Al-Ubaid and M. A. Soliman, 1990, "On the Non-Monotonic Behaviour of Methane Steam Reforming Kinetics", *Chemical Engineering Science*, Vol. 45, pp.491-501.

Eriksson, S., M. Wolf, A. Schneider, J. Mantzaras, F. Raimondi, M. Boutonnet and S. Jaras, 2006, "Fuel-Rich Catalytic Combustion of Methane in Zero Emissions Power Generation Processes", *Catalysis Today*, Vol. 117, pp. 447-453.

Fogler, H. S., 1999, *Elements of Chemical Reaction Engineering*, Prentice Hall, New Jersey.

Froment, G. F. and K. B. Bischoff, 1990, *Chemical Reactor Analysis and Design*, J. Wiley, New York.

Fukuhara, C., H. Ohkura, K. Gonohe and A. Igarashi, 2005, "Low-Temperature Water-Gas Shift Reaction of Plate-Type Copper-Based Catalysts on an Aluminium Plate Prepared by Electroless Plating", *Applied Catalysis A: General*, Vol. 279, pp. 195-203.

Galvita, V. and K. Sundmacher, 2005, "Hydrogen Production from Methane by Steam Reforming in a Periodically Operated Two-Layer Catalytic Reactor", *Applied Catalysis A: General*, Vol. 289, pp. 121-127.

Gasteiger, H. A., J. E. Panels and S. G. Yan, 2004, "Dependence of PEM Fuel Cell Performance on Catalyst Loading", *Journal of Power Sources*, Vol. 127, pp. 162-171.

Ghenciu, A. F., 2002, "Review of Fuel Processing Catalysts for Hydrogen Production in PEM Fuel Cell Systems", *Current Opinion in Solid State and Materials Science*, Vol. 6, pp. 389-399.

Golunski, S., 1998, "HotSpot^{TM} Fuel Processor", *Platinum Metals Review*, Vol. 42, pp. 2-7.

Haruta, M., S. K. Tsubota, T. Kobayashi, H. Kageyama, M. J. Genet and B. Delmon, 1993, "Low-Temperature Oxidation of CO over Gold Supported on TiO_2, α-Fe_2O_3 and Co_3O_4", *Journal of Catalysis*, Vol. 144, pp. 175-192.

Heck, R. M. and R. J. Farrauto, 1995, *Catalytic Air Pollution Technology: Commercial Technology*, Van Nostrand Reinhold, New York.

Heinzel, A., B. Vogel and P. Hübner, 2002, "Reforming of Natural Gas – Hydrogen Generation for Small Scale Stationary Fuel Cell Systems", *Journal of Power Sources*, Vol. 105, pp. 202-207.

Hickman, D. A. and L. D. Schmidt, 1992, "Synthesis Gas Formation by Direct Oxidation of Methane over Pt Monoliths", *Journal of Catalysis*, Vol. 138, pp. 267 -282.

Hickman, D. A. and L. D. Schmidt, 1993, "Production of Syngas by Direct Catalytic Oxidation of Methane", *Science*, Vol. 259, pp. 343- 346.

Hirschenhofer, J. H., D. B. Stauffer, R. R. Engleman and M. G. Klett, 1998, *Fuel Cell Handbook*, 4th ed., DOE/FETC-99/1076, US Department of Energy, Federal Energy Technology Center, Morgantown, WV.

Hoang, D. L. and S. H. Chan, 2004, "Modeling of a Catalytic Autothermal Methane Reformer for Fuel Cell Applications", *Applied Catalysis A: General*, Vol. 268, pp. 207-216.

Holladay, J. D., E. O. Jones, M. Phelps and J. Hu, 2002, "Microfuel Processor for Use in a Miniature Power Supply", *Journal of Power Sources*, Vol. 108, pp. 21-27.

Holladay, J. D., Y. Wang and E. Jones, 2004a, "Review of Developments in Portable Hydrogen Production Using Microreactor Technology", *Chemical Reviews*, Vol. 104, pp. 4767-4790.

Holladay, J. D., E. O. Jones, R. A. Dagle, G. G. Xia, C. Cao and Y. Wang, 2004b, "High Efficiency and Low Carbon Monoxide Micro-Scale Methanol Processors", *Journal of Power Sources*, Vol. 131, pp. 69-72.

Horny, C., L. Kiwi-Minsker and A. Renken, 2004, "Micro-Structured String-Reactor for Autothermal Production of Hydrogen", *Chemical Engineering Journal*, Vol. 101, pp. 3-9.

Idakiev, V., T. Tabakova, Z. Y. Juan and B. L. Su, 2004, "Gold Catalysts Supported on Mesoporous Titania for Low-temperature Water–gas Shift Reaction", *Applied Catalysis A: General*, Vol. 270, pp. 135-141.

InnovaTek, Inc., InnovaGen® Fuel Processor, http://www.tekkie.com/docs/InnovaGen.pdf, viewed on 14 March 2007.

Jamal Y. and M. L. Wyszynski, 1994, "On-board Hydrogen Generation of Hydrogen-Rich Gaseous Fuels – A Review", *International Journal of Hydrogen Energy*, Vol. 19, pp. 557-572.

Jensen, K. F., 2001, "Microreaction Engineering - Is Small Better?", *Chemical Engineering Science*, Vol. 56, pp. 293-303.

Ji, P., H. J. V. D. Kooi and J. D. S. Arons, 2003, "Simulation and Thermodynamic Analysis of Conventional and Oxygen Permeable CPO Reactors", *Chemical Engineering Science*, Vol. 58, pp. 2921-2930.

Jiang, C. 1992, *Studies of the Production of Hydrogen from Methanol Steam Reforming at Low Temperatures*, Ph.D. Dissertation, University of New South Wales.

Jiang, C., D. L. Trimm and M. S. Wainwright, 1995, "New Technology for Hydrogen Production by the Catalytic Oxidation and Steam Reforming of Methanol at Low Temperatures", *Chemical Engineering Technology*, Vol. 18, pp. 1-6.

Jin, R., Y. Chen, W. Li, W. Cui, Y. Ji, C. Yu and Y. Jiang, 2000, "Mechanism for Catalytic Partial Oxidation of Methane to Syngas over a Ni/Al_2O_3 Catalyst", *Applied Catalysis A: General*, Vol. 201, pp. 71-80.

Joensen, F. and J. R. Rostrup-Nielsen, 2002, "Conversion of Hydrocarbons and Alcohols for Fuel Cells", *Journal of Power Sources*, Vol. 105, pp. 195-201.

Johnson, B. R., N. L. Canfield, D. N. Tran, R. A. Dagle, X. S. Li, J. D. Holladay and Y. Wang, 2007, "Engineered SMR Catalysts Based on Hydrothermally Stable, Porous, Ceramic Supports for Microchannel Reactors", *Catalysis Today*, Vol. 120, pp. 54-62.

Kahlich, M. J., H. A. Gasteiger and R. J. Behm, 1997, "Kinetics of the Selective CO Oxidation in H_2-Rich Gas on Pt/Al_2O_3", *Journal of Catalysis*, Vol. 171, pp. 93-105.

Kahlich, M. J., H. A. Gasteiger and R. J. Behm, 1999, "Kinetics of the Selective CO Oxidation in H_2-Rich Gas on $Au/\alpha\text{-}Fe_2O_3$", *Journal of Catalysis*, Vol. 182, pp. 430-440.

Kamarudin, S. K., W. R. W. Daud, A. Md. Som, A. W. Mohammad, S. Takriff and M. S. Masdar, 2004, "The Conceptual Design of a PEMFC System via Simulation", *Chemical Engineering Journal*, Vol. 103, pp. 99-113.

Kang, I. and J. Bae, 2006, "Autothermal Reforming Study of Diesel for Fuel Cell Applications", *Journal of Power Sources*, Vol. 159, pp. 1283-1290.

Karakaya, M., 2006, *Dynamic Simulation of Indirect Partial Oxidation Reactor for Methane Conversion to Hydrogen*, M.S. Thesis, Boğaziçi University.

Keiski, R. L., O. Desponds, Y. F. Chang and G. A. Somorjai, 1993, "Kinetics of the Water-gas Shift Reaction over Several Alkane Activation and Water-gas Shift Catalysts", *Applied Catalysis A: General*, Vol. 101, pp. 317-338.

Kolb, G. and V. Hessel, 2004, "Micro-Structured Reactors for Gas Phase Reactions", *Chemical Engineering Journal*, Vol. 98, pp. 1-38.

Kopasz, J. P., D. Applegate, L. Miller, H. K. Liao and S. Ahmed, 2005, "Unraveling the Maze: Understanding of Diesel Reforming Through the Use of Simplified Fuel Blends", *International Journal of Hydrogen Energy*, Vol. 30, pp. 1243-1250.

Kvamsdal, H. M., H. F. Svendsen, T. Hertsberg and O.Olsvik, 1999, "Dynamic Simulation and Optimization of a Catalytic Steam Reformer", *Chemical Engineering Science*, Vol. 54, 2697-2706.

Laosiripojana, N. and S. Assabumrungrat, 2006, "Hydrogen Production from Steam and Autothermal Reforming of LPG over High Surface Area Ceria", *Journal of Power Sources*, Vol. 158, pp. 1348-1357.

Larentis, A.L., N. S. de Resende, V. M. M. Salim and J. C. Pinto, 2001, "Modeling and Optimization of the Combined Carbon Dioxide Reforming and Partial Oxidation of Natural Gas", *Applied Catalysis A: General*, Vol. 215, pp. 211-224.

Larminie, J. and A. L. Dicks, 2003, *Fuel Cell Systems Explained*, 2nd ed., West Sussex: J. Wiley, Chichester.

Lattner, J. R. and M. P. Harold, 2004, "Comparison of Conventional and Membrane Reactor Fuel Processors for Hydrocarbon-based PEM Fuel Cell Systems", *International Journal of Hydrogen Energy*, Vol. 29, pp. 393-417.

Lee, D. and S. T. Oyama, 2002, "Gas Permeation Characteristics of a Hydrogen Selective Supported Silica Membrane", *Journal of Membrane Science*, Vol. 210, pp. 291-306.

Lee, D., H. C. Lee, K. H. Lee and S. Kim, 2007, "A Compact and Highly Efficient Natural Gas Fuel Processor for 1-kW Residential Polymer Electrolyte Membrane Fuel Cells", *Journal of Power Sources*, Vol. 165, pp. 337-341.

Lee, S. H. D., D. V. Applegate, S. Ahmed, S. G. Calderone and T. L. Harvey, 2005, "Hydrogen from Natural Gas: Part I – Autothermal Reforming in an Integrated Fuel Processor", *International Journal of Hydrogen Energy*, Vol. 30, pp. 829-842.

Lei, Y., N. W. Cant and D. L. Trimm, 2005, "Kinetics of the Water-gas Shift Reaction over a Rhodium-promoted Iron-chromium Oxide Catalyst", *Chemical Engineering Journal*, Vol. 114, pp. 81-85.

Lian, H. L., M. J. Jia, W. C. Pan, W. X. Zhang and D. Z. Jiang, 2006, "Copper Promoted Au/ZnO-CuO Catalysts for Low Temperature Water-gas Shift Reaction", *Chemical Research in Chinese Universities*, Vol. 22, pp. 99-102.

Liguras, D. K., K. Goundani and X. E. Verykos, 2004, "Production of Hydrogen for Fuel Cells by Catalytic Partial Oxidation of Ethanol over Structured Ni Catalysts", *Journal of Power Sources*, Vol. 130, pp. 30-37.

Lin, S.H., Y. H. Chen, C. C. Yu, Y. C. Liu and C. H. Lee, 2005, "Modelling an Experimental Methane Fuel Processor", *Journal of Power Sources*, Vol. 148, pp. 45-53.

Litster, S. and G. McLean, 2004, "PEM Fuel Cell Electrodes", *Journal of Power Sources*, Vol. 130, pp. 61-76.

Ma, L., 1995, *Hydrogen Production from Steam Reforming of Light Hydrocarbons in an Autothermic System*, Ph.D. Dissertation, University of New South Wales.

Ma, L. and D. L. Trimm, 1996, "Alternative Catalyst Bed Configurations for the Autothermic Conversion of Methane to Hydrogen", *Applied Catalysis A: General*, Vol. 138, pp. 265-273.

Ma, L., D. L. Trimm and C. Jiang, 1996, "The Design and Testing of an Autothermal Reactor for the Conversion of the Light Hydrocarbons to Hydrogen I. The Kinetics of the Catalytic Oxidation of Light Hydrocarbons", *Applied Catalysis A: General*, Vol 138, pp. 275-283.

Men, Y., H. Gnaser, R. Zapf, V. Hessel, C. Ziegler and G. Kolb, 2004, "Steam Reforming of Methanol over $Cu/CeO_2/g\text{-}Al_2O_3$ Catalysts in a Microchannel Reactor", *Applied Catalysis A: General*, Vol. 277, pp. 83-90.

Ming, Q., T. Healey, L. Allen and P. Irving, 2002, "Steam Reforming of Hydrocarbon Fuels", *Catalysis Today*, Vol. 77, pp. 51-64.

Muradov, N., 2003, "Emission-Free Fuel Reformers for Mobile and Portable Fuel Cell Applications", *Journal of Power Sources*, Vol. 118, pp. 320-324.

Muradov, N. and T. N. Veziroğlu, 2005, "From Hydrocarbon to Hydrogen-Carbon to Hydrogen Economy", *International Journal of Hydrogen Energy*, Vol. 30, pp. 225-237.

Numaguchi, T. and K. Kikuchi, 1988, "Intrinsic Kinetics and Design Simulation in a Complex Reaction Network: Steam-Methane Reforming", *Chemical Engineering Science*, Vol. 43, 2295-2301.

O'Hayre, R., S. J. Lee, S. W. Cha and F. B. Prinz, 2002, "A Sharp Peek in the Performance of Sputtered Platinum Fuel Cells at Ultra-Low Platinum Loading", *Journal of Power Sources*, Vol. 109, pp. 483-493.

Opoku-Gyamfi, K. and A. A. Adesina, 1999, "Kinetic Studies of CH_4 Oxidation over $Pt\text{-}NiO/d\text{-}Al_2O_3$ in a Fluidised Bed Reactor", *Applied Catalysis A: General*, Vol. 180, pp. 113-122.

Oyama, S. T., D. Lee, P. Hacarlioglu and R. F. Saraf, 2004, "Theory of Hydrogen Permeability in Nonporous Silica Membranes", *Journal of Membrane Science*, Vol. 244, pp. 45-53.

Özkara, S. and A. E. Aksoylu, 2003, "Selective Low Temperature Carbon Monoxide Oxidation in H_2-rich Gas Streams over Activated Carbon Supported Catalysts", *Applied Catalysis A: General*, Vol. 251, pp. 75-83.

Özyönüm, G. N., 2002, *Kinetics of Selective CO Oxidation in Hydrogen Rich Streams Over Pt-Co-Ce/Al_2O_3 Catalyst*, M.S. Thesis, Boğaziçi University.

Panagiotopoulou, P. and D. I. Kondarides, 2004, "Effect of Morphological Characteristics of TiO_2-supported Noble Metal Catalysts on Their Activity for the Water–gas Shift Reaction", *Journal of Catalysis*, Vol. 225, pp. 327-336.

Pena, M. A., J. P. Gomez and J. L. G. Fierro, 1996, "New Catalytic Routes for Syngas and Hydrogen Production", *Applied Catalysis A: General*, Vol. 144, pp. 7-57.

Perry, R. H. and D. W. Green, 1997, *Perry's Chemical Engineers' Handbook*, 7th ed., McGraw-Hill, USA.

Persson, K., A. Ersson, A. Colussi, A. Trovarelli and S. G. Jaras, 2006, "Catalytic Performance of Methane over Bimetallic Pd-Pt Catalysts: The Influence of Support Materials", *Applied Catalysis B: Environmental*, Vol. 66, pp. 175-185.

Polman, E. A., J. M. Der Kinderen and F. M. A. Thuis, 1999, "Novel Compact Steam Reformer for Fuel Cells with Heat Generation by Catalytic Combustion Augmented by Induction Heating", *Catalysis Today*, Vol. 47, pp. 347-351.

Prabhu, A. K. and S. T. Oyama, 2000, "Highly Hydrogen Selective Ceramic Membranes: Application to the Transformation of Greenhouse Gases", *Journal of Membrane Science*, Vol. 176, pp. 233-248.

Prabhu, A. K., A. Liu, L. G. Lovell and S. T. Oyama, 2000, "Modeling of the Methane Reforming Reaction in Hydrogen Selective Membrane Reactors", *Journal of Membrane Science*, Vol. 177, pp. 83-95.

Qi, A., S. Wang, G. Fu, C. Ni and D. Wu, 2005, "La-Ce-Ni-O Monolithic Perovskite Catalysts Potential for Gasoline Autothermal Reforming System", *Applied Catalysis A: General*, Vol. 281, pp. 233-246.

Qi, A., B. Peppley and K. Karan, 2007, "Integrated Fuel Processors for Fuel Cell Application: A Review", *Fuel Processing Technology*, Vol. 88, pp. 3-22.

Radhakrishnan, R., R. R. Willigan, Z. Dardas and T. H. Vanderspurt, 2006, "Water Gas Shift Activity and Kinetics of Pt/Re Catalysts Supported on Ceria-zirconia Oxides", *Applied Catalysis B: Environmental*, Vol. 66, pp. 23-28.

Rakass, S., H. Oudghiri-Hassani, P. Rowntree and N. Abatzoglou, 2006, "Steam Reforming of Methane Over Unsupported Nickel Catalyst", *Journal of Power Sources*, Vol. 158, pp. 485-496.

Ralph, T. R. and G. A. Hards, 1998, "Powering the Cars and Homes for Tomorrow", *Chemistry & Industry*, Vol. 9, pp. 337-342.

Rase, H. F., 1990, *Fixed-bed Reactor Design and Diagnostics: Gas-phase Reactions*, Butterworth Publishers, London.

Recupero, V., L. Pino, A. Vita, F. Cipiti, M. Cordaro and M. Lagana, 2005, "Development of a LPG Fuel Processor for PEFC Systems: Laboratory Scale Evaluation of Autothermal Reforming and Preferential Oxidation Subunits", *International Journal of Hydrogen Energy*, Vol. 30, pp. 963-971.

Reuse, P., A. Renken, K. Haas-Santo, O. Görke and K. Schubert, 2004, "Hydrogen Production for Fuel Cell Application in an Autothermal Micro-Channel Reactor", *Chemical Engineering Journal*, Vol. 101, pp. 133-141.

Ross, J. R. H., 1974, *Surface and Defect properties of Solids*, in M. W. Roberts and J. M. Thomas (Eds.), *Chemical Society*, Vol. 4, pp.34, London.

Rossignol, C., S. Arrii, F. Morfin, L. Piccolo, V. Caps and J-L. Rousset, 2005, "Selective Oxidation of CO over Model Gold-Based Catalysts in the Presence of H_2", *Journal of Catalysis*, Vol. 230, pp. 476-483.

Rostrup-Nielsen, J. R., 1973, "Activity of Nickel Catalysts for Steam Reforming of Hydrocarbons", *Journal of Catalysis*, Vol. 31, pp. 173-199.

Rostrup-Nielsen, J. R., 1984, "Catalytic Steam Reforming", in J. R. Anderson and M. Boudart (Eds.), *Catalysis, Science & Technology*, Vol 5., pp. 1-117, Springer-Verlag, Berlin.

Rostrup-Nielsen, J. R., 1998, "Methane Conversion", in D. M. Bibley (Eds.), Elsevier, Amsterdam.

Ruettinger, W. F. and R. J. Farrauto, 2004, *Suppression of Methanation Activity Platinum Group Metal Water-Gas Shift Catalysts*, US6790432B2.

Ryi, S. K., J. S. Park, S. H. Choi, S. H. Cho and S. H. Kim, 2005, "Novel Micro Fuel Processor for PEMFCs with Heat Generation by Catalytic Combustion", *Chemical Engineering Journal*, Vol. 113, pp. 47-53.

Saito, M., K. Tomoda, I. Takahara, K. Murata and M. Inaba, 2003, "Effects of Pretreatments of Cu/ZnO-based Catalysts on Their Activities for the Water-gas Shift Reaction", *Catalysis Letters*, Vol. 89, pp. 11-13.

Santarelli, M. G. and M. F. Torchio, 2007, "Experimental Analysis of the Effects of the Operating Variables on the Performance of a Single PEMFC", *Energy Conversion and Management*, Vol. 48, pp. 40-51.

Satyapal, S., J. Petrovic, C. Read, G. Thomas and G. Ordaz, 2007, "The U.S. Department of Energy's National Hydrogen Storage Project: Progress towards Meeting Hydrogen-Powered Vehicle Requirements", *Catalysis Today*, Vol. 120, pp. 246-256.

Schmidt, L. D., E. J. Klein, C. A. Leclerc, J. J. Krummenacher and K. N. West, 2003, "Syngas in Milisecond Reactors: Higher Alkanes and Fast Lightoff", *Chemical Engineering Science*, Vol. 58, pp. 1037-1041.

Schmidt, V. M., P. Bröcherhoff, B. Höhlein, R. Menzer and U. Stimmung, 1994, "Utilization of Methanol for Polymer Electrolyte Fuel Cells in Mobile Systems", *Journal of Power Sources*, Vol. 49, pp. 299-313.

Schubert, M. M., A. Venugopal, M. J. Kahlich, V. Plzak and R. J. Behm, 2004, "Influence of H_2O and CO_2 on the Selective CO Oxidation in H_2-rich Gases over Au/α-Fe_2O_3", *Journal of Catalysis*, Vol. 222, pp. 32-40.

Schumacher, B., Y. Denkwitz, V. Plzak, M. Kinne and R. J. Behm, 2004, "Kinetics, Mechanism and the Influence of H_2 on the CO Oxidation Reaction on a Au/TiO_2 Catalyst", *Journal of Catalysis*, Vol. 224, pp. 49-462.

Sedmak, G., S. Hocevar and J. Levec, 2003, "Kinetics of Selective CO Oxidation in Excess of H_2 over the Nanostructured $Cu_{0.1}Ce_{0.9}O_{2-y}$ Catalyst", *Journal of Catalysis*, Vol. 213, pp. 135-150.

Sekizawa, K., S. Yano, K. Eguchi and H. Arai, 1998, "Selective Removal of CO in Methanol Reformed Gas over Cu-Supported Mixed Metal Oxides", *Applied Catalysis A: General*, Vol. 169, pp. 291-297.

Selen, B., 2003, *Production of Hydrogen from Light Hydrocarbons via Indirect Partial Oxidation on Bimetallic Catalysts*, M.S. Thesis, Boğaziçi University.

Seo, D. J., W. L. Yoon, Y. G. Yoon, S. H. Park, G. G. Park and C. S. Kim, 2004, "Development of a Micro Fuel Processor for PEMFCs", *Electrochimica Acta*, Vol. 50, pp. 719-723.

Sinnot, R. K., 1993, *Coulson's & Richardson's Chemical Engineering, Design*, Vol. 6., 2nd ed., Butterworth–Heinemann, London.

Sirijaruphan, A., J. G. Goodwin Jr., R. W. Rice, D. Wei, K. R. Butcher, G. W. Roberts and J. J. Spivey, 2005a, "Metal Foam Supported Pt Catalysts for the Selective Oxidation of CO in Hydrogen", *Applied Catalysis A: General*, Vol. 281, pp. 1-9.

Sirijaruphan, A., J. G. Goodwin Jr., R. W. Rice, D. Wei, K. R. Butcher, G. W. Roberts and J. J. Spivey, 2005b, "Effect of Metal Foam Supports on the Selective Oxidation of CO on Fe-Promoted Pt/γ-Al_2O_3", *Applied Catalysis A: General*, Vol. 281, pp. 11-18.

Son, I. H., M. Shamsuzzoha and A. M. Lane, 2002, "Promotion of Pt/γ-Al_2O_3 by New Pretreatment for Low-Temperature Preferential Oxidation of CO in H_2 for PEM Fuel Cells", *Journal of Catalysis*, Vol. 210, pp. 460-465.

Song, C., 2002, "Fuel Processing for Low-Temperature and High-Temperature Fuel Cells. Challenges and Opportunities for Sustainable Development in the 21st Century", *Catalysis Today*, Vol. 77, pp. 17-49.

Springman, S., M. Bohnet, A. Docter, A. Lamm and G. Eigenberger, 2004, "Cold Start Simulations of a Gasoline Based Fuel Processor for Mobile Fuel Cell Applications", *Journal of Power Sources*, Vol. 128, pp. 13-24.

Sun, J., J. DesJardins, J. Buglass and K. Liu, 2005, "Noble Metal Water Gas Shift Catalysis: Kinetic Study and Reactor Design", *International Journal of Hydrogen Energy*, Vol. 30, pp. 1259-1264.

Tabakova, T., V. Idakiev, D. Andreeva and I. Mitov, 2000, "Influence of the Microscopic Properties of the Support on the Catalytic Activity of Au/ZnO, Au/ZrO_2, Au/Fe_2O_3, Au/Fe_2O_3–ZnO, Au/Fe_2O_3–ZrO_2 Catalysts for the WGS Reaction", *Applied Catalysis A: General*, Vol. 202, pp. 91-97.

Thomas, C. E., B. D. James, F. D. Lomax Jr and I. F. Kuhn Jr, 2000, "Fuel Options for the Fuel Cell Vehicle: Hydrogen, Methanol or Gasoline?", *International Journal of Hydrogen Energy*, Vol. 25, pp. 551-567.

Thomas, S. and R. A. Dawe, 2003, "Review of Ways to Transport Natural Gas Energy from Countries Which Do Not Need the Gas for Domestic Use", *Energy*, Vol. 28, pp. 1461-1477.

Tonkovich, A. Y., J. L. Zilka, M. J. LaMont, Y. Wang and R. S. Wegeng, 1999, "Microchannel Reactors for Fuel Processing Applications. I. Water Gas Shift Reactor", *Chemical Engineering Science*, Vol. 54, pp. 2947-2951.

Trimm, L. and Z. İ. Önsan, 2001, "On-board Fuel Conversion for Hydrogen-Fuel-Cell-Driven Vehicles", *Catalysis Reviews: Science and Engineering*, Vol.43, pp. 31-84.

Trimm, D. L. and C. W. Lam, 1980, "The Combustion of Methane on Platinum-Alumina Fibre Catalysts", *Chemical Engineering Science*, Vol. 35, pp. 1405-1413.

Trimm, D. L., 1983, "Catalytic Combustion", *Applied Catalysis*, Vol. 7, pp. 249-282.

Trimm, D. L., 1999, "Catalysts for the Control of Coking During Steam Reforming", *Catalysis Today*, Vol. 49, pp. 3-10.

Twigg, M. V. (editor), 1989, *Catalyst Handbook*, Wolf Scientific Text: London.

Utaka, T. K., K. Sekizawa and K. Eguchi, 2000, "CO Removal by Oxygen-Assisted Water Gas Shift Reaction over Supported Cu Catalysts", *Applied Catalysis A: General*, Vol. 194-195, pp. 21-26.

Veser, G., 2001, “Experimental and Theoretical Investigation of H_2 Oxidation in a High-Temperature Catalytic Microreactor”, *Chemical Engineering Science*, Vol. 56, pp. 1265-1273.

Veser, G. And L. D. Schmidt, 1996, “Ignition and Extinction in the Catalytic Oxidation of Hydrocarbons over Platinum”, *AIChE Journal*, Vol. 42, pp. 1077-1087.

Watanabe, M., H. Igarashi, M. Suzuki, Y. Sasaki and H. Uchida, 1997, “Removal of Carbon Monoxide from Hydrogen-Rich Fuels by Selective Oxidation Over Platinum Catalyst Supported on Zeolite”, *Applied Catalysis A: General*, Vol. 159, pp. 159-169.

Xiu, G, P. Li and A. E. Rodrigues, 2003, “Adsorption-Enhanced Steam-Methane Reforming with Intraparticle-Diffusion Limitations”, *Chemical Engineering Journal*, Vol. 95, pp. 83-93.

Xu, J. and G. F. Froment, 1989, “Methane Steam Reforming, Methanation and Water-Gas Shift: I. Intrinsic Kinetics”, *AIChE Journal*, Vol. 35, pp. 88-96.

Yoshida, H., T. Nakajima, Y. Yazawa and T. Hattori, 2007, “Support Effect on Methane Combustion over Palladium Catalysts”, *Applied Catalysis B: Environmental*, Vol. 71, pp. 70-79.

Zalc, J. M. and D. G. Löffler, 2002, “Fuel Processing for PEM Fuel Cells: Transport and Kinetic Issues of System Design”, *Journal of Power Sources*, Vol. 111, pp. 58-64.

Zhao, S., T. Luo and R. J. Gorte, 2004, “Deactivation of the Water-gas Shift Activity of Pd/Ceria by Mo”, *Journal of Catalysis*, Vol. 221, pp. 413-420.